

Issue 3

2017 | Volume 13

The Journal on Advanced Studies in Theoretical and Experimental Physics,
including Related Themes from Mathematics

PROGRESS IN PHYSICS



“All scientists shall have the right to present their scientific research results, in whole or in part, at relevant scientific conferences, and to publish the same in printed scientific journals, electronic archives, and any other media.” — Declaration of Academic Freedom, Article 8

ISSN 1555-5534

PROGRESS IN PHYSICS

A quarterly issue scientific journal, registered with the Library of Congress (DC, USA). This journal is peer reviewed and included in the abstracting and indexing coverage of: Mathematical Reviews and MathSciNet (AMS, USA), DOAJ of Lund University (Sweden), Scientific Commons of the University of St. Gallen (Switzerland), Open-J-Gate (India), Referativnyi Zhurnal VINITI (Russia), etc.

Electronic version of this journal:
<http://www.ptep-online.com>

Advisory Board

Dmitri Rabounski,
Editor-in-Chief, Founder
Florentin Smarandache,
Associate Editor, Founder
Larissa Borissova,
Associate Editor, Founder

Editorial Board

Pierre Millette
millette@ptep-online.com
Andreas Ries
ries@ptep-online.com
Gunn Quznetsov
quznetsov@ptep-online.com
Felix Scholkmann
scholkmann@ptep-online.com
Ebenezer Chifu
chifu@ptep-online.com

Postal Address

Department of Mathematics and Science,
University of New Mexico,
705 Gurley Ave., Gallup, NM 87301, USA

Copyright © *Progress in Physics*, 2017

All rights reserved. The authors of the articles do hereby grant *Progress in Physics* non-exclusive, worldwide, royalty-free license to publish and distribute the articles in accordance with the Budapest Open Initiative: this means that electronic copying, distribution and printing of both full-size version of the journal and the individual papers published therein for non-commercial, academic or individual use can be made by any user without permission or charge. The authors of the articles published in *Progress in Physics* retain their rights to use this journal as a whole or any part of it in any other publications and in any way they see fit. Any part of *Progress in Physics* howsoever used in other publications must include an appropriate citation of this journal.

This journal is powered by \LaTeX

A variety of books can be downloaded free from the Digital Library of Science:
<http://fs.gallup.unm.edu/ScienceLibrary.htm>

ISSN: 1555-5534 (print)

ISSN: 1555-5615 (online)

Standard Address Number: 297-5092

Printed in the United States of America

July 2017

Vol. 13, Issue 3

CONTENTS

Douari J. The Curved Space is the Electrified Flat Space	139
Elmaghraby K. E. Configuration Mixing in Particle Decay and Reaction	150
Consiglio J. Are Energy and Space-time Expanding Together?	156
Caritá L. A., Rodrigues I., Puerari I., Schiavo L. E. C. A. Using the SALI Method to Distinguish Chaotic and Regular Orbits in Barred Galaxies with the LP-Vicode Program	161
Mayhew K. W. A New Perspective for Kinetic Theory and Heat Capacity	166
Marquet P. Exotic Matter: A New Perspective	174
Zhang T. X. Testing 5D Gravity with LIGO for Space Polarization by Scalar Field	180

Information for Authors

Progress in Physics has been created for rapid publications on advanced studies in theoretical and experimental physics, including related themes from mathematics and astronomy. All submitted papers should be professional, in good English, containing a brief review of a problem and obtained results.

All submissions should be designed in L^AT_EX format using *Progress in Physics* template. This template can be downloaded from *Progress in Physics* home page <http://www.ptep-online.com>

Preliminary, authors may submit papers in PDF format. If the paper is accepted, authors can manage L^AT_EX typing. Do not send MS Word documents, please: we do not use this software, so unable to read this file format. Incorrectly formatted papers (i.e. not L^AT_EX with the template) will not be accepted for publication. Those authors who are unable to prepare their submissions in L^AT_EX format can apply to a third-party payable service for LaTeX typing. Our personnel work voluntarily. Authors must assist by conforming to this policy, to make the publication process as easy and fast as possible.

Abstract and the necessary information about author(s) should be included into the papers. To submit a paper, mail the file(s) to the Editor-in-Chief.

All submitted papers should be as brief as possible. Short articles are preferable. Large papers can also be considered. Letters related to the publications in the journal or to the events among the science community can be applied to the section *Letters to Progress in Physics*.

All that has been accepted for the online issue of *Progress in Physics* is printed in the paper version of the journal. To order printed issues, contact the Editors.

Authors retain their rights to use their papers published in *Progress in Physics* as a whole or any part of it in any other publications and in any way they see fit. This copyright agreement shall remain valid even if the authors transfer copyright of their published papers to another party.

Electronic copies of all papers published in *Progress in Physics* are available for free download, copying, and re-distribution, according to the copyright agreement printed on the titlepage of each issue of the journal. This copyright agreement follows the *Budapest Open Initiative* and the *Creative Commons Attribution-Noncommercial-No Derivative Works 2.5 License* declaring that electronic copies of such books and journals should always be accessed for reading, download, and copying for any person, and free of charge.

Consideration and review process does not require any payment from the side of the submitters. Nevertheless the authors of accepted papers are requested to pay the page charges. *Progress in Physics* is a non-profit/academic journal: money collected from the authors cover the cost of printing and distribution of the annual volumes of the journal along the major academic/university libraries of the world. (Look for the current author fee in the online version of *Progress in Physics*.)

The Curved Space is the Electrified Flat Space

Jamila Douari

Department of Science, University of North Florida, 1 UNF Drive 32224, Jacksonville, Florida, USA.
High Energy Section, The Abdus Salam International Center for Theoretical Physics, Trieste, Italy.
E-mail: jdouari@hotmail.com

The responsibility of the electric field E in the modification of the nature of the space is proved. We investigate the way the fundamental strings are related to super-gravity background of D5-branes; i.e. once the endpoints of the D-strings are electrified the flat space becomes curved. We study the electrified relative and overall transverse perturbations of fuzzy funnel solutions of intersecting (N, N_f) -strings and D5-branes in flat and super-gravity backgrounds respectively. As a result the perturbations have a discontinuity which corresponds to a zero phase shift realizing Polchinski's open string Neumann boundary condition. And once the electric field E is turned on in flat space these perturbations decrease and when E is close to the critical value $1/\lambda$ the perturbations disappear forever and the string coupling becomes strong. At this stage the space is considered curved and the electric field is responsible for this effect. This phenomenon is also enhanced by the behavior of the potential V associated to the perturbations Φ on the funnel solutions under the influence of the electric field. The potential goes too fast to $-\infty$ when E goes to the critical value $1/\lambda$ in flat space which looks like a kink to increase the velocity for Φ to disappear. But in curved space and close to the intersecting point we do not find any perturbation for all E and there is no effect of E on V and this is a sign to the absence of the perturbation effects in super-gravity background. This clarifies the existence of a relation between the electric field and the super-gravity background.

1 Introduction

The present work proves the fact that the flat space becomes curved because of the presence of the electric field. We use the non-Abelian Dirac-Born-Infeld (DBI) effective action for this study. Many results using this action have dealt with brane intersections and polarization [1–3, 5, 6, 18]. The study of brane intersections has given a realization of non-commutative geometry in the form of so-called fuzzy funnels [7–13]. In the context of time dependence in string theory from the effective D-brane action, we expect that the hyperplanes can fluctuate in shape and position as dynamical objects.

We deal with the branes intersection problem of (N, N_f) -strings with D5-branes in flat and curved spaces by treating the relative and overall transverse perturbations. And it will be devoted to extend the research begun in [9, 12, 13]. The duality of intersecting D1-D3 branes in the low energy effective theory in the presence of electric field is found to be broken in [11] but the duality of intersecting D1-D5 branes discussed in [12] is unbroken in the same theory with the electric field switched on which allows us to be more interested by the study of the intersecting D1-D5 branes.

We observe, in section 2, that the most lowest energy is gotten as the electric field E is approximately its critical value $1/\lambda$ ($\lambda = 2\pi\ell_s^2$ and ℓ_s the string length) and also as E is going to $1/\lambda$ the physical radius is going to the highest value and then D5-brane is getting bulky.

The analysis we give in sections 3 and 4 proves that the perturbations have a discontinuity which corresponds to zero

phase shift and then the string is Polchinski's open string obeying Neumann boundary condition. Hence the endpoints lie on the hyperplane are still free to move in.

We also look for more effects of E on the perturbations and the associated potentials. The behavior of the perturbations in both backgrounds is as follows: in flat space (section 3), the perturbations are disappearing because of the presence of E and when $E \approx 1/\lambda$ we end by no perturbation and our system is stable; and in curved space (section 4) we did not get any perturbation for all E which means the presence of the super-gravity does not allow any perturbation to appear in the same way that E does in flat space.

The effect of E on the potentials associated to the perturbations in flat and curved spaces is the following: the potential is going down too fast to a very low amplitude minima ($-\infty$) in flat space as E is going to its maxima, this is interpreted as inducing an increase in the velocity of the perturbation to disappear; and in curved space the effect of E on the potential is absent.

The comparison of the flat and curved cases leads us to say if E or super-gravity is present then the perturbations should be absent. This looks like E affects the flat background of D5-brane and transformed it to super-gravity background where the objects are stable. Consequently, we can think of E and super-gravity as dual.

It's known that in curved space the string coupling g_s is strong. And from our study the electric field E is fixed in terms of g_s by the relation $E = \frac{1}{\lambda}(1 + (N/N_f g_s)^2)^{-1/2}$. Then

if $E \approx 1/\lambda$ that means $N_f g_s \gg 1$ and g_s is strong. In this case the system should be described by Quantum Field Theory (QFT) in curved space where no perturbations show up. Hence our electric field is sending us to another theory such that our space is not flat any more.

The effect of the electric field is clear in this work. E increases the volume of D5-brane and decreases the low energy of the system and changes the nature of the background from flat to curved and tells us the system should now be studied in QFT in curved space.

We start the study by introducing D1 ⊥ D5 branes and discussing the influence of the electric field on the low energy and the volume of D5-brane in section 2. We give the solutions of the linearized equations of motion of the relative transverse perturbations in flat space and we treat the effect of the electric field on the perturbations and the associated potentials in section 3. Then in section 4, we study the overall transverse perturbations and their associated potentials in zero and non-zero modes propagating on a dyonic string in the super-gravity background of the orthogonal D5-branes and we look for the effect of the electric field in this case. The discussion and conclusion are presented in section 5.

2 Intersecting D1 and D5 branes

Let's briefly review the non-abelian viewpoint of the (N, N_f) -strings which grow into D5-branes by using non-commutative coordinates [7, 15, 18]. The dual picture is the intersecting D5 and D1 branes such that (N, N_f) -strings can end on D5-branes, but they must act as sources of second Chern class or instanton number in the world volume theory of the D5-branes. Hence D5 world volume description is complicated because of the second chern term which is not vanishing. The most important feature of the intersecting D1-D5 branes is the fact that the duality of this system discussed in [12] in the low energy effective theory with the electric field switched on is unbroken.

In the present description, the fundamental N_f strings are introduced by adding a U(1) electric field denoted $F_{\tau\sigma} = EI_N$, with I_N the $N \times N$ identity matrix. In fact the electric field turns the N D-strings into a (N, N_f) -strings by dissolving the fundamental string degrees of freedom into the world volume.

For a fixed E we consider the quantization condition on the displacement $D = \frac{N_f}{N}$ such that

$$D \equiv \frac{1}{N} \frac{\delta S}{\delta E} = \frac{\lambda^2 T_1 E}{\sqrt{1 - \lambda^2 E^2}}.$$

Then the electric field is expressed in terms of string coupling g_s and the number of fundamental strings N_f ,

$$E = \frac{1}{\lambda} \left(1 + \left(\frac{N}{N_f g_s} \right)^2 \right)^{-1/2}. \tag{1}$$

The electric field is turned on and the system dyonic is described by the action

$$S = -T_1 \int d^2\sigma \times \text{STr} \left[-\det \left(\eta_{ab} + \lambda F_{ab} \lambda \partial_a \Phi^j - \lambda \partial_b \Phi^i Q^{ij} \right) \right]^{\frac{1}{2}} \tag{2}$$

with $i, j = 1, \dots, 5$, $a, b = \tau, \sigma$ and using $T = 1/\lambda g_s$ such that $\lambda = 2\pi l_s^2$ with l_s is the string length, g_s is the string coupling and $Q_{ij} = \delta_{ij} + i\lambda[\Phi_i, \Phi_j]$. The funnel solution is given by suggesting the ansatz

$$\Phi_i(\sigma) = \mp \hat{R}(\sigma) G_i \tag{3}$$

$i = 1, \dots, 5$, where $\hat{R}(\sigma)$ is the (positive) radial profile and G_i are the matrices constructed by Castellino, Lee and Taylor in [14]. We note that G_i are given by the totally symmetric n -fold tensor product of 4×4 Euclidean gamma matrices, such that $\frac{1}{2}[G^i, G^j]$ are generators of SO(5) rotations, and that the dimension of the matrices is related to the integer n by $N = (n+1)(n+2)(n+3)/6$. The funnel solution (3) has the following physical radius

$$R(\sigma) = \sqrt{c} \lambda \hat{R}(\sigma) \tag{4}$$

with c is the Casimir associated with the G_i matrices, given by $c = n(n+4)$, and the funnel solution is

$$\Phi_i(\sigma) = \pm \frac{R(\sigma)}{\lambda \sqrt{c}} G_i. \tag{5}$$

We compute the determinant in (2) and we obtain

$$S = -NT_1 \int d^2\sigma \sqrt{1 - \lambda^2 E^2 + (R')^2} \left(1 + 4 \frac{R^4}{c\lambda^2} \right). \tag{6}$$

This result only captures the leading large N contribution at each order in the expansion of the square root. Using the action (6), we can derive the lowest energy ξ_{min} as the electric field is present and $E \in]0, 1/\lambda[$, (the low energy in the case of intersecting D1-D5 branes when the electric field is absent was discussed in [15])

$$\xi = NT_1 \int d\sigma \left[\left(\sqrt{1 - \lambda^2 E^2} \mp R' \left(\frac{8R^4}{c\lambda^2} + \frac{16R^8}{c^2\lambda^4} \right)^{\frac{1}{2}} \right)^2 + \left(R' \pm \sqrt{1 - \lambda^2 E^2} \left(\frac{8R^4}{c\lambda^2} + \frac{16R^8}{c^2\lambda^4} \right)^{\frac{1}{2}} \right)^2 \right]^{\frac{1}{2}}$$

and

$$\xi_{min} = NT_1 \sqrt{1 - \lambda^2 E^2} \int \left(1 + \frac{4R^4}{c\lambda^2} \right)^2 d\sigma. \tag{7}$$

such that

$$R' = \mp \sqrt{1 - \lambda^2 E^2} \left(\frac{8R^4}{c\lambda^2} + \frac{16R^8}{c^2\lambda^4} \right)^{\frac{1}{2}}. \tag{8}$$

The lowest energy (7) can be rewritten in the following expression

$$\begin{aligned} \xi_{min} = & N_f g_s T_1 \frac{1 - \lambda^2 E^2}{\lambda E} \int_0^\infty d\sigma + \\ & + \frac{6N}{c} T_5 \sqrt{1 - \lambda^2 E^2} \int_0^\infty \Omega_4 R^4 dR + \\ & + NT_1 \sqrt{1 - \lambda^2 E^2} \int_0^\infty dR - \Delta\xi. \end{aligned} \tag{9}$$

In this equation, $T_5 = T_1 / (2\pi l_s)^4$ and we can interpret the four terms as follows; the first term is the energy of N_f strings and the second is the energy of $6N/c \approx n$ (for large N) D5-branes and the third is of N D-strings running out radially across D5-brane world volume and the last term is a binding energy

$$\begin{aligned} \Delta\xi = & 2NT_1 \sqrt{1 - \lambda^2 E^2} \times \\ & \times \int_0^\infty du u^4 \left(1 + \frac{1}{2u^4} - \sqrt{1 + \frac{1}{u^4}} \right) \\ & \approx 1.0102 T_1 l_s N c^{\frac{1}{4}} \sqrt{1 - \lambda^2 E^2}. \end{aligned} \tag{10}$$

This equation shows that the lowest energy is gotten more lowest as the value of electric field is more important.

The equation (6) can be solved in the dyonic case by considering various limits. For small R , the physical radius of the fuzzy funnel solution (5) is found to be

$$R(\sigma) \approx \frac{\lambda \sqrt{c}}{2\sqrt{2} \sqrt{1 - \lambda^2 E^2} \sigma} \tag{11}$$

and for large R the solution is

$$R(\sigma) \approx \left(\frac{\lambda^2 c}{\sqrt{18} \sqrt{1 - \lambda^2 E^2} \sigma} \right)^{\frac{1}{3}} \tag{12}$$

with an upper bound on the electric field $E < 1/\lambda$ for both cases.

According to equations (11) and (12), we remark that as the higher order terms in the BI action would effect a transition from the universal small R behavior to the ‘‘harmonic’’ expansion at large R (σ goes to zero). The effect we get at this stage when the electric field is turned on is that R is going up faster as σ goes to zero once E reaches approximately $1/2\lambda$ as shown in Fig. 1, and we are on D5-brane. It looks like the electric field increases the velocity of the transition from strings to D5-branes world volume. Also we remark that D5 brane got highest radius once E close to its critical value.

The equations (9) and (12) give us the impression that the presence of the electric field is an important phenomena; it decreases the low energy and makes the D5-brane more voluminous.

In the following sections, we include a perturbation in the D5-brane configuration by simply adding lower and higher order symmetric polynomials in the G^i to the matrix configuration. We study the spatial perturbations of the moving D1-branes as the electric field is switched on.

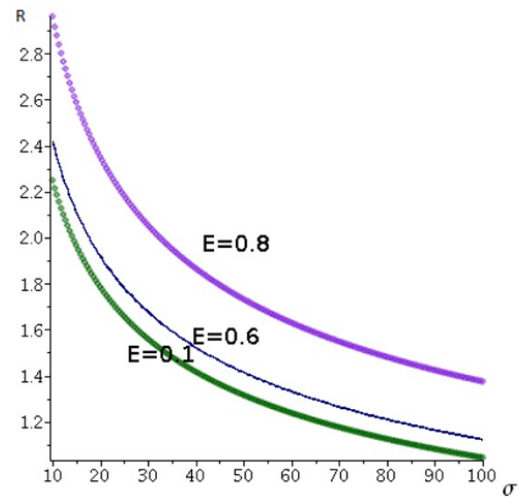


Fig. 1: Large radius.

3 Flat space

In this section, we examine the propagation of the perturbations on the fuzzy funnel by considering dyonic strings in flat background. We discuss the relative transverse perturbations which are transverse to the string, but parallel to the D5-brane world volume (i.e. along $X^{1,\dots,5}$). The overall transverse perturbations were studied in [13].

We give the relative transverse perturbations in the following form

$$\delta\phi^i(\sigma, t) = f^i(\sigma, t) I_N, \tag{13}$$

as zero mode with $i = 1, \dots, 5$ and I_N the identity matrix. By inserting this perturbation into the full (N, N_f) -string action (2), together with the funnel (6) the action is found to be

$$\begin{aligned} S \approx & -NT_1 \int d^2\sigma \left[(1 - \lambda^2 E^2) A - \right. \\ & \left. - (1 - \lambda E) \frac{\lambda^2}{2} (f^i)^2 + \frac{(1 + \lambda E)\lambda^2}{2A} (\partial_\sigma f^i)^2 + \dots \right] \end{aligned} \tag{14}$$

with

$$A = \left(1 + \frac{4R(\sigma)^4}{c\lambda^2} \right)^2. \tag{15}$$

Then, in large and fixed n the equations of motion are

$$\left(\frac{1 - \lambda E}{1 + \lambda E} \left\{ 1 + \frac{n^2 \lambda^2}{16(1 - \lambda^2 E^2)^2 \sigma^4} \right\}^2 \partial_\tau^2 - \partial_\sigma^2 \right) f^i = 0. \tag{16}$$

Let’s suggest that

$$f^i = \Phi(\sigma) e^{-i\omega\tau} \delta\lambda^i,$$

in the direction of δx^i with Φ is a function of σ and the equations of motion become

$$\left(-\frac{1 - \lambda E}{1 + \lambda E} \left(1 + \frac{n^2 \lambda^2}{16(1 - \lambda^2 E^2)^2 \sigma^4} \right)^2 w^2 - \partial_\sigma^2 \right) \Phi = 0 \quad (17)$$

which can be rewritten as

$$\left(-\frac{1 - \lambda E}{1 + \lambda E} \left(\frac{n^2 \lambda^2}{8(1 - \lambda^2 E^2)^2 \sigma^4} + \frac{n^4 \lambda^4}{16^2(1 - \lambda^2 E^2)^4 \sigma^8} \right) w^2 - \partial_\sigma^2 \right) \Phi = \frac{1 - \lambda E}{1 + \lambda E} w^2 \Phi. \quad (18)$$

Since the equation looks complicated, we simplify the calculations by dealing with asymptotic analysis; we start by the system in small and then large σ limits.

3.1 Small σ region

In this region, we see that σ^8 dominates and the equation of motion is reduced to

$$\left(-\partial_\sigma^2 + V(\sigma) \right) \Phi = \frac{1 - \lambda E}{1 + \lambda E} w^2 \Phi \quad (19)$$

for each direction δx^i , with the potential

$$V(\sigma) = -\frac{w^2 n^4 \lambda^4}{16^2(1 + \lambda E)^5(1 - \lambda E)^3 \sigma^8}. \quad (20)$$

The progress of this potential is shown in Fig. 2; when we are close to the D5-brane the potential is close to zero and once E is turned on it gets negative values until E is close to its maxima, we see this potential goes down too fast to a very low amplitude minima ($-\infty$). This phenomenon should have a physical meaning! This could be thought as a kink to increase the Φ 's velocity to push the perturbation to disappear.

To solve (19), we consider the total differential on the perturbation. Let's denote $\partial_\sigma \Phi \equiv \Phi'$. Since Φ depends only on σ we find $\frac{d\Phi}{d\sigma} = \partial_\sigma \Phi$. We rewrite (19) in this form

$$\frac{1}{\Phi} \frac{d\Phi'}{d\sigma} = -w^2 \left[\frac{n^4 \lambda^4}{16^2(1 + \lambda E)^5(1 - \lambda E)^3 \sigma^8} + 1 \right]. \quad (21)$$

An integral formula can be written as follows

$$\int_0^{\Phi'} \frac{d\Phi'}{\Phi} = - \int_0^\sigma w^2 \left[\frac{n^4 \lambda^4}{16^2(1 + \lambda E)^5(1 - \lambda E)^3 \sigma^8} + 1 \right] d\sigma \quad (22)$$

which gives

$$\frac{\Phi'}{\Phi} = -w^2 \left[-\frac{n^4 \lambda^4}{16^2(1 + \lambda E)^5(1 - \lambda E)^3 \times 7\sigma^7} + \sigma \right] + \alpha. \quad (23)$$

We integrate again the following

$$\int_0^\Phi \frac{d\Phi}{\Phi} = - \int_0^\sigma d\sigma \times \left(w^2 \left[-\frac{n^4 \lambda^4}{16^2 7(1 + \lambda E)^5(1 - \lambda E)^3 \sigma^7} + \sigma \right] + \alpha \right). \quad (24)$$

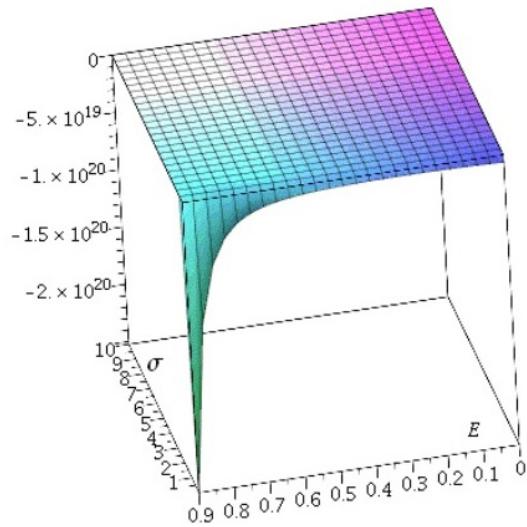


Fig. 2: Potential associated to the relative transverse perturbations in small region in flat space.

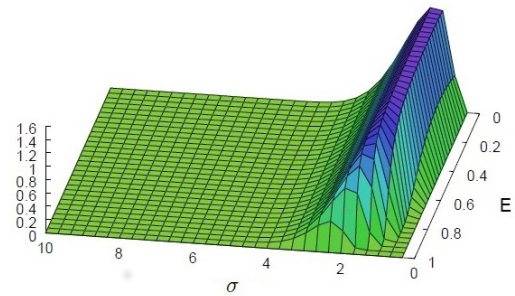


Fig. 3: Relative transverse perturbations in small region in flat space.

We get

$$\ln \Phi = -w^2 \left[-\frac{n^4 \lambda^4}{16^2 42(1 + \lambda E)^5(1 - \lambda E)^3 \sigma^6} + \frac{\sigma^2}{2} \right] + \alpha\sigma + \beta \quad (25)$$

and the perturbation in small σ region is found to be

$$\Phi(\sigma) = \beta e^{-w^2 \left[-\frac{n^4 \lambda^4}{16^2 42(1 + \lambda E)^5(1 - \lambda E)^3 \sigma^6} + \frac{\sigma^2}{2} \right] + \alpha\sigma} \quad (26)$$

with β and α are constants.

We plot the progress of the obtained perturbation. First we consider the constants $\beta = 1 = \alpha$, then the small spatial coordinate in the interval $[0, 10]$ with the unit of $\lambda = 1$, $w = 1$ and $n \approx 10^3$ with the electric field in $[0, 1]$.

As shown in Fig. 3, close to D5-brane there is perturbation. We remark that as E goes up, the perturbation goes down. And when $E \approx 1/\lambda$ we observe no perturbation effects.

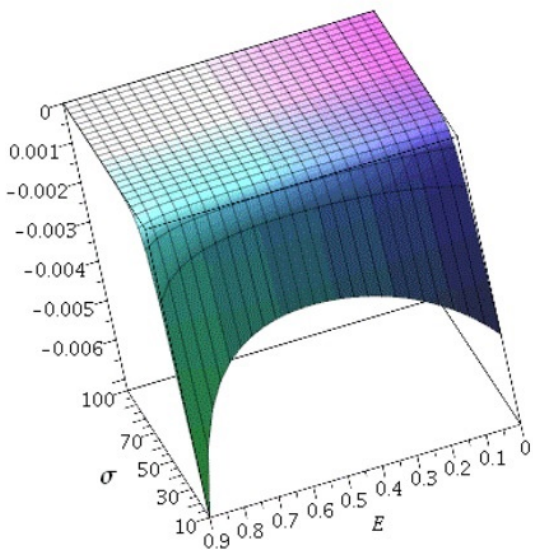


Fig. 4: Potential of relative transverse perturbations in large region in flat space.

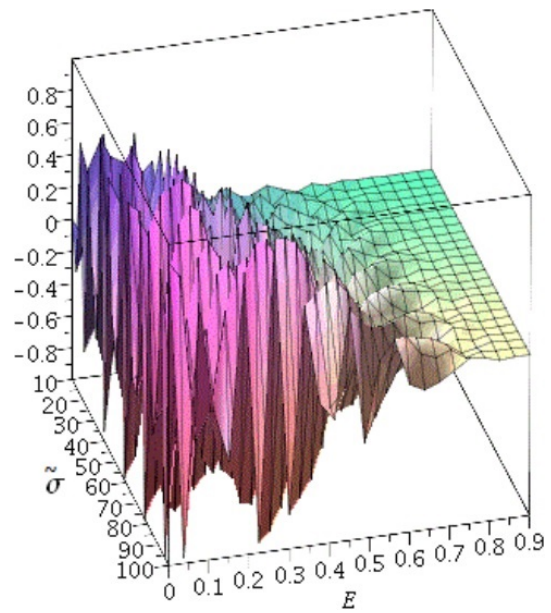


Fig. 5: Relative transverse perturbations in large region in flat space.

At this stage, according to (1) the string coupling gets strong $N_f g_s \gg 1$ which means the system background is changed. We know that with strong coupling the system should be in super-gravity background where the perturbations are no more. Consequently, the presence of E kills the perturbation and moves the system from flat to super-gravity background.

3.2 Large σ region

By considering large σ limit the equation of motion (18) becomes

$$(-\partial_\sigma^2 + V(\sigma))\Phi = \frac{1 - \lambda E}{1 + \lambda E} w^2 \Phi \tag{27}$$

with the potential

$$V(\sigma) = -\frac{w^2 n^2 \lambda^2}{8(1 + \lambda E)^3 (1 - \lambda E) \sigma^4} \tag{28}$$

By plotting the progress of this potential (Fig. 4) we remark that when σ goes faraway from the D5-brane the potential vanishes approximately for all values of the electric field. And close to D5-brane the potential gets negative values. The effect of E is very clear; as E goes up V slows down the decreasing until the medium of E , then V decreases too fast until its minimum value for E going up to its critical value.

Consequently, the electric field has the same effect on V in both regions of σ ; as E goes to its maxima V goes to its minima.

To solve (27) we rewrite it in the following form

$$\left(\partial_{\tilde{\sigma}}^2 + \frac{\kappa^2}{\tilde{\sigma}^4} + 1\right)\Phi = 0, \tag{29}$$

with

$$\tilde{\sigma} = \sqrt{\frac{1 - \lambda E}{1 + \lambda E}} w \sigma \tag{30}$$

and

$$\kappa^2 = \frac{n^2 \lambda^2}{8w^2(1 + \lambda E)(1 - \lambda E)^3} \tag{31}$$

Eq. (29) is a Schrödinger equation for an attractive singular potential $\propto \tilde{\sigma}^{-4}$ and depends on the single coupling parameter κ with constant positive Schrödinger energy. The solution is then known by making the following coordinate change

$$\chi(\tilde{\sigma}) = \int_{\tilde{\sigma}}^{\tilde{\sigma}} dy \sqrt{1 + \frac{\kappa^2}{y^4}} \tag{32}$$

and

$$\Phi = \left(1 + \frac{\kappa^2}{\tilde{\sigma}^4}\right)^{-\frac{1}{4}} \tilde{\Phi} \tag{33}$$

Thus, (29) becomes

$$(-\partial_\chi^2 + V(\chi))\tilde{\Phi} = 0 \tag{34}$$

with

$$V(\chi) = \frac{5\kappa^2}{\left(\tilde{\sigma}^2 + \frac{\kappa^2}{\tilde{\sigma}^2}\right)^3} \tag{35}$$

Then, the perturbation is found to be

$$\Phi = \left(1 + \frac{\kappa^2}{\tilde{\sigma}^4}\right)^{-\frac{1}{4}} e^{\pm i\chi(\tilde{\sigma})} \tag{36}$$

which has the following limit; since we are in large σ region $\Phi \sim e^{\pm i\chi(\tilde{\sigma})}$. This is the asymptotic wave function in the region $\chi \rightarrow +\infty$, while around $\chi \sim 0$, i.e. $\tilde{\sigma} \sim \sqrt{k}$ and $\sigma \sim n\lambda/2\sqrt{2}w^2(1-\lambda E)^2$, $\Phi \sim 2^{-\frac{1}{4}}$.

Owing to the plotting of the progress of this perturbation (Fig. 5), by considering the real part of the function, the perturbation solution is totally different from the one gotten in the small σ limit (26). Hence the perturbations have a discontinuity and the system is divided into two regions which implies Neumann boundary conditions and the end of an open string can move freely on the brane in the dyonic case, which means the end of a string on D5-brane can be seen as an electrically charged particle.

Fig. 5 shows that the perturbation is slowing down as E is turned on then starts to disappear once E reaches the value $1/2\lambda$. The perturbation disappears when E is too close to $1/\lambda$ for all values of σ . The effect of E is very surprising! The presence of E stops the perturbations.

No electric field means the intersecting point is in high perturbation. Then as E is turned on the perturbations decrease. When E is close to its critical value the perturbations are no more. They are killed by E . This phenomena matches very well with the fact that g_s becomes strong ($N_f g_s \gg 1$) at this point according to the relation (5) such that $E \approx 1/\lambda$. Consequently, we can suggest that the presence of the electric field changes the background of D-branes from flat to super-gravity background (where the string coupling is strong).

4 Curved space

We extend the investigation of the intersecting D1-D5 branes to curved space. We consider again the presence of electric field and the resulting configuration is a bound state of fundamental strings and D-strings. Under these conditions the bosonic part of the effective action is the non-abelian BI action

$$S = -T_1 \int d^2\sigma e^{-\phi} S Tr \left[-\det(P(G_{ab} + G_{ai}(Q^{-1} - \delta)^{ij}G_{jb} + \lambda F_{ab})) \det Q^{ij} \right]^{\frac{1}{2}} \quad (37)$$

with T_1 the D1-brane tension, G the bulk metric, (for simplicity we set the Kalb-Ramond two form B to be zero), ϕ the dilaton and F the field strength, $a, b = \tau, \sigma$ and $i, j = 1, 2, 3, 4, 5$. Furthermore, P denotes the pullback of the bulk space time tensors to each of the brane world volume. The matrix Q is given by $Q_j^i = \delta_j^i + i\lambda [\phi^i, \phi^k] G_{kj}$, with ϕ^i are the transverse coordinates to the D1-branes.

We consider the super-gravity background and the metric of n D5-branes

$$\begin{aligned} ds^2 &= \frac{1}{\sqrt{h}} \eta_{\mu\nu} dx^\mu dx^\nu + \sqrt{h} (d\sigma^2 + \sigma^2 d\Omega_3^2) \\ e^{-\phi} &= \sqrt{h} \\ h &= 1 + \frac{L^2}{\sigma^2} \end{aligned} \quad (38)$$

with $\mu, \nu = \tau, \sigma$ and $L = n l_s^2 g_s$.

4.1 Zero mode

In our work we treat E as a variable to discuss its influence on the perturbations. We investigate the perturbations in the super-gravity background of an orthogonal 5-brane in the context of dyonic strings growing into D5-branes. The study is focused on overall transverse perturbations in the *zero mode*; $\delta\phi^i = f^i(\tau, \sigma)I$, $i = 6, 7, 8, 9$ and I is $N \times N$ identity matrix.

The action describing the perturbed intersecting D1-D5 branes in the super-gravity background is

$$\begin{aligned} S &\equiv -NT_1 e^{-\phi} \int d^2\sigma \left[G_{\tau\tau} G_{\sigma\sigma} (1 + \lambda E) - \frac{\lambda^2}{2} (1 - \lambda^2 E^2) G_{\sigma\sigma} G_{ii} (f^i)^2 + \frac{\lambda^2}{2} (1 + \lambda E) G_{\tau\tau} G_{ii} (f^i)^2 + \dots \right] \\ &\equiv -NT_1 \int d^2\sigma \sqrt{h} \left[1 + \lambda E - \frac{\lambda^2 \alpha_i}{2h} (1 - \lambda^2 E^2) (f^i)^2 + \frac{\lambda^2 \sqrt{h} \alpha_i}{2} (1 + \lambda E) (f^i)^2 + \dots \right] \end{aligned} \quad (39)$$

where $h(\sigma) = e^{-2\phi} = 1 + L^2/\sigma^2$, $f^i = \partial_\tau f^i$, $(f^i)' = \partial_\sigma f^i$, $G_{\tau\tau} = h^{-1/2} G_{\sigma\sigma} = \sqrt{h} e^{-\phi}$ and $G_{ii} = \alpha_i$ with α_i some real numbers.

The equations of motion of the perturbations are found to be

$$\left(\frac{1 - \lambda E}{h^{3/2}} \partial_\tau^2 - \partial_\sigma^2 + \frac{L^2}{h\sigma^3} \partial_\sigma \right) f^i = 0. \quad (40)$$

If we consider $\tilde{\sigma}^2 = \sigma^2 + L^2$ the equations of motion become

$$\left(\frac{1 - \lambda E}{\sqrt{h}} \partial_\tau^2 - \partial_{\tilde{\sigma}}^2 \right) f^i(\tilde{\sigma}, t) = 0. \quad (41)$$

We define the perturbations as

$$f^i(\tilde{\sigma}, t) = \Psi(\tilde{\sigma}) e^{-i\omega\tau} \delta x^i \quad (42)$$

with δx^i ($i = 6, 7, 8, 9$) the direction of the perturbation and (41) becomes

$$\left(-w^2(1 - \lambda E) \frac{\tilde{\sigma}}{\sqrt{\tilde{\sigma}^2 - L^2}} - \partial_{\tilde{\sigma}}^2 \right) \Psi = w^2(1 - \lambda E) \Psi \quad (43)$$

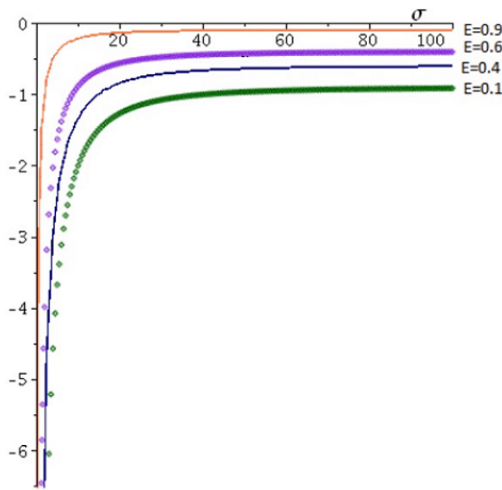


Fig. 6: Potential in curved space for zero mode.

with the potential

$$V = -w^2(1 - \lambda E) \frac{\tilde{\sigma}}{\sqrt{\tilde{\sigma}^2 - L^2}} = -w^2(1 - \lambda E) \frac{\sqrt{\sigma^2 + L^2}}{\sigma}.$$

Fig. 6 shows the variation of the potential V in terms of σ . We remark approximately the absence of the potential for all large values of σ and V goes to zero as E goes to $1/\lambda$. When σ is too close to zero, in this case V is negative and goes down too quick for all E and the potential is not that low. In addition, in the curved space the effect of E is approximately absent.

Let's solve the differential equation (43). As we see this is Heun's equation and the solution is the perturbation

$$\begin{aligned} \Psi = & (-\tilde{\sigma}^2 + L^2) \times \\ & \times \left[\eta \text{HeunC} \left(0, \frac{-1}{2}, 1, \frac{1}{4} w^2(1 - \lambda E)L^2, \frac{1}{2} + \right. \right. \\ & + \frac{1}{4} (-L^2 + L^2)w^2(1 - \lambda E), \tilde{\sigma}^2/L^2 \Big) + \\ & + \beta \text{HeunC} \left(0, \frac{1}{2}, 1, \frac{1}{4} w^2(1 - \lambda E)L^2, \frac{1}{2} + \right. \\ & \left. \left. + \frac{1}{4} (-L^2 + L^2)w^2(1 - \lambda E), \tilde{\sigma}^2/L^2 \right) \right] \tilde{\sigma} \end{aligned} \quad (44)$$

with η and β are constants.

We tried to plot the perturbation (44) for small region of σ (the radius of funnel solution is too large) and there is no perturbation in this region. The intersecting point is stable in super-gravity background even if the electric field is present.

Fig. 7 shows the variation of the perturbation in terms of the electric field E and the coordinate $\tilde{\sigma}$ in large region such that the radius of funnel solution is too small. We set $\lambda = 1$, $w = 1$ and $n = 10^2$. The perturbation is showing up as a peak

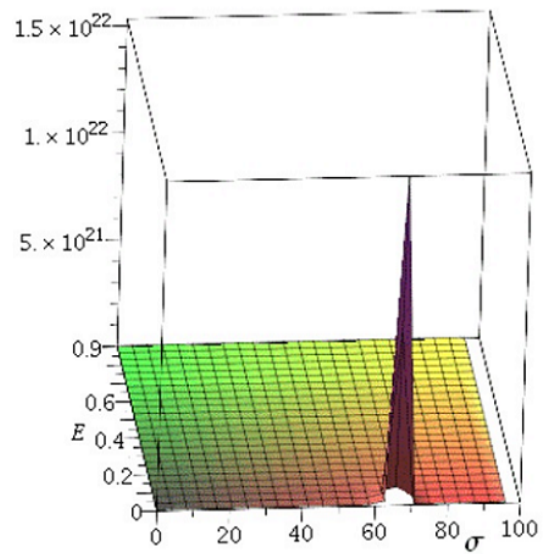


Fig. 7: Overall transverse perturbations in curved space for zero mode.

for a while and for low electric field. In general we observe approximately no perturbation effects for all E in this case.

The important remark we obtain by comparing the influence of E on the perturbation in flat and curved spaces is that E kills the perturbation in flat space (Fig. 3, Fig. 5) and turns the string coupling to be strong and then the flat space in this case becomes curved when E reaches its critical value, but when the space is already curved the influence of E is absent. This observation leads us to think that E is strongly related in some way to the super-gravity background.

4.2 Non-zero modes

Let's now consider the *non-zero modes*, the perturbations can be written in the form

$$\delta\phi^m(\sigma, t) = \sum_{\ell=1}^{N-1} \psi_{i_1 \dots i_\ell}^m G^{i_1} \dots G^{i_\ell}$$

and $\psi_{i_1 \dots i_\ell}^m$ are completely symmetric and traceless in the lower indices. We get two terms added to the action (39) to describe the present system $[\phi^i, \delta\phi^m]^2$ and $[\partial_\sigma \phi^i, \partial_t \delta\phi^m]^2$. Then in the equation of motion (40) these two terms $[\phi^i, [\phi^j, \delta\phi^m]]$ and $[\partial_\sigma \phi^i, [\partial_\sigma \phi^j, \partial_t^2 \delta\phi^m]]$ appeared. We have $\phi^i = RG^i$ and by straightforward calculations we have

$$\begin{aligned} [G^i, [G^j, \delta\phi^m],] &= \sum_{\ell < N}^{N-1} \psi_{i_1 \dots i_\ell}^m [G^i, [G^j, G^{i_1} \dots G^{i_\ell}]] \\ &= \sum_{\ell < N}^{N-1} \psi_{i_1 \dots i_\ell}^m \epsilon^{i_1 \dots i_\ell} G^{i_1} \dots G^{i_\ell}, \\ &= \sum_{\ell < N}^{N-1} 4\ell(\ell + \beta) \delta\phi_\ell^m \end{aligned} \quad (45)$$

with $\epsilon^{i_1 \dots i_\ell}$ antisymmetric tensor and β a real number. To obtain a specific spherical harmonic on 4-sphere, we have

$$[\phi^i, [\phi^i, \delta\phi_\ell^m]] = \frac{\ell(\ell + \beta)\lambda^2 c}{2(1 - \lambda^2 E^2)\sigma^2} \delta\phi_\ell^m, \tag{46}$$

$$[\partial_\sigma \phi^i, [\partial_\sigma \phi^i, \partial_\tau^2 \delta\phi_\ell^m]] = \frac{\ell(\ell + \beta)\lambda^2 c}{2(1 - \lambda^2 E^2)\sigma^4} \partial_\tau^2 \delta\phi_\ell^m.$$

Then for each mode we set $\delta\phi_\ell^m = f_\ell^m(\tilde{\sigma})e^{-i\omega\tau}\delta x^m$ with f_ℓ^m some function for each mode. Then the equations of motion will be in this form

$$(-\partial_{\tilde{\sigma}}^2 + V(\tilde{\sigma}))f_\ell^m(\tilde{\sigma}) = -w^2(1 - \lambda E)f_\ell^m(\tilde{\sigma}) \tag{47}$$

with $V(\tilde{\sigma}) = V_1 + V_2 + V_3$ and

$$V_1 = -w^2(1 - \lambda E) \frac{\tilde{\sigma}}{\sqrt{\tilde{\sigma}^2 - L^2}} = -w^2(1 - \lambda E) \frac{\sqrt{\sigma^2 + L^2}}{\sigma} \tag{48}$$

$$V_2 = \frac{\ell(\ell + \beta)\lambda^2 c}{2(\tilde{\sigma}^2 - L^2)} = \frac{\ell(\ell + \beta)\lambda^2 c}{2\sigma^2} \tag{49}$$

$$V_3 = \frac{\ell(\ell + \beta)\lambda^6 c w^2 \alpha^i \alpha^m}{24(1 - \lambda^2 E^2)(\tilde{\sigma}^2 - L^2)^2} = \frac{\ell(\ell + \beta)\lambda^6 c w^2 \alpha^i \alpha^m}{24(1 - \lambda^2 E^2)\sigma^4}. \tag{50}$$

These expressions can be treated by taking into account the limits of σ such as σ goes to zero and the infinity.

For small σ , V_3 dominates and in large σ , $V_1 + V_2$ will dominate. From now on, it is clear that the system in the present background will get different potentials and perturbations from region to other which support the idea of Neumann boundary condition in super-gravity background.

We start by small σ region, and the plot of V_3 (Fig. 8) shows that if σ goes to zero then the potential goes to $+\infty$. Physically this behavior should mean something! This could be a sign to the absence of the perturbation effects and the influence of E is absent.

We remark that the electric field does not have any influence on the perturbations in non-zero mode at the presence of the super-gravity background.

Then the perturbation for each mode ℓ is gotten (see (51) at the top of the next page) with b_1 and b_2 are constants and $d = \ell(\ell + \beta)\lambda^6 n(n + 1)\alpha^i \alpha^m w^2$. We tried to plot this function but noway we could not get any perturbation for the values $\lambda = 1, w = 1$ and for all $E, \ell > 4$ and $n > 1$ in the region $\sigma \in [0, 10]$.

Also the potential shows up with little values by comparison to the case of small region and for all E which means E does not change anything in the case of curved space.

Let's move to the large σ . As σ goes to infinity we see the potential goes to zero (Fig. 9) but when σ approaches the small σ region the potential goes up too quick and reaches the maximum value, approximately for all E . Then the electric field does not have influence on the behavior of the potential in curved space.

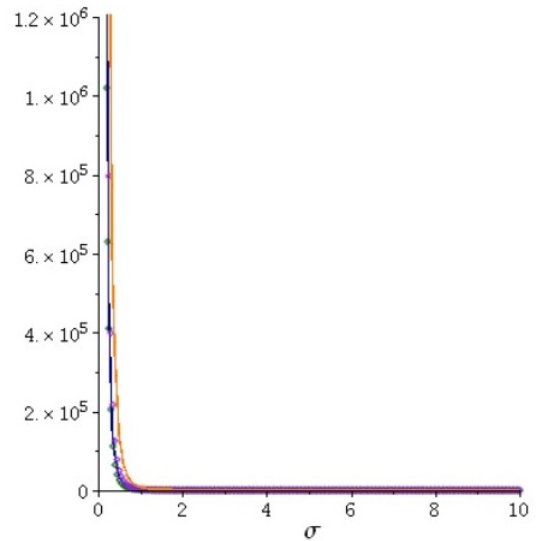


Fig. 8: Potential in curved space for non-zero mode for different values of E in small region.

The perturbation for each mode is (see (52)) with a_1 and a_2 are real constants. We tried to plot this function for all $E, \ell = 10$ and $n = 10^2$, and no perturbations appear which is consistent with the nature of space. Since the system is in super-gravity background, there is no perturbations then no influence of electric field.

5 Discussion and conclusion

In the low energy effective theory with the electric field E is switched on, we proved in [11] that the duality of intersecting D1-D3 branes is broken and in [12] the duality of intersecting D1-D5 branes is unbroken. Hence, it is interesting to know more about the effect of the electric field, and the intersecting D1-D5 branes looks more important as a system.

We consider the non-abelian Born-Infeld (BI) dynamics of the dyonic string such that the electric field E has a limited value. If we suppose there is no excitation on transverse directions then the action of D1-branes is

$$S = -NT_1 \int d^2\sigma \sqrt{1 - \lambda^2 E^2}.$$

The limit of E attains a maximum value $E_{max} = 1/\lambda$ just as there is an upper limit for the velocity in special relativity. In fact, if E is constant, after T-duality along the direction of E the speed of the brane is precisely λE so that the upper limit on the electric field follows from the upper limit on the velocity. Hence if this critical value arises such as $E_{max} > 1/\lambda$ the action ceases to make physical sense and the system becomes unstable. Since the string effectively carries electric charges of equal sign at each of its endpoints, as E increases the charges start to repel each other and stretch the string. For

$$\begin{aligned}
 f_\ell^m = & b_1 \text{HeunT} \left(\frac{-3 \cdot 2^{1/3} d (-1 + \lambda^2 E^2) (-1 + \lambda E)}{\lambda^2 (-d (-1 + \lambda^2 E^2))^{4/3}}, 0, \frac{\frac{1}{2} d \lambda^2 L^2 (-1 + \lambda^2 E^2) 2^{2/3}}{(-d (-1 + \lambda^2 E^2))^{2/3}}, \frac{12^{1/3} (-6d (-1 + \lambda^2 E^2))^{1/6} \lambda \tilde{\sigma}}{6} \right) \\
 & \exp \left(- \frac{\frac{1}{24} \lambda^3 \tilde{\sigma} \left(\frac{2}{3} \sqrt{-6d (-1 + \lambda^2 E^2)} \tilde{\sigma}^2 (-d (-1 + \lambda^2 E^2))^{2/3} + d L^2 2^{2/3} 12^{1/3} (-6 (-1 + \lambda^2 E^2))^{1/6} (-1 + \lambda^2 E^2) \right)}{(-d (-1 + \lambda^2 E^2))^{2/3}} \right) \\
 & + b_2 \text{HeunT} \left(\frac{-3 \cdot 2^{1/3} d (-1 + \lambda^2 E^2) (-1 + \lambda E)}{\lambda^2 (-d (-1 + \lambda^2 E^2))^{4/3}}, 0, \frac{\frac{1}{2} d \lambda^2 L^2 (-1 + \lambda^2 E^2) 2^{2/3}}{-d (-1 + \lambda^2 E^2)^{2/3}}, - \frac{12^{1/3} (-6d (-1 + \lambda^2 E^2))^{1/6} \lambda \tilde{\sigma}}{6} \right) \\
 & \exp \left(\frac{\frac{1}{24} \lambda^3 \tilde{\sigma} \left(\frac{2}{3} \sqrt{-6d (-1 + \lambda^2 E^2)} \tilde{\sigma}^2 (-d (-1 + \lambda^2 E^2))^{2/3} + d L^2 2^{2/3} 12^{1/3} (-6d (-1 + \lambda^2 E^2))^{1/6} (-1 + \lambda^2 E^2) \right)}{(-d (-1 + \lambda^2 E^2))^{2/3}} \right)
 \end{aligned} \tag{51}$$

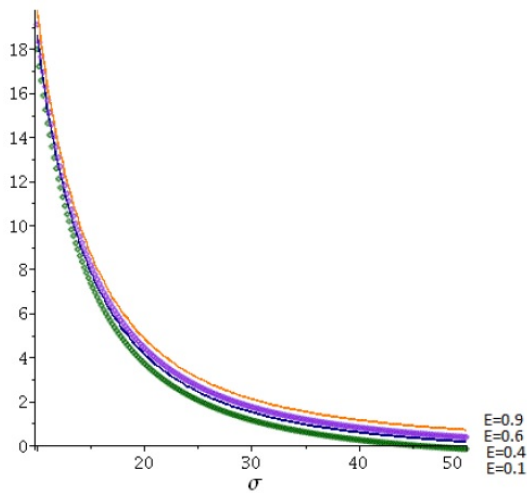


Fig. 9: Potential in curved space for non-zero modes in large region.

E larger than the critical value, the string tension T_1 can no longer hold the strings together.

In this context, we have treated in this project in particular the perturbations of a set of (N, N_f) -strings ending on a collection of n orthogonal D5-branes in lowest energy world volume theory. The fundamental strings ending on an orthogonal D5-branes act as an electric point sources in the world volume theory of D5-brane and the perturbations in both flat and curved spaces were studied from this point of view.

We showed in section 2 that the semi-infinite fuzzy funnel is a minimum energy configuration by imposing singular boundary conditions that have interesting physical interpretation in terms of D-brane geometries. And to consider the lowest energy effective theory the electric field should be present.

We found the lowest energy

$$\begin{aligned}
 \xi_{min} = & N_f g_s T_1 \frac{1 - \lambda^2 E^2}{\lambda E} \int_0^\infty d\sigma + \\
 & + \frac{6N}{c} T_5 \sqrt{1 - \lambda^2 E^2} \int_0^\infty \Omega_4 R^4 dR + \\
 & + N T_1 \sqrt{1 - \lambda^2 E^2} \int_0^\infty dR - \\
 & - 1.0102 T_1 l_s N c^{\frac{1}{4}} \sqrt{1 - \lambda^2 E^2}
 \end{aligned}$$

by considering E switched on in the low energy effective theory. The energy of intersecting D1-D5 branes is found to be a sum of four parts depending on the electric field E and all these energies are decreasing as E goes to $1/\lambda$. The first is for N_f fundamental strings extending orthogonally away from the D5-branes and the second for the n D5-branes and the third for the N D-strings extending out radially in D5-branes and the fourth is the binding energy.

In this theory, the transition between the universal behavior at small radius of the funnel solution and the harmonic behavior at large one in terms of electric field is mentioned too. When the electric field is turned on the physical radius of the fuzzy funnel solution $R(\sigma) \approx (\lambda^2 c / \sqrt{18} \sqrt{1 - \lambda^2 E^2} \sigma)^{\frac{1}{2}}$ is going up faster as σ goes to zero (the intersecting point) and E reaches approximately $1/2\lambda$ which looks like the electric field increases the velocity of the transition from strings to D5-branes world volume. Then D5-branes get highest radius once E is close to $1/\lambda$ which interprets the increasing of the volume of the D5-branes under the effect of the electric field (Fig. 1).

In section 3, we have investigated the relative transverse perturbations of the funnel solutions of the intersecting D1-D5 branes in flat space and the associated potentials in terms of the electric field $E \in]0, 1/\lambda[$ and the spatial coordinate σ . We find that too close to the intersecting point the potential is

$$\begin{aligned}
f_\ell^m = & a_1 \text{HeunC} \left(0, \frac{\sqrt{2w^2L^4(\lambda E - 1) + L^2 - 4\lambda^2cl(l + \beta)}}{2L}, -2, \frac{w^2L^2(\lambda E - 1)}{8}, \frac{5}{4} - \frac{w^2L^2(\lambda E - 1)}{8}, \right. \\
& \left. \frac{2\tilde{\sigma}^2 - 2\tilde{\sigma}\sqrt{\tilde{\sigma}^2 - L^2} - L^2}{L^2} \right) \left(\sqrt{\tilde{\sigma}^2 - L^2} + \tilde{\sigma} \right) \frac{L - \sqrt{2w^2L^4(\lambda E - 1) + L^2 - 4\lambda^2cl(l + \beta)}}{2L} \\
& + a_2 \text{HeunC} \left(0, -\frac{\sqrt{2w^2L^4(\lambda E - 1) + L^2 - 4\lambda^2cl(l + \beta)}}{2L}, -2, \frac{w^2L^2(\lambda E - 1)}{8}, \frac{5}{4} - \frac{w^2L^2(\lambda E - 1)}{8}, \right. \\
& \left. \frac{2\tilde{\sigma}^2 - 2\tilde{\sigma}\sqrt{\tilde{\sigma}^2 - L^2} - L^2}{L^2} \right) \left(\sqrt{\tilde{\sigma}^2 - L^2} + \tilde{\sigma} \right) \frac{L + \sqrt{2w^2L^4(\lambda E - 1) + L^2 - 4\lambda^2cl(l + \beta)}}{2L}
\end{aligned} \tag{52}$$

close to zero and once E is turned on it gets negative values until E is close to its maxima, we see this potential goes down too fast to a very low amplitude minima $-\infty$ (Figs. 2,4) and away from the intersecting point there is approximately no potential for all E . This is interpreted as inducing an increase in the velocity of the perturbation to disappear at the intersecting point toward the D5-brane world volume. Figs. 3,5 show that when E goes to its maxima there is no perturbation effects. Hence the presence of E kills in general the perturbations. At this stage, according to (1) the string coupling starts to get strong which means the system background is changing.

In curved space, we have studied the same system by looking for the effect of electric field on the perturbations and the associated potentials in zero (Figs. 6,7) and non zero-modes (Figs. 8,9) of the overall transverse perturbations in section 4. It was surprisingly that too close to the intersecting point; i.e. at large physical radius of D5-brane, we could not find any perturbation and also there is approximately no influence of E on potentials. The effect of E appears only when we are too far away from the intersecting point where the radius is too small and still E makes the perturbations to disappear on the strings. In general we do not see the influence of E in curved space.

The main and very important feature we got from this investigation is the following; the presence of electric field flux on the strings changes the background of the system. We proved explicitly that when the coupling is going to be strong which means E goes to its critical value we should move to QFT to describe the system where no perturbations exist. In curved space the influence of the electric field appears for too small radius of funnel solution which means for large spatial coordinate σ of strings and this phenomena decreases from zero mode to non-zero modes but when the radius is important as σ goes to zero there is no effect of E . By contrast in the case of flat space that was very clear when E is turned on the perturbations change their behavior in general. E forces

them to disappear as it is close to the critical value and in meantime the string coupling is getting strong.

The string coupling is strong means $N_f g_s \gg 1$ and $g_s \approx N/N_f$ since $E \approx 1/\lambda$ which is the critical value and if the electric field exceeds this value the system will be non-physical phenomena as discussed above and to be out of this problem we should choose another theory to describe our system.

In the case of weak coupling $N_f g_s \ll 1$ the electric field will be approximately $E \approx N_f g_s / \lambda N$ and the condition matches our perturbative phenomena $E \in [0, 1/\lambda]$. We mention here that if E goes to zero then $N_f g_s$ does too which means the number of fundamental strings decreases and simply the endpoints of the strings loose their electric charges and vice-versa.

In curved space, we can say the electric field E has no effect on the intersecting point. We can connect then the phenomena to the electric field E and the string coupling g_s such as E and g_s are connected by the relation (5). We see that once E is turned on and goes up g_s is getting stronger. At the critical point, E reaches its maxima and g_s is strong then the space should become curved. Hence we can remark at this stage that the effect of E looks like it transforms the flat space to curved one. In this context we can say there is a one-to-one map between the super-gravity background and the electric field that we should look for!

Acknowledgements

The author would like to thank the Abdus Salam International Center for Theoretical Physics, Trieste, for the invitation and the hospitality during the stage in which this paper was done.

Received on February 18, 2017

References

1. Polchinski J. Tasi Lectures on D-branes. arXiv: hep-th/9611050; Leigh R. *Modern Physics Letters A*, 1989, v. 4, 2767.
2. Callan C. G. and Maldacena J. M. *Nuclear Physics B*, 1998, v. 513, 198. arXiv: hep-th/9708147; Bhattacharyya R. and Douari J. *Journal of High Energy Physics*, 2005, v. 12, 012.

3. Brecher D., *Physics Letters B*, 1998, v.442, 117; Cook P., De Mello Koch R. and Murugan J. *Physics Review D*, 2003, v. 68, 126007. arXiv: hep-th/9804180. arXiv: hep-th/0306250; Constable N. R., Myers R. C. and Tafjord O. *Physics Review D*, 2000, v. 61, 106009. arXiv: hep-th/9911136.
4. Lee S., Peet A. and Thorlacius L. *Nuclear Physics B*, 1998, v. 514, 161. arXiv: hep-th/9710097; Kastor D. and Traschen J. *Physics Review D*, 1999, v. 61, 024034. arXiv: hep-th/9906237.
5. Constable N. R., Myers R. C., Tafjord O. *Physics Review D*, 2000, v. 61, 106009. arXiv: hep-th/9911136; Myers R. C. *Classical Quantum Gravity*, 2003, v. 20, S347–S372. arXiv: hep-th/0303072.
6. Gibbons G. W. *Nuclear Physics B*, 1998, v. 514, 603. arXiv: hep-th/9709027; Howe P. S., Lambert N. D. and West P. C. *Nuclear Physics B*, 1998, v. 515, 203. arXiv: hep-th/9709014; Banks T., Fischler W., Shenker S. H. and Susskind L. *Physics Review D*, 1997, v. 55, 5112. arXiv: hep-th/9610043; Kabat D. and Taylor W. *Advances in Theoretical and Mathematical Physics*, 1998, v. 2, 181. arXiv: hep-th/9711078; Rey S. arXiv: hep-th/9711081; Myers R. C. *Journal of High Energy Physics*, 1999, v. 9912, 022. arXiv: hep-th/9910053.
7. Constable N. R., Myers R. C. and Tafjord O. *Physics Review D*, 2000, v. 61, 106009. arXiv: hep-th/9911136.
8. Bhattacharyya R. and De Mello Koch R. arXiv: hep-th/0508131; Papageorgakis C., Ramgoolam S., Toumbas N. arXiv: hep-th/0510144; Papageorgakis C., Ramgoolam S. *International Journal of Modern Physics A*, 2006, v. 21. arXiv: hep-th/0603239.
9. Douari J. *Physics Letters B*, 2007, v. 644, 83–87. arXiv: hep-th/0603037.
10. Thomas S., Ward J. *Journal of High Energy Physics*, 2006, v. 0611, 019. arXiv: hep-th/0602071; *Physics Review D*, 2005, v. 72, 083519. arXiv: hep-th/0504226v3.
11. Bhattacharyya R. and Douari J. *Journal of High Energy Physics*, 2005, v. 12, 012.
12. Douari J. *Physics Letters B*, 2007, v. 656, 233–242. arXiv: hep-th/0610156.
13. Douari J. *Nuclear Physics B*, 2009, v. 808, 592–612. arXiv: hep-th/0803.0065.
14. Castelino J., Lee S. and Taylor W. *Nuclear Physics B*, 1998, v. 526, 334. arXiv: hep-th/9712105.
15. Constable N. R., Myers R. C., Tafjord O. *Journal of High Energy Physics*, 2001, v. 0106, 023. arXiv: hep-th/0102080.
16. Gibbons G. W. *Nuclear Physics B*, 1998, v. 514, 603–639. arXiv: hep-th/9709027.
17. Tseytlin A. A. *Nuclear Physics B*, 1997, v. 501, 41. arXiv: hep-th/9701125; Tseytlin A. A. arXiv: hep-th/9908105; Myers R. C. *Journal of High Energy Physics*, 1999, v. 9912, 022. arXiv: hep-th/9910053.
18. Lee S., Peet A. and Thorlacius L. *Nuclear Physics B*, 1998, v. 514, 161. arXiv: hep-th/9710097; Constable N. R., Myers R. C. and Tafjord O. *Physics Review D*, 2000, v. 61, 106009. arXiv: hep-th/9911136.
19. Grosse H., Klimcik C. and Presnajder P. *Communications in Mathematical Physics*, 1996, v. 180, 429. arXiv: hep-th/9602115.
20. Savvidy K. G. and Savvidy G. K. *Nuclear Physics B*, 1999, v. 561, 117–124. arXiv: hep-th/9902023.

Configuration Mixing in Particle Decay and Reaction

Elsayed K. Elmaghraby

Experimental Nuclear Physics Department, Nuclear Research Center, Atomic Energy Authority, Cairo 13759, Egypt.
E-mail: e.m.k.elmaghraby@gmail.com

Recent controversy on the existence (versus non-existence) of variability in the observation of decay rate can be settled by considering mixing in decay configuration. Variability in decay rate was investigated based on the available information of beta decay rate data, solar neutrino flux, and energy distribution. Full systematic analysis of the oscillatory behavior was carried out. Based on the zero threshold energy for neutrino absorption in beta emitters, a model for configuration mixing between two distinct beta disintegration modes β^{ν} -disintegration (electron from neutrino interaction) and the β^{-} -disintegration (electron from natural decay) was proposed. The phenomenon of variability in beta decay rate was related to the possible exothermic neutrino absorption by unstable nuclei which, in principle, should include the whole range of flux energies involving flux with energy below the ^{71}Ga threshold at 0.23 MeV. These two disintegration modes occur independently and model for their apparent mixing rate was proposed. The configuration mixing between the two modes cause depletion of radioactive nuclei which is subject to change with seasonal solar neutrino variability. Ability to detect this variability was found to be dependent on the Q-value of the β^{ν} disintegration and detection instrument setup. Value of neutrino cross section, weighted by the ratio between β^{ν} and β^{-} detection efficiencies, was found to be in the range 10^{-44} to 10^{-36} cm^2 . For experiments that uses the end point to determine the neutrino mass, interference due to mixing should be taken into account.

1 Introduction

Anomalous behavior in radioisotopes activity was reported by several scientists, they considered it as influence of solar proximity and activity. Several scientist are in favor of the influence of solar activity/distance on the decay rate. Early results of Alburger et al. [3] are based on normalizing the count rate ratio of $^{32}\text{Si}/^{32}\text{P}$ decay rate. Siegert et al. [34] had reported oscillatory behavior of ^{226}Ra , ^{152}Eu , and ^{154}Eu . Jenkins et al. [44] had studied these cases and reported several new data and measurements. Most investigator had reported seasonal relation between oscillatory behavior and the earth's position with respect to its sun's orbit; referring to the neutrino influence to the decay process.

Several other scientists oppose the connection between sun and the phenomenon. In one of the oppose thoughts, scientists may consider the rare neutrino events in experiments like Ice Cube and Sudbury Neutrino Observatory [2]; yet, the energy threshold of there detection system may not fall below ^{71}Ga border at 0.233 MeV (3.5-5 MeV for electron scattering [7], 1.44 MeV for $d(\nu_e, e)pp$ interaction.) In all measurements, no relation between half-life and the existence of this phenomenon was reported. Several other oppose reports, based on measurements by different techniques, were published, see Refs. [5, 8, 10, 11, 29].

In the present work, full systematic analysis and treatment of the oscillatory behavior was performed in order to reconcile these viewpoints. Based on the zero threshold energy for neutrino absorption beta emitters, a model for configuration

mixing between distinct β^{ν} -disintegration (the electrons from neutrino interaction) and the β^{-} -disintegration (the electrons from natural decay) was proposed.

2 Model for analysis

The majority of solar neutrino are with electron flavor associated with proton burn-up processes ($\phi_{\nu_e, pp} = 6 \pm 0.8 \times 10^{10} \text{ cm}^{-2} \text{ s}^{-1}$) with maximum energy around 0.41 MeV [1]. During solar flares protons stimulates production of pions / muons; π^+ (π^-) decays into ν_{μ} ($\bar{\nu}_{\mu}$) with μ^+ (μ^-), later partners decay and emit ν_e ($\bar{\nu}_e$) together with $\bar{\nu}_{\mu}$ (ν_{μ}) [30] total flux is of order $10^9 \text{ cm}^{-2} \text{ s}^{-1}$ and has energy up to 10 MeV.

Rare reaction of neutrino with stable isotopes is attributed to its small coupling with W^{\pm} and Z^0 bosons, and higher threshold of reaction kinematics. Coupling with Z^0 may be not appreciated due to non-existence of flavor changing neutral currents. If happened, an electron neutrino in the vicinity of the nucleus couples with a W boson emitting a β^{ν} and induces beta transformation in the nucleus. Threshold energy of neutrino capture in ^{37}Cl is about 0.813 MeV compared to 0.233 MeV in ^{61}Ga , these isotopes are used as monitor for ^8Be neutrinos. Radioactive isotopes, on the other hand, have excess energy to deliver due to positive Q-values as illustrated in Table 1. Hence, one can conclude that the solar influence on the *apparent* decay rate is associated mixing of specific mode of *disintegration* in consequence of neutrino capture in nuclei with the natural disintegration rate. The apparent decay rate of radioactive isotopes, λ' may be split into two terms; a term for usual disintegration of the nucleus labelled

λ_d and a terms for neutrino interaction. Presumably, neutral current will contribute to scattering only. β^- -decay rate is proportional to the matrix element of the decay, $|M_d|^2$ while the reaction terms are associated with matrix elements of neutrino interaction with charged current, $|M_{\nu W^\pm}|^2$.

$$N(t)\lambda' = N(t)\lambda_d + N(t) \sum_{\text{flavors}} \phi_\nu(t) N_N \langle K_{\beta^\nu}(Q) \rangle \sigma_{\nu n} \quad (1)$$

The summation is taken over all possible neutrino flavors. Here, $N(t)$ is the number of nuclei at time t , $\langle K(Q) \rangle$ is the factor representing the modification of nucleon properties in the nuclear medium, which can be investigated by nucleon induced nuclear reactions [12, 13]; $\langle K(Q) \rangle$ depends on the Q -value of the reaction and the state of the nucleus upon interaction. The in-medium neutrino cross section σ_ν can replace $\langle K(Q) \rangle \sigma_{\nu n}$.

The flux would be altered with the change in earth to sun distance R . Hence the time varying function is inversely proportional to the area of a sphere centered at sun. The radius vector has the form

$$R = a \frac{1 - \epsilon^2}{1 + \epsilon \cos(\theta)}, \quad \theta \approx \omega t. \quad (2)$$

Where ϵ is the eccentricity of earth's orbit (now, 0.0167 [35]) and the cosine argument is the angle relative to the distance of closest approach (2-4 January) in which value equals to $R = a(1 - \epsilon)$. $\omega = 2\pi/T_\omega$ is the average orbital velocity, and T_ω is the duration of earth's years in days. The approximate sign is introduced because earth's spend much more time at larger distance from the sun than in the near distances. Assuming that the average flux ($\phi_\nu^{(0)}$) occurs at time t_0 during the revolution around the sun, the flux at any other time will be

$$\phi_\nu(t) = \phi_\nu^{(0)} F(t), \quad (3)$$

$$F(t) = \frac{(1 + \epsilon \cos(\omega t))^2}{(1 + \epsilon \cos(\omega t_0))^2}. \quad (4)$$

Here, $\phi_\nu^{(0)}$ is the average flux of neutrinos reaching earth's surface (about $6.65 \times 10^{10} \text{ cm}^{-2}\text{s}^{-1}$ as average of all sun's producing routes [37], in which only $2.3 \times 10^6 \text{ cm}^{-2}\text{s}^{-1}$ are from ^8Be . Comparison between $F(t)$ (taking $t_0 = 0$) and normalized seasonal variation of ^8Be neutrons (data taken from Yoo et al. [46] and normalised to its yearly average) is represented in Fig. 1. $F(t)$ gives the averaged trend of Yoo et al. data within the experimental uncertainty of measurement.

For simplicity, and due to nature of available data of being related to oscillatory behavior, effect of cosmological neutrinos will be disregarded. Additionally, non-predominant radioactive isotopes should have the neutrino-induced beta disintegration of contribution much smaller than that of the β^- -decay; hence, λ_d can be replaced by the laboratory decay constant, λ , with good precision. The apparent decay rate for specific interaction current can be described by the formulae

$$\lambda' \Rightarrow \lambda + \phi_\nu^{(0)} N_N \sigma_\nu F(t). \quad (5)$$

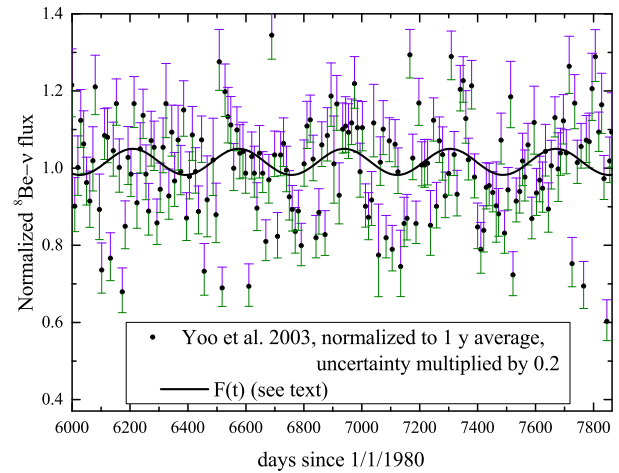


Fig. 1: Normalized measurements of ^8Be neutrino variation by Yoo et al. [46] in comparison with predictions of $F(t)$ function in Eq. 4.

Where, $\phi_\nu^{(0)}$, N_N , and $\sigma_\nu = \langle K \rangle \sigma_{\nu n}$ are related to the considered current and the disintegrated nucleus. Differential nuclear decay rate is simply described by the rate equation $dN(t)/dt = -N(t)\lambda'$. Upon integration, the number of survived nuclei become

$$N(t) = N(0) \exp\left(-\lambda t - \mu\left(1 + \frac{\epsilon^2}{2}\right)t\right) \times \exp\left(-2\epsilon\mu\left(1 + \frac{\epsilon}{4} \cos(\omega t)\right) \sin(\omega t)\right), \quad (6)$$

$$\mu = \frac{\phi_\nu^{(0)} N_N \sigma_\nu}{\omega (1 + \epsilon \cos(\omega t_0))^2}.$$

The first exponential represent the *depletion* of nuclei with neutrino interaction together with the radioactive decay. The second exponential can be represented as

$$1 + \sum_{i=1}^{\infty} \frac{(-1)^i}{i!} \left(2\epsilon\mu\left(1 + \frac{\epsilon}{4} \cos(\omega t)\right) \sin(\omega t)\right)^i. \quad (7)$$

The value of $2\epsilon\mu \ll 1$; hence, only the first term in the summation is effective. I.e.,

$$N(t) = e^{-\lambda t - \mu\left(1 + \frac{\epsilon^2}{2}\right)t} \left(N(0) - A\left(1 + \frac{\epsilon}{4} \cos(\omega t)\right) \sin(\omega t)\right), \quad (8)$$

which reveal seasonal variability. The amplitude of the oscillation is $A = 2N(0)\epsilon\mu$ with the depletion factor $\exp\left(-\lambda t - \mu\left(1 + \frac{\epsilon^2}{2}\right)t\right)$; depletion factor reaches unity for long-lived isotopes with relative short-term measurements.

The method of normalization of data, mentioned in context, is intended to remove the effect of isotope decay rate and give the residual of neutrino interaction. So, when normalized to 1, the normalized fraction (proportional to decay rate or detector count) becomes

$$\overline{N(t)} = \left(1 - A e^{-\lambda t} e^{-\mu\left(1 + \frac{\epsilon^2}{2}\right)t} \left(1 + \frac{\epsilon}{4} \cos(\omega t)\right) \sin(\omega t)\right). \quad (9)$$

Similarly, for normalization of the ratio between two isotope 1 and 2,

$$\frac{\overline{N_{1/2}(t)}}{N_2(0)} \approx 1 - 2 \frac{N_1(0)}{N_2(0)} e^{-(\lambda_1 - \lambda_2)t} e^{-(\mu_1 - \mu_2)\left(1 + \frac{\epsilon}{2}\right)t} \times \frac{\epsilon \mu_1 \left(1 + \frac{\epsilon}{4} \cos(\omega t)\right) \sin(\omega t)}{1 - 2\epsilon \mu_2 \left(1 + \frac{\epsilon}{4} \cos(\omega t)\right) \sin(\omega t)}. \quad (10)$$

Which is not a complete sinusoidal variation. The amplitude and depletion factors in case of two activity ratio becomes

$$A_{1/2} = 2 \frac{N_1(0)}{N_2(0)} \frac{\epsilon \mu_1}{1 - 2\epsilon \mu_2} e^{-(\lambda_1 - \lambda_2)t} e^{-(\mu_1 - \mu_2)\left(1 + \frac{\epsilon}{2}\right)t}. \quad (11)$$

This depletion term can be ignored if both isotopes have comparable half-life and mass.

3 Discussion

Normalized oscillatory data, were collected for the decay of isotopes given in Table 1. Because we need to have a starting point, data retrieved relative to 1 Jan. 1980. The time shift, t_0 , was obtained using least square fitting of every data set with Eq. 9 by shifting time with free parameter—say t_1 . Results are illustrated in Table 1 in which a shift of $-120 \pm 14(1\sigma\text{-stat.}) \pm 5(1\sigma\text{-syst.})$ days was found; i.e. the average flux received on earth from the sun occurs around end of October (or, alternatively, May first.) This is consistent with data given in measurement of ^8Be neutrino variation by Yoo et al. [46].

Before going further in the discussion, we must apprehend measurement techniques and circumstance of each experiment. The correlation between earth sun distance and decay rate for ^{32}Si and ^{226}Ra was reported by Jenkins et al. [17] based on Alburger et al. [3] and Siegert et al. [34]; those measurements are based on the β spectrum measurements. Alburger and coworkers used end-window gas-flow proportional counter system and a liquid/plastic scintillation detectors and Siegert and coworkers used both 4π ionization chamber and Ge and Si semiconductor detectors with reference to ionization chamber measurements. Same group of Ref. [17] and others in later work [24] had measured the ^{54}Mn using the 834.8 keV γ -line during 2 years without significant seasonal variation, they only report a connection with solar storm. Similar results appeared after solar flare [16]. Variation of ^{36}Cl decay rate was reported by BNL group [18] using Geiger-Müller counter and in PTB-2014 measurements [22] using the triple-to-double coincidence ratio liquid scintillation counting system. PTB-2014 detection system excluded the idea of time varying decay rate while the BNL measurements prove the phenomenon. Power spectrum analysis [15, 18, 20, 26, 40, 43] reveal several spectral frequencies especially at 1 y^{-1} . Some explanations of seasonal variation of decay rate were related to decoherence in gravitational field [36] and internal sun modes [42]. An experiment was performed for ^{222}Rn decay in controlled environment showed

dependence on the angular emission of gamma ray [39] and daily behavior [9, 19, 44]; however Bellotti et al. [9] excluded the sun influenced decay rate in support with their earlier work [8]. Ware et al. [45] returned the variation to change in the pressure of counting chamber during the seasonal variation.

Opposition to the connection between sun's and the variability phenomenon of apparent decay rate came out as a consequence of measurements, as well. No significant deviations from exponential decay are observed in Cassini spacecraft power production due to the decay of ^{238}Pu [11]. Bellotti et al. [8] studied decay of ^{40}K , ^{137}Cs and ^{232}Th using NaI and Ge detectors with no significant effect of earth-sun distance. Same results had been reported by Alexeyev et al. [5] in the alpha decay of ^{214}Po measured by α -particle absorption. However, Stancil et al. [38] detected seasonal variation in the gamma transition in ^{214}Po due to ^{214}Bi decay in radium chain. Others [4] had reported seasonal variation in life time of ^{214}Po . Recently, Pommé et al. [29] re-performed measurements in several laboratories by all possible measurement techniques including ionisation chamber, HPGe detector, silicon detector, proportional counter, anti-coincidence counting, triple-to-double coincidence, liquid scintillation, CsI(Tl) spectrometer, internal gas counting. They returned the phenomenon to lower stability of instruments. Bikit et al [10] investigated the ^3H decay rate by measured by liquid scintillation and related the fluctuation of the high-energy tail of the beta spectrum to instrumental instability.

The techniques of measurements is different among these two parties. Among all measurements given above, all techniques that are based on detecting β -radiation, or combined β - γ -radiation coming from its daughter, had signaled variability. Which can be explained as a consequence of the mixing between β^+ and β^- disintegrations. In such case, both terms in Eq. 5 are effective and the apparent decay rate should be influenced by solar proximity and activity. On the other hand, techniques that uses specific decay parameter such as specific γ -line from β^+ - or α -decay may not be able to recorded any variability because the oscillatory part of configuration mixing in Eq. 5 is not operative. With pure α -emitters like ^{241}Am and ^{226}Ra , the mixing oscillatory term will change sign and time shift of half-period may appear. In accordance to Siegert et al. [34] results, time shift of a half period in the fluctuation measured between $4\pi\gamma$ -ionization chamber measurement of ^{226}Ra and measurements of $^{152,154}\text{Eu}$ by GeLi semiconductor detectors was found. Hence, both parties concluded existence or non-existence of the phenomenon based on their technique of measuring it. Each team draw the correct picture of his viewpoint; that is determined by whether the mixing part of Eqs. 5 and 9 were taken into account or not.

The β^+ energy spectrum should, in principle, reflects the energy distribution of neutrino and the structure of residual nucleus. In β^+ -decay, all energy of neutrino plus the major contribution of mass excess (Q-value) is transferred to the

Table 1: Data of seasonal variability of radioactive disintegration. Unit of $\xi\sigma_v$ is cm^2 , Q -value is calculated from AME2003 atomic mass evaluation [6] in the unit of MeV; t_1 is the time shift in days.

Isotope	Ref	$A \times 10^4$	$-t_1$	$\xi\sigma_v \times 10^{41}$	Q	E_{th}
^3H	[21, 27]	$5.29 \pm 2 \pm 6$	-10 ± 30	$1.8 \pm 0.4 \pm 2 \times 10^{-6}$	0.0186	0
^3H	[14]	$38.4 \pm 0.8 \pm 35$	138 ± 1	$13 \pm 0.1 \pm 12 \times 10^{-6}$	0.0186	0
^{32}Si	[3]	$10.8 \pm 2 \pm 5$	109 ± 12	$1.15 \pm 0.01 \pm 0.5 \times 10^{-3}$	0.2243	0
$^{32}\text{Si}/^{36}\text{Cl}$	[3, 15, 17]	$15.8 \pm 0.67 \pm 7$	126 ± 5			
^{36}Cl	[18]	$19 \pm 0.9 \pm 10$	160 ± 5	$4.52 \pm 0.01 \pm 2.4$	0.7097	0
^{152}Eu	[31, 32, 41]	$8.4 \pm 0.3 \pm 2$	113 ± 3	$3.51 \pm 0.01 \pm 0.79$	1.8197	0
^{154}Eu	[31, 32, 41]	$8.5 \pm 0.4 \pm 3$	121 ± 2	$8.7 \pm 0.004 \pm 3$	1.9688	0
^{214}Bi	[38]	$31 \pm 2 \pm 17$	119 ± 6	$39.7 \pm 0.02 \pm 22$	3.2701	0
^{214}Bi	[38]	$30 \pm 2 \pm 12$	118 ± 5	$38.5 \pm 0.02 \pm 15$	3.2701	0
^{85}Kr	[32, 41]	$7.2 \pm 0.35 \pm 1.5$	113 ± 3		0.687	0
^{90}Sr	[32, 41]	$8.8 \pm 0.4 \pm 2$	121 ± 3		0.546	0
^{108}Ag	[32, 41]	$8.6 \pm 0.3 \pm 2$	126 ± 2		1.76	0
^{133}Ba	[32, 41]	$6.18 \pm 0.6 \pm 4$	119 ± 5		-2.061	2.061
^{226}Ra	[15, 17]	$10.1 \pm 0.3 \pm 3$	105 ± 20	$83 \pm 0.02 \pm 20 \times 10^{-3}$	diverse	
^{226}Ra	[34]	$11.9 \pm 0.2 \pm 2$	125 ± 2	$99 \pm 0.01 \pm 20 \times 10^{-3}$	diverse	

beta particle. The higher the Q -value, the higher the energy of the emitted β^v . This is another source of disagreement among both teams supporting and declining the phenomenon. Observation of the phenomenon is determined by the ability of their system to detect β^v or the specific γ -transition or mass loss subsequent the disintegration. Detection volume, in general, is selective to a band of radiation energy. Ionization chamber detects gamma radiation and fraction of beta radiation above few hundreds eV [31]. Additionally, higher energy of β^v have higher value of detection efficiency. Counting of β^v , and β^- , and/or their corresponding γ -ray from nuclei, have different efficiencies due to difference in energy distribution and endpoint (c.f. [33]); literally, β^v has no end-point. Hence, each count rate must be related to its efficiency; i.e. the amplitude of the variation must be modified by a ratio—say ξ —between β^v counting efficiency and β^- counting efficiency; which depends on the β^v energy and the measurement setup. If variation occurs, it would be reflected on the counting rate. The value of $\xi\sigma_v$ represent a weighted cross section and it was calculated as a whole in Table 1.

The amplitude of the variability was obtained from each dataset by fitting using Eq. 9; results are represented in Table 1. The value of $N(0)$ (alternatively, mass or activity) was found for ^3H (assuming 1-20 g of $^3\text{H}_2\text{O}$ as for PTB measurements catalogue of activity standards [25]), ^{32}Si (0.0477 g of $^{32}\text{SiO}_2$ [3]), ^{36}Cl (0.4 μCi [22]), ^{152}Eu (40 MBq [31, 32, 41]), ^{154}Eu (2.5 MBq [31, 32, 41]), and ^{214}Bi (2 μCi [38]), see Table 1. Mass, activity, and/or number of decaying atoms were not reported for other datasets. Then, the value ($\xi\sigma_v$) are calculated only for the said isotopes. A plot for the variation of $\xi\sigma_v$ with Q -value is represented in Fig. 2. The known limit of

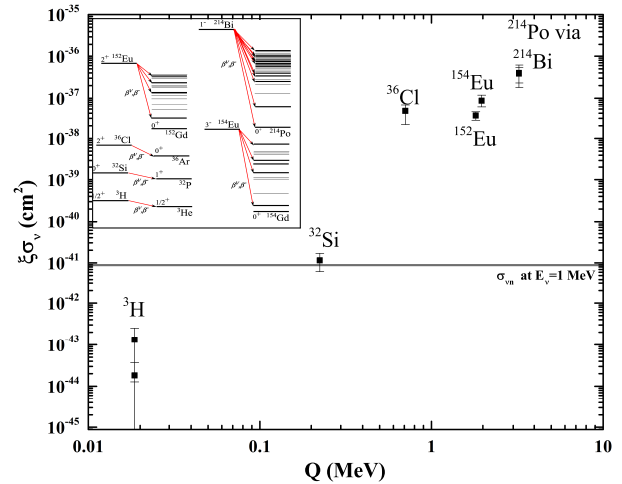


Fig. 2: Value of the reduced cross section $\xi\sigma_v$ in the unit of cm^2 in correlation with the Q -value of the possible β^v -disintegration. Line represent the value of $\sigma_{vn} = 0.881 \times 10^{-38} E_v (\text{GeV}) \text{cm}^2$ at $E_v = 1 \text{ MeV}$. Insert: possible disintegration probabilities of represented isotopes to levels in daughter nuclei.

ν_e -neutron cross section is $\sigma_{vn} = 0.881 \times 10^{-38} E_v (\text{GeV}) \text{cm}^2$ which is represented by the line in Fig. 2 for electron neutrino with $E_v = 1 \text{ MeV}$ considering $\xi = 1$. The increase of $\xi\sigma_v$ with Q -value confirms the mentioned hypothesis of existence of instrumental setting participation in the detection of the variability of apparent decay rate.

In the insert of Fig. 2, decay schemes of said isotopes are represented. The β^v spectrum is expected to have definite spectrum corresponding to direct transition to levels in daugh-

ter nuclei in similarity to neutrinoless double beta decay; one of the possible broadening that could occur is due to original energy distribution of neutrinos. Sensitive detector like KATRINE [23] can be used to detect such energy distribution in ${}^3\text{H}$; fortunately, neutrinoless double beta decay cannot occur in case of ${}^3\text{H}$ without fission of the whole nucleus. Disintegration of ${}^3\text{H}$, ${}^{32}\text{Si}$ and ${}^{36}\text{Cl}$ have single possible transition for both β^{ν} and β^{-} decays. The maximum energy of β^{ν} - ${}^3\text{H}$ decay is expected to be 0.42 MeV with $\xi\sigma_{\nu} = 1.82 \pm 0.4$ stat. ± 2 syst. $\times 10^{-44}$ cm² as calculated from Pomme et al. [27] data, and 13.2 ± 0.1 stat. ± 11 syst. $\times 10^{-44}$ cm² as calculated from Falkenberg [14] data. Systematic uncertainties are mostly related to unknown mass of the material. The BNL data of ${}^{226}\text{Ra}$ and other data of radium had been evaluated but was not represented in Fig. 2. ${}^{226}\text{Ra}$ has threshold for β^{ν} decay of 0.641 MeV, its daughters have possible beta decay probability, that is why variability can be observed [15, 17, 31, 32, 34, 41]. The phenomenon disappeared when α -detection system is used [28].

4 Conclusion

Rare mixed configuration between neutrino induced beta disintegration and natural beta disintegration may exist. These two distinct classes of beta decay could, in principle, explain the variation of apparent decay rate of radioactive isotopes with sun proximity. The circumstances of detection and instrumental ability determine whether to detect pure natural disintegration or the mixed mode. Configuration mixing between β^{ν} and β^{-} is, presumably, happen among all existing β^{-} emitters. The mixing in configuration of decay and reaction can be extended to all particles and nuclei. It must be taken into account in the in high precision measurements of neutrino mass. Mixing may be of significance for nucleosynthesis in astronomical object.

Received on April 26, 2017

References

- Abdurashitov J. N., Gavrin V. N., Gorbachev V. V., Gurkina P. P., Ibragimova T. V., Kalikhov A. V., Khairnasov N. G., Knodel T. V., Mirmov I. N., Shikhin A. A., Veretenkin E. P., Yants V. E., Zatsepin G. T., Bowles T. J., Elliott S. R., Teasdale W. A., Nico J. S., Cleveland B. T. and Wilkerson J. F. Measurement of the Solar Neutrino Capture Rate With Gallium Metal: III. Results for the 2002-2007 Data-Taking Period. *Physical Review C*, 2009, v. 80, 015807.
- Aharmim B. et al. Determination of the ν_e and Total ${}^8\text{B}$ Solar Neutrino Fluxes Using the Sudbury Neutrino Observatory Phase I Data Set. *Physical Review C*, 2007, v. 75, 045502.
- Alburger D., Harbottle G. and Norton E. Half-Life of ${}^{32}\text{Si}$. *Earth and Planetary Science Letters*, 1986, v. 78 (2-3), 168–176.
- Alexeyev E. N., Gavriljuk Y. M., Gangapshev A. M., Kazalov V. V., Kuzminov V. V., Panasenko S. I. and Ratkevich S. S. Results of a Search for Daily and Annual Variations of the ${}^{214}\text{Po}$ Half-Life at the Two Year Observation Period. *Physics of Particles and Nuclei*, 2016, v. 47, 986–994.
- Alexeyev E., Alekseenko V., Gavriljuk J., Gangapshev A., Gezhaev A., Kazalov V., Kuzminov V., Panasenko S., Ratkevich S. and Yakimenko S. Experimental Test of the Time Stability of the Half-Life of Alpha-Decay ${}^{214}\text{Po}$ Nuclei. *Astroparticle Physics*, 2013, v. 46, 23–28.
- Audi G., Wapstra A. H. and Thibault C. The AME2003 Atomic Mass Evaluation: (II). Tables, Graphs and References. *Nuclear Physics*, 2003, v. A729, 337.
- Bellini G. et al. Measurement of the Solar ${}^8\text{B}$ Neutrino Rate With a Liquid Scintillator Target and 3 MeV Energy Threshold in the Borexino Detector. *Physical Review D*, 2010, v. 82, 033006.
- Bellotti E., Brogгинi C., Carlo G. D., Laubenstein M. and Menegazzo, R. Search for Correlations Between Solar Flares and Decay Rate of Radioactive Nuclei. *Physics Letters*, 2013, v. B720, 116–119.
- Bellotti E., Brogгинi C., Carlo G. D., Laubenstein M. and Menegazzo R. Precise Measurement of the ${}^{222}\text{Rn}$ Half-Life: A Probe to Monitor the Stability of Radioactivity. *Physics Letters*, 2015, v. B743, 526–530.
- Bikit K., Nikolov J., Bikit I., Mrda D., Todorovic N., Forkapic S., Slivka J., and Veskovic M. Reinvestigation of the Irregularities in the ${}^3\text{H}$ decay. *Astroparticle Physics*, 2013, v. 47, 38–44.
- Cooper P. S. Searching for Modifications to the Exponential Radioactive Decay Law with the Cassini Spacecraft. *Astroparticle Physics*, 2009, v. 31(4), 267–269.
- Elmaghraby E. K. PHASE-OTI: A pre-equilibrium model code for nuclear reactions calculations. *Computer Physics Communications*, 2009, v. 180, 1694–1699.
- Elmaghraby E. K. Initial exciton configuration in (p,n) pre-equilibrium emission reactions. *Physical Review C*, 2008, v. 78, 014601.
- Falkenberg E. D. Radioactive decay caused by neutrinos? *Apeiron*, 2001, v. 8 (2), 32.
- Javorek II D., Sturrock P., Lasenby R., Lasenby A., Buncher J., Fischbach E., Gruenwald J., Hofst A., Horan T., Jenkins J., Kerford J., Lee R., Longman A., Mattes J., Morreale B., Morris D., Mudry R., Newport J., O'Keefe D., Petrelli M., Silver M., Stewart C. and Terry B. Power Spectrum Analyses of Nuclear Decay Rates. *Astroparticle Physics*, 2010, v. 34 (3), 173–178.
- Jenkins J. H. and Fischbach E. Perturbation of Nuclear Decay Rates During the Solar Flare of 2006 December 13. *Astroparticle Physics*, 2009, v. 31 (6), 407–411.
- Jenkins J. H., Fischbach E., Buncher J. B., Gruenwald J. T., Krause D. E. and Mattes J. J. Evidence of Correlations Between Nuclear Decay Rates and Earth-Sun Distance. *Astroparticle Physics*, 2009, v. 32 (1), 42–46.
- Jenkins J. H., Herminghuysen K. R., Blue T. E., Fischbach E., Javorek II D., Kauffman A. C., Mundy D. W., Sturrock P. A. and Talnagi J. W. Additional Experimental Evidence for a Solar Influence on Nuclear Decay Rates. *Astroparticle Physics*, 2012, v. 37, 81–88.
- Jenkins J. H., Mundy D. W. and Fischbach E. Analysis of Environmental Influences in Nuclear Half-Life Measurements Exhibiting Time-Dependent Decay Rates. *Nuclear Instruments and Methods in Physics Research A*, 2010, v. 620 (2-3), 332–342.
- Jenkins J., Fischbach E., Javorek II D., Lee R. and Sturrock P. Concerning the Time Dependence of The Decay Rate of ${}^{137}\text{Cs}$. *Applied Radiation and Isotopes*, 2013, v. 74, 50–55.
- Kossert K., Broda R., Cassette P., Ratel G. and Zimmerman B. Uncertainty Determination for Activity Measurements by Means of the TDCR Method and the CIEMAT/NIST Efficiency Tracing Technique. *Metrologia*, 2015, v. 52 (3), S172.
- Kossert K. and Nahle O. J. Long-Term Measurements of ${}^{36}\text{Cl}$ to Investigate Potential Solar Influence on the Decay Rate. *Astroparticle Physics*, 2014, v. 55, 33–36.
- Mertens S. Status of the KATRIN Experiment and Prospects to Search for keV-Mass Sterile Neutrinos in Tritium β -decay. *Physics Procedia*, 2015, v. 61, 267–273.

24. Mohsinaly T., Fancher S., Czerny M., Fischbach E., Gruenwald J., Heim J., Jenkins J., Nistor J. and O'Keefe D. Evidence for Correlations Between Fluctuations in ^{54}Mn Decay Rates and Solar Storms. *Astroparticle Physics*, 2016, v. 75, 29–37.
25. NIST. SRM 4927F - Hydrogen-3 water radioactivity standard. Accessed 3 Feb 2017, 2017.
26. O'Keefe D., Morreale B. L., Lee R. H., Buncher J. B., Jenkins J. H., Fischbach E., Gruenwald T., Javorek II D. and Sturrock P. A. Spectral Content of $^{22}\text{Na}/^{44}\text{Ti}$ Decay Data: Implications for a Solar Influence. *Astrophysics and Space Science*, 2013, v. 344 (2), 297–303.
27. Pomme S., Stroh H., Paepen J., Ammel R. V., Marouli M., Altitzoglou T., Hult M., Kossert K., Nahle O., Schrader H., Juget F., Bailat C., Nedjadi Y., Bochud F., Buchillier T., Michotte C., Courte S., van Rooy M. W., van Staden M. J., Lubbe J., Simpson B. R. S., Fazio A., Felice P. D., Jackson T. W., Wyngaardt W. M. V., Reinhard M. I., Golya J., Bourke S., Roy T., Galea R., Keightley J. D., Ferreira K. M., Collins S. M., Ceccatelli A., Verheyen L., Bruggeman M., Vodenik B., Korun M., Chisté V., and Amiot M.-N. On Decay Constants and Orbital Distance to the Sun—Part II: Beta Minus Decay. *Metrologia*, 2017, v. 54 (1), 19.
28. Pomme S., Stroh H., Paepen J., Ammel R. V., Marouli M., Altitzoglou T., Hult M., Kossert K., Nahle O., Schrader H., Juget F., Bailat C., Nedjadi Y., Bochud F., Buchillier T., Michotte C., Courte S., van Rooy M. W., van Staden M. J., Lubbe J., Simpson B. R. S., Fazio A., Felice P. D., Jackson T. W., Wyngaardt W. M. V., Reinhard M. I., Golya J., Bourke S., Roy T., Galea R., Keightley J. D., Ferreira K. M., Collins S. M., Ceccatelli A., Verheyen L., Bruggeman M., Vodenik B., Korun M., Chisté V., and Amiot M.-N. On Decay Constants and Orbital Distance to the Sun—Part I: Alpha Decay. *Metrologia*, 2017, v. 54 (1), 1.
29. Pommé S., Stroh H., Paepen J., Ammel R. V., Marouli M., Altitzoglou T., Hult M., Kossert K., Nähle O., Schrader H., Juget F., Bailat C., Nedjadi Y., Bochud F., Buchillier T., Michotte C., Courte S., van Rooy M., van Staden M., Lubbe J., Simpson B., Fazio A., Felice P. D., Jackson T., Wyngaardt W. V., Reinhard M., Golya J., Bourke S., Roy T., Galea R., Keightley J., Ferreira K., Collins S., Ceccatelli A., Unterweger M., Fitzgerald R., Bergeron D., Pibida L., Verheyen L., Bruggeman M., Vodenik B., Korun M., Chiste V. and Amiot M.-N. Evidence Against Solar Influence on Nuclear Decay Constants. *Physics Letters*, 2016, v. B761, 281–286.
30. Ryazhskaya O., Volkova L. and Zatsepin, G. Neutrinos from Solar Flares at the Earth. *Nuclear Physics - Proceedings Supplements* 2002, v. B110, 358–360.
31. Schrader H. Ionization Chambers. *Metrologia*, 2007, v. 44 (4), S53–S66.
32. Schrader H. Half-Life Measurements of Long-Lived Radionuclides—New Data Analysis and Systematic Effects. *Applied Radiation and Isotopes*, 2010 v 68 (7-8), 1583–1590.
33. Schrader H. Calibration and Consistency of Results of an Ionization-Chamber Secondary Standard Measuring System for Activity. *Applied Radiation and Isotopes*, 2000, v. 52 (3), 325–334.
34. Siegert H., Schrader H. and Schatzig U. Half-Life Measurements of Europium Radionuclides and the Long-Term Stability of Detectors. *Applied Radiation and Isotopes*, 1998, v. 49 (9-11) 1397–1401.
35. Simon J. L., Bretagnon P., Chapront J., Chapront-Touze M., Francou G. and Laskar J. Numerical Expressions for Precession Formulae and Mean Elements for the Moon and the Planets. *Astronomy and Astrophysics*, 1994, v. 282, 663–683.
36. Singleton D., Inan N. and Chiao R. Y. Neutrino Induced Decoherence and Variation in Nuclear Decay Rates. *Physics Letters*, 2015, v. A379 (12-13), 941–946.
37. Soler F., Froggatt C. and Muheim F. Neutrinos in Particle Physics, Astrophysics and Cosmology. Scottish Graduate Series. Taylor & Francis, 2008.
38. Stancil D. D., Yegen S. B., Dickey D. A. and Gould C. R. Search for Possible Solar Influences in Ra-226 Decays. *Results in Physics*, 2017, v. 7, 385–406.
39. Steinitz G., Kotlarsky P. and Piatibratova O. Observations of the Relationship Between Directionality and Decay Rate of Radon in a Confined Experiment. *The European Physical Journal Special Topics*, 2015, v. 224 (4), 731–740.
40. Sturrock P. A., Buncher J. B., Fischbach E., Gruenwald J. T., Javorek II D., Jenkins J. H., Lee R. H., Mattes J. J. and Newport J. R. Power Spectrum Analysis of Physikalisch-Technische Bundesanstalt Decay-Rate Data: Evidence for Solar Rotational Modulation. *Solar Physics*, 2010, v. 267 (2), 251–265.
41. Sturrock P. A., Fischbach E., and Jenkins J. Analysis of Beta-Decay Rates for Ag-108, Ba-133, Eu-152, Eu-154, Kr-85, Ra-226, and Sr-90, Measured at the Physikalisch-Technische Bundesanstalt from 1990 to 1996. *The Astrophysical Journal*, 2014, v. 794 (1), 42.
42. Sturrock P., Bertello L., Fischbach E., Javorek II D., Jenkins J., Kosovichev A. and Parkhomov A. An Analysis of Apparent R-Mode Oscillations in Solar Activity, the Solar Diameter, the Solar Neutrino Flux, and Nuclear Decay Rates, with Implications concerning the Sun's Internal Structure and Rotation, and Neutrino Processes. *Astroparticle Physics*, 2013, v. 42, 62–69.
43. Sturrock P., Parkhomov A., Fischbach E. and Jenkins J. Power Spectrum Analysis of LMSU (Lomonosov Moscow State University) Nuclear Decay-Rate Data: Further Indication of R-Mode Oscillations in an Inner Solar Tachocline. *Astroparticle Physics*, 2012, v. 35 (11), 755–758.
44. Sturrock P., Steinitz G., Fischbach E., Parkhomov A. and Scargle J. Analysis of Beta-Decay Data Acquired at the Physikalisch-Technische Bundesanstalt: Evidence of a Solar Influence. *Astroparticle Physics*, 2016, v. 84, 8–14.
45. Ware M. J., Bergeson S. D., Ellsworth J. E., Groesbeck M., Hansen J. E., Pace D. and Peatross J. Instrument for Precision Long-Term β -Decay Rate Measurements. *Review of Scientific Instruments*. 2015, v. 86 (7), 073505.
46. Yoo J. et al. Search for Periodic Modulations of the Solar Neutrino Flux in Super-Kamiokande-I. *Physical Review D*, 2003, v. 68, 092002.

Are Energy and Space-time Expanding Together?

Jacques Consiglio

52, Chemin de Labarthe. 31600 Labastidette. France. E-mail: Jacques.Consiglio@gmail.com

Assuming the universe has permanent critical density gives energy non-conservation, a linear increase of the universe total energy as a function of time. It enables to compute the universe densities of matter, dark matter, and dark energy as distinct effects of a unique source, where dark matter is stress. We show coherence with the Schwarzschild and the Schwarzschild-de Sitter solutions from which we compute the term Λ as geometrical effect of expansion. In this context, we show that MOND is consequence of the universe expansion and compute its parameter value and time evolution.

1 Introduction

This paper follows [1], where we find that energy “is” the universe expansion, and complements the analysis. But here we proceed from side-thinking: The next theory of gravity, if any, will have to recover the Einstein field equations (EFE). Therefore correlations between quantities considered independent in general relativity (GR), are instructive as to the object and contents of a better theory. Then in order to find new correlations we shall rely on a) the geometry of existing EFE solutions, and b) one coincidence which is critical density.

1.1 Coincidences

According to the Planck mission (PM) 2015 results [10], it seems that the universe has critical density:

$$\rho_T = \frac{3 H^2}{8\pi G}, \quad (1)$$

where G is Newton’s constant, and H the Hubble parameter. Note, with respect to [1], that we compute ρ_T from (1) instead of the total dark fields density. Taking $H = 1/T$, where T is the universe age and the distance to the cosmological event horizon $R_U = c T$, it also reads:

$$2 G = \frac{R_U c^2}{M_T}, \quad (2)$$

where $M_T c^2$ is the total energy of the observed universe. Then (1-2) uncovers a symmetry of the Schwarzschild solution:

$$\frac{R_s}{r} = \frac{R_U M}{M_T r}, \quad (3)$$

where gravity is the interaction of all energies of the observed universe; that is to say Mach’s principle. But (1) also reads:

$$M_T c^2 = \frac{P_p T}{2}, \quad (4)$$

which means that the energy of the observed universe grows linearly according to half the Planck power $P_p = c^5/G$. We see that the same equation (1) takes 4 forms which can be

given very large significance ranging from the simplest system (3) to cosmology (4) and the absence of a big bang. Now take the Bekenstein-Hawking area-entropy law:

$$S = \frac{K A c^3}{4 G \hbar}, \quad (5)$$

which states that the entropy S associated with an event horizon is its area A divided by $4G$ [2] [3] (where K and \hbar are Boltzmann and the reduced Planck constants respectively). It also applies to the de Sitter cosmological event horizon [4] seen at R_U :

$$S = \frac{4\pi K R_U^2 c^3}{4 G \hbar}. \quad (6)$$

Now injecting (1) in (6) gives:

$$\frac{\hbar}{K} \times \frac{S}{M_T c^2} = 2\pi T, \quad (7)$$

which means that the ratio between entropy S and energy $M_T c^2$ at any given epoch, “is cosmic time” – or the opposite, entropy is accumulation of action in the manner of an old de Broglie conjecture about the physical significance of $h S = K A$ which associates an action A and an entropy S to any piece of energy.

Using GR the probability for the “coincidence” (1) to be observed is about zero, there is not even a theoretical reason for the order of magnitude to ever come out; secondly (2) and (7) establish a simple, clear, and unexpected quantitative fit between gravity, cosmic time, energy, and entropy – where energy is not supposed to be. So maybe this is a big deal and we shall assume that (1) is not a coincidence but a law of nature ruling the universe expansion together with its energy.

Consider now the FLRW metric with a positive cosmological term and homogeneous density - that is to say the Λ CDM model. Assuming that (1) is not just a coincidence implies that it is valid at any epoch; then using (4) since the FLRW metric describes a simple 4-ball, we can slice it with 4-spheres centered at the origin, of radius r and thickness $2l_p$ (both along the light cone), and each slice adds an identical energy increment M_p , the non-reduced Planck mass, and it looks like the universe is a Planck power space-time generator.

The visible matter field exists “now” at the surface of the 4-sphere while M_T , as defined from R_U , is causal and occupies the light cone. Then a geometrical ratio exists between the two quantities, which evolve together. Simple integration gives $2\pi^2$ the 4-sphere surface coefficient and removing the “surface” we get the total dark field density ρ_D :

$$\rho_D = \rho_T \times \frac{2\pi^2}{1 + 2\pi^2} = 8.98 \times 10^{-27} \text{ kg m}^{-3}, \quad (8)$$

which agrees with PM results. The difference $\rho_V = \rho_T - \rho_D$ is the visible matter density and represents 4.82% of the total density ρ_T where the PM found 4.86 (8)%.

So, computing matter density ρ_V from geometry and (1) is totally abnormal in GR; we can even say irrelevant. But at the opposite, if those quantities *and others* are calculable, GR is incomplete and we can even say that it misses a fundamental point. In the remainder of this paper we shall analyze the consequences of (1) and (8) and check if nature agrees.

1.2 Premises

Noether’s theorem is the basis of conservation laws; it is used to evaluate energy conservation, and it works perfectly in quantum field theory. In GR, an area in which energy is assumed constant is defined by physical rods and clocks.

But how do we measure the rod? Essentially by decree of conservation. We define a-priori what a meter is and the postulate is that a rod does not evolve; up to now, there is no experimental results which is recognized to require any change to this postulate. But we cannot physically compare rods between distinct epochs. Even though GR studies the transfers of clocks and rods between distinct space-time locations, it assumes that no hidden source comes to expand its energy – and this is what (2) states: G is assumed constant, then the total energy M_T evolves in proportion of R_U , and we measure that the observable universe radius $R_U = c T$ grows.

It can be interpreted in different manners and we have to choose one that can be logically understood and requires minimal hypothesis. In the next sections we shall proceed from the four premises hereafter which were chosen appropriately, explaining how (2) physically works; we shall then use three EFE solutions to show coherence with existing theory and unexplained experimental data. Premises are:

- P1: The universe proceeds from the FLRW metric with cosmological term $\Lambda > 0$.
- P2: The observable matter field (particles) rests at the surface of a 4-sphere.
- P3: A mechanism exists inflating the 4-sphere and expanding masses and energy; both effects are simultaneous.

P4: The metric expansion includes inflation of the 4-sphere radius and a reduction of particles wavelengths; energy condenses permanently and progressively.

Those premises are easily justified:

- P1 agree with the best verified model, and
- P2 is direct consequences of the “coincidences”.
- P3 and P4 must be taken together; the feed mechanism in P3 could be just the radial expansion of a 4-ball in a preexisting 4-dimensional space filled with constant energy density. The sphere expands and masses increase reducing wavelengths; this is permanent and progressive condensation, hence P4.

2 The dark fields and the expansions

2.1 Expansion in the Schwarzschild solution

We first use the Schwarzschild solution to study the effects of (2) and expansion at different heights in the gravitational pit of a central mass M (the basic test case) and assume the system far away from other gravitational sources. With respect to (2), M_T is variable in time but constant in space ($M_T \sim T$), so M is also variable in time. At the opposite since gravitation is a retarded interaction, the metric in r is retarded and the Schwarzschild solution must be modified accordingly. Hence, using P3-P4, r and M (or R_s) expand; with respect to [1], introducing new ad-hoc parameters α, β to separate the effects of energy and space expansion, we write from (2):

$$\frac{R_s}{r} = \frac{R_U M}{M_T r} \rightarrow \frac{R_U M}{M_T r} \times \frac{1 - \alpha Hr/c}{1 + \beta Hr/c}. \quad (9)$$

Gravitation is retarded; a signal goes from M to r . Hence the correction at the numerator of (9) denotes that when the signal was emitted the mass M was lesser than expected in GR. Secondly, the additional delay we introduce comes from expansion. Then at the denominator, r “looks” advanced because the signal dilutes more than with a static r , and we expect $\beta = 1$. Second order limited development yields:

$$\frac{R_U M}{M_T r} \rightarrow \frac{R_U M}{M_T r} - (\alpha + \beta) \frac{M}{M_T} + \beta(\alpha + \beta) \frac{M r}{M_T R_U}. \quad (10)$$

Now examine this expression:

- The first term is nominal and now corresponds to a static field.
- The middle term cannot be seen negligible since it addresses identically all masses of the universe. It must be integrated to M_T , giving -1 which is the flat metric and it denotes its production; from (8), $\alpha + \beta = 2\pi^2$.
- Therefore the right hand term must also be integrated to M_T giving Hr/c , or a cosmological term Hc with unit of acceleration; and we find $\beta = 1$.

Note that we use a limited development in r so we cannot integrate to R_U , but we can still integrate to M_T as the middle term of (10) requires. Overall, after integration to M_T we get:

$$\frac{2GM}{rc^2} = \frac{R_U M}{M_T r} \rightarrow \frac{2GM}{rc^2} - 1 + \frac{r}{R_U}. \quad (11)$$

We shall now analyze this modified solution and show that the two new terms correspond to dark energy (DE) and dark matter (DM) – meaning exactly.

2.2 Dark energy and dark matter

The limited development above corresponds to a unique field that we split in three non-independent components. In [1], we analyzed the relations between the two new components; we showed that considering the first as an energy field X and the second as stress leads to:

$$M_{se(R)} c^2 = \frac{1}{2} \int_0^R (4\pi \rho_X r^2) (H_R c r) dr = \frac{3}{8} M_{X(R)} c^2,$$

where $M_{X(R)}$ is the energy of the field X in a 3-sphere of radius $R \ll R_U$, while $M_{se(R)} c^2$ is the stress given by the acceleration Hc , which is equivalent to a potential Hcr . (Note that in the integral energy is given by acceleration, then kinetic energy $p^2/2m$; thus the factor $1/2$.) Therefore:

$$\frac{M_{se(R)}}{M_{X(R)}} = \frac{3}{8} = 0.375, \quad (12)$$

which agrees with the ratio of DM to DE given by the PM:

$$\frac{\Omega_C}{\Omega_{DE}} = \frac{0.2589}{0.6911} = 0.3746, \quad (13)$$

and, since M_{se} is stress, identification is trivial; X is dark energy which creates stress interpreted as dark matter. Now we solve the system of equations and coincidences:

$$\rho_D = 2\pi^2 \rho_V = \frac{2\pi^2}{2\pi^2 + 1} \rho_T = \frac{11}{8} \rho_{DE} = \frac{11}{3} \rho_C. \quad (14)$$

It leaves no freedom or randomness in cosmological energies. In GR theory, those energy densities give four distinct effects:

- ρ_{DE} provides with a *decreasing* repelling force at the origin of expansion and then of the flat metric.
- ρ_C is stress due to the same repelling force; in the EFE stress comes in the stress-energy tensor, like mass, and then this result agrees with the Λ CDM model.
- ρ_V lies at the 4-sphere surface and non-homogeneity creates deviations to the flat metric.
- ρ_T is their sum and has critical density.

Each density finds its appropriate places in the EFE, and we can use M_T and R_U to replace G in the equations; we could compute $\Lambda = 8\pi G \rho_{DE}$ but we shall deduce it differently.

2.3 Λ and the CDM

In recent papers, [5–7] P. Marquet formally showed that a varying cosmological term restores in the EFE a conserved energy-momentum *true tensor* of matter and gravity with a massive source:

$$G^{\alpha\beta} = \frac{8\pi G}{c^4} [(T^{\alpha\beta})_{\text{matter}} + (t^{\alpha\beta})_{\text{gravity}}], \quad (15)$$

Here $(t^{\alpha\beta})_{\text{gravity}}$ includes a background field tensor which persists in the absence of matter:

$$(t^{\alpha\beta})_{\text{background}} = \frac{c^3}{8\pi G} \delta_{\beta}^{\alpha} (\Xi/2), \quad (16)$$

where $\Xi/2$ is the variation of cosmological constant Λ . As a result the de Sitter-Schwarzschild metric is slightly modified:

$$1 - \frac{R_s}{r} - \frac{\Lambda r^2}{3} \rightarrow 1 - \frac{R_s}{r} - \frac{\Lambda + \delta\Lambda}{3} r^2,$$

which we identify term to term with (11). But recall that the factor $1/3$ in this metric is given by integration, it is then irrelevant for a correspondence with a derivative. We also introduce a parameter k to solve:

$$k\Lambda + k\delta\Lambda \leftrightarrow -1 + \frac{r}{R_U}, \quad (17)$$

which means that since Λ is a constant, integration to R_U is now possible and will give the flat metric like in (11); then:

$$-k\Lambda \int_0^{R_U} r^2 dr = 1 \rightarrow k\Lambda = \frac{1}{3R_U^3}. \quad (18)$$

Then for any r we have $k\delta\Lambda(r) = -1/r^2$. Integrating the last term to the full solid angle (as stress), multiplying by $1/2$ for kinetic energy and identifying with Hr/c gives:

$$\begin{aligned} \frac{1}{2} \int 4\pi k\delta\Lambda(r) r^2 dr &= \int 2\pi k dr = \frac{Hr}{c} \\ \rightarrow k &= \frac{H}{2\pi c} = \frac{1}{2\pi R_U}, \end{aligned} \quad (19)$$

where k is also the ratio entropy/energy on the right-hand side of (7). Here it links the expansion of R_U (\sim energy) to that of DE ($\sim \Lambda$) through $2\pi R_U$. Now we have completed the correspondence and using (18) and (19) we get:

$$\Lambda = \frac{2\pi c}{3HR_U^3} = \frac{2\pi}{3R_U^2} = 1.229 \times 10^{-52} \text{ m}^{-2}. \quad (20)$$

The standard Λ CDM estimate is:

$$\Lambda \approx 1.19 \times 10^{-52} \text{ m}^{-2}, \quad (21)$$

and then our reasoning on energy expansion is appropriate. But we found that the dark field has a unique source since

$\rho_{DE} \rightarrow \rho_{DM}$; then extending the source unicity to ρ_V explains the difference between (20) and (21) as the share of dark energy invested at the surface, its share of ρ_V . Picking Λ in (20) and following the ratios in (8) and (14):

$$\frac{\Lambda}{1 + \frac{1}{2\pi^2} \times \frac{8}{11}} = 1.185 \times 10^{-52} \text{ m}^{-2}, \quad (22)$$

which is well within precision of (21); here the complimentary $3/11$ of ρ_V comes from stress (12) in agreement with (8) where ρ_V is the surface.

3 The classical field

As shown in [1], using the Bohr hydrogen model (or inspecting the Dirac equation), we find the effects of $Hc/2\pi$ when elementary particles mass increase linearly in time, and abusively computing with respect to a fixed frame:

$$\frac{da_0}{dt} = \frac{Hc}{2\pi\nu}, \quad (23)$$

where a_0 is the Bohr radius and ν the electron pulsation ($E = h\nu$). In quantum theory, distances like a_0 are quantized as the inverse of mass, but in gravity the classical force is given by a product of masses, which doubles the effect. Then in the very weak gravitational field the acceleration Hc gives measurable effects in the form of anomalous acceleration; in circular orbit it will be:

$$a_{Hc} = \frac{Hc}{2\pi} = 1.10 \times 10^{-10} \text{ m s}^{-2}, \quad (24)$$

like in (7) and (19). Then Newton's theory is no more the weak field limit of GR as it also needs $R_U \rightarrow \infty$. Now a_{Hc} is in range with Milgrom's modified Newton dynamics (MOND) limit acceleration [8, 9], which estimate is:

$$a_0 = 1.20 (\pm 0.2) \times 10^{-10} \text{ m s}^{-2}. \quad (25)$$

Then we shall recover MOND in the weak field/circular orbit problem. In the modified Schwarzschild solution in (11), the term Hc denotes that the classical potential is permanently becoming steeper. Then a_{Hc} has specific direction; it just amplifies the local Newton acceleration. The simple sum gives:

$$A = \frac{GM}{r^2} + a_{Hc}. \quad (26)$$

Applying a force to an object in free fall gives reaction, so denoting A_N the Newton acceleration we can write:

$$A_N \left(1 + \frac{a}{A_N}\right) \Rightarrow -a, \quad (27)$$

where $-a$ corresponds to the effect of inertia, as a reaction to a non-gravitational acceleration a when A_N and a are parallel. In GR this equation is given by the field transformation in

weak accelerations. Now denoting A_{eff} the effective acceleration in circular orbit we have $A_{eff} \Rightarrow 0$; meaning that it is A_{eff} that transforms the field, and not A_N . Then in order to link A_N , A_{eff} and A_{Hc} , we must write:

$$A_N = \frac{f}{m} = A_{eff} \left(1 + \frac{a_{Hc}}{A_{eff}}\right)^{-1}, \quad (28)$$

where, since (27) defines the field transformation, the denominator of the right-hand side formally removes a_{Hc} from A_{eff} and then recovers the Newton force. This equation is MOND simple interpolation function; needless to list the wide range of astrophysical data it fits. It is then a formal approximation of the modified Schwarzschild solution in (11). QED.

4 The Hubble parameter and accelerated expansion

The parameters $\alpha = 2\pi^2 - 1$ and $\beta = 1$ in (9), which values are deduced reasoning on (10), show that the contribution of space expansion to the metric is trivial ($\beta = 1$), and the contribution of mass expansion is $1/2\pi^2$. Therefore the observable r , which depends on massive clocks and rulers, expands more than simple space expansion. Then we can approximate the metric state at distance r from the observer with:

$$d\tau(r)^2 \approx d\tau(0)^2 \times \left(\frac{2\pi^2}{2\pi^2 + \frac{R_U - r}{R_U}}\right)^2. \quad (29)$$

Therefore, measurements of the Hubble parameter from the CMB spectrum ($r \rightarrow R_U$) will give a value different from and larger than $H = 1/T$; we find:

$$H = \frac{1}{T} \rightarrow H_{CMB}^0 = \frac{2\pi^2 H}{2\pi^2 + 1} = 67.53 \text{ km/s/Mpc}, \quad (30)$$

which agrees with the PM results:

$$H_{CMB}^0 = 67.74 \pm 0.46 \text{ km/s/Mpc}.$$

Eq. (29) gives other measurable effects:

- When measuring H^0 from baryon acoustic oscillations (BAO) for which T is also close to zero, the same discrepancy appears, $H_{BAO}^0 \approx H_{CMB}^0$ as shown in [10].
- At the opposite, $H = 1/T = 71.1 \text{ km/s/Mpc}$ is compatible with most recent Hubble space telescope data [11] taken from SN1A ($73.24 \pm 1.73 \text{ km/s/Mpc}$, currently valid at $\sim 2 - 3\sigma$), for which $r \rightarrow 0$.
- A simple plot shows that the denominator of (29) permanently gives the illusion of accelerating expansion.

Last, the symmetry in (1) is:

$$\lambda R_U = \text{const}, \quad (31)$$

where λ is the Compton wavelength of any piece of energy. Taking the universe mass and $\lambda_T = h/M_T c$ yields:

$$\lambda_T \frac{T}{2} = l_p t_p,$$

where l_p and t_p are the non-reduced Planck length and time respectively. It gives immediate significance to those units as they define the symmetry of the field expansion versus condensation. It denotes an inversion between spaces and times which reads:

$$\frac{T}{t_p} = \frac{2l_p}{\lambda_T}, \quad (32)$$

and a similar equation also applies to any mass. Hence the energy scales corresponding to l_p and t_p are epoch-relative like clocks and rulers, and also other Planck units (M_p , P_p). It just means that the laws of nature are constant but that the scale at which they apply vary in time.

It makes a big difference when thinking of quantum gravity which is expected to solve the big bang problem, because (32) is a symmetry linking the expansions of space-time and energy in a non-linear manner. To show this, from (32) and since energies increase, we find that at any given epoch:

$$R_U = c T_0 \int t_p/t, \quad (33)$$

where the quantum of time t_p replaces dt , and T_0 is a constant. Integration gives a logarithm which implies that the universe radius as observed from loopback time at any epoch, but assuming energy conservation, starts with inflation.

5 Conclusion

Overall, we found 9 strong correlations (*) giving distinct numerical results agreeing with unexplained experimental data in several domains of cosmology and astrophysics. We also find inflation for which a quantitative fit is out of reach, and the illusion of accelerating expansion. All come from a single assumption, a limited development, and classical solutions of the Einstein field equations.

The correlations above are totally irrelevant in GR, and also in QFT, but nature agrees at all scales. Hence the answer to the title is positive, and then GR and QFT miss the most important point which is that the expansion of space-time is identical to the expansion of energy. That is to say that space-time and energy are the same phenomenon. Importantly, all correlations are geometrical and all calculus use as input only one parameter, namely the universe age T , and natural constants G and c ; then the next theory uses geometry and has no free parameters.

Acknowledgements

Many thanks to Patrick Marquet for interesting discussions and for pointing to his results.

Received on April 29, 2017

*With (1), (8), (12–13), (19), (20), (23), (24–25), (28), and (30).

References

1. Consiglio J. Energy is the Expansion. *Progress in Physics*, 2017, v. 13 (2), 102–105.
2. Bekenstein J.D. Black Holes and Entropy. *Phys. Rev. D*, 1973, v. 7, 2333.
3. Hawking S.W. Particle Creation by Black Holes. *Commun. Math. Phys.*, 1975, v. 43, 199.
4. Gibbons G.W. and Hawking S.W. Cosmological Event Horizons, Thermodynamics, and Particle Creation. *Phys. Rev.*, 1977, v. D 15, 2738.
5. Marquet P. The Gravitational Field : A New Approach. *Progress in Physics*, 2013, v. 3, 62–66.
6. Marquet P. Vacuum Background Field in General Relativity. *Progress in Physics*, 2016, v. 12, 314–316.
7. Marquet P. Some Insights on the Nature of the Vacuum Background Field in General Relativity. *Progress in Physics*, 2016, v. 12, 366–367.
8. Milgrom M. A Modification of the Newtonian Dynamics as a Possible Alternative to the Hidden Mass Hypothesis. *Astrophysical Journal*, 1983, v. 270, 365–370.
9. Milgrom M. MOND Theory. arXiv: astro-ph/1404.7661v2.
10. The Planck Collaboration. Planck 2015 Results. I. Overview of Products and Scientific Results. arXiv: astro-ph/1502.01582.
11. Riess A. G., Macri L. M., Hoffmann S. L., Scolnic D., Casertano S., Filippenko A. V., Tucker B. E., Reid M. J., Jones D. O. A 2.4% Determination of the Local Value of the Hubble Constant. arXiv: astro-ph/1604.01424.

Using the SALI Method to Distinguish Chaotic and Regular Orbits in Barred Galaxies with the LP-VIcode Program

Lucas Antonio Caritá^{1,2,3}, Irapuan Rodrigues², Ivânio Puerari³ and Luiz Eduardo Camargo Aranha Schiavo²

¹Instituto Federal de Educação, Ciência e Tecnologia de São Paulo, IFSP, São José dos Campos, Brasil.

²Universidade do Vale do Paraíba, UNIVAP, São José dos Campos, Brasil.

³Instituto Nacional de Astrofísica, Óptica y Electrónica, INAOE, Puebla, México.

The Smaller Alignment Index (SALI) is a new mathematical tool for chaos detection in the phase space of Hamiltonian Dynamical Systems. With temporal behavior very specific to movements ordered or chaotic, the SALI method is very efficient in distinguishing between chaotic and regular movements. In this work, this method will be applied in the study of stellar orbits immersed in a gravitational potential of barred galaxies, once the motion of a test particle, in a rotating barred galaxy model is given by a Hamiltonian function. Using an analytical potential representative of a galaxy with bar (two degrees of freedom), we integrate some orbits and apply SALI in order to verify their stabilities. In this paper, we will discuss a few cases illustrating the trajectories of chaotic and regular orbits accompanied by the graph containing the behavior of SALI. All calculations and integrations were performed with the LP-VIcode program.

1 Introduction

One of the schemes more used to classify galaxies according to their morphology was proposed by Edwin Powell Hubble. Basically, the Hubble fork separates galaxies in two types: regular spirals (S) and barred spirals (SB). The galaxy bar, spiral arms and even galactic rings are structures that can be interpreted as disturbance to axisymmetric potential of the galactic disk.

In this work, we study the nature of some orbits immersed in analytical potentials with two degrees of freedom representing barred galaxies. In order to do this, we applied the Smaller Alignment Index (SALI) [9–13], which is a mathematical tool for distinguishing regular and chaotic motions in the phase space of Hamiltonian Dynamical Systems in analytical gravitational potentials. It is possible because the motion of a test particle in a rotating barred galaxy model is given by a Hamiltonian function.

The orbits integration and the SALI calculation were performed using the LP-VIcode program [2]. The LP-VIcode is a fully operational code in Fortran 77 that calculates efficiently 10 chaos indicators for dynamic systems, regardless of the number of dimensions, where SALI is one of them. To construct our barred galaxies models, two different sets of parameters were extracted from the paper of Manos and Athanassoula [5].

The main purpose of this paper is to show some regular and chaotic orbits, where the stability study was done using the SALI method. Such orbits were taken immersed in a mathematical model for the gravitational potential that simulates a barred galaxy in a system with two degrees of freedom.

2 Methodology

2.1 The SALI method

Considering a Hamiltonian flow (N degrees of freedom), an

orbit in the $2N$ -dimensional phase space with initial condition $P(0) = (x_1(0), \dots, x_{2N}(0))$ and two different initial deviation vectors from the initial point $P(0)$, $w_1(t)$ and $w_2(t)$, we define the Smaller Alignment Index (SALI) by:

$$\text{SALI}(t) = \min \{ \|\widehat{w}_1(t) + \widehat{w}_2(t)\|, \|\widehat{w}_1(t) - \widehat{w}_2(t)\| \} \quad (1)$$

where $\widehat{w}_i(t) = w_i(t)/\|w_i(t)\|$ for $i \in \{1, 2\}$.

In the case of chaotic orbits, $\text{SALI}(t)$ falls exponentially to zero as follows:

$$\text{SALI}(t) \propto e^{-(L_1 - L_2)t} \quad (2)$$

where L_1 and L_2 are the biggest Lyapunov Exponents.

When the behavior is ordered, SALI oscillates in non-zero values, that is:

$$\text{SALI}(t) \approx \text{constant} > 0, t \rightarrow \infty. \quad (3)$$

Therefore, there is a clear distinction between orderly and chaotic behavior using this method.

2.2 Gravitational potential of a barred galaxy

We apply the SALI method in the study of stellar orbits immersed in a gravitational potential of barred galaxies, once the movement of a test particle in a rotating three-dimensional model of a barred galaxy is given by the Hamiltonian:

$$\begin{aligned} H(x, y, z, p_x, p_y, p_z) = \\ = (p_x^2 + p_y^2 + p_z^2) + \Phi_T(x, y, z) + \Omega_b(xp_y - yp_x) \end{aligned} \quad (4)$$

where the bar rotates around z ; x and y contain respectively the major and minor axes of the galactic bar, Φ_T is the gravitational potential (which will be described later), and Ω_b represents the standard angular velocity of the bar.

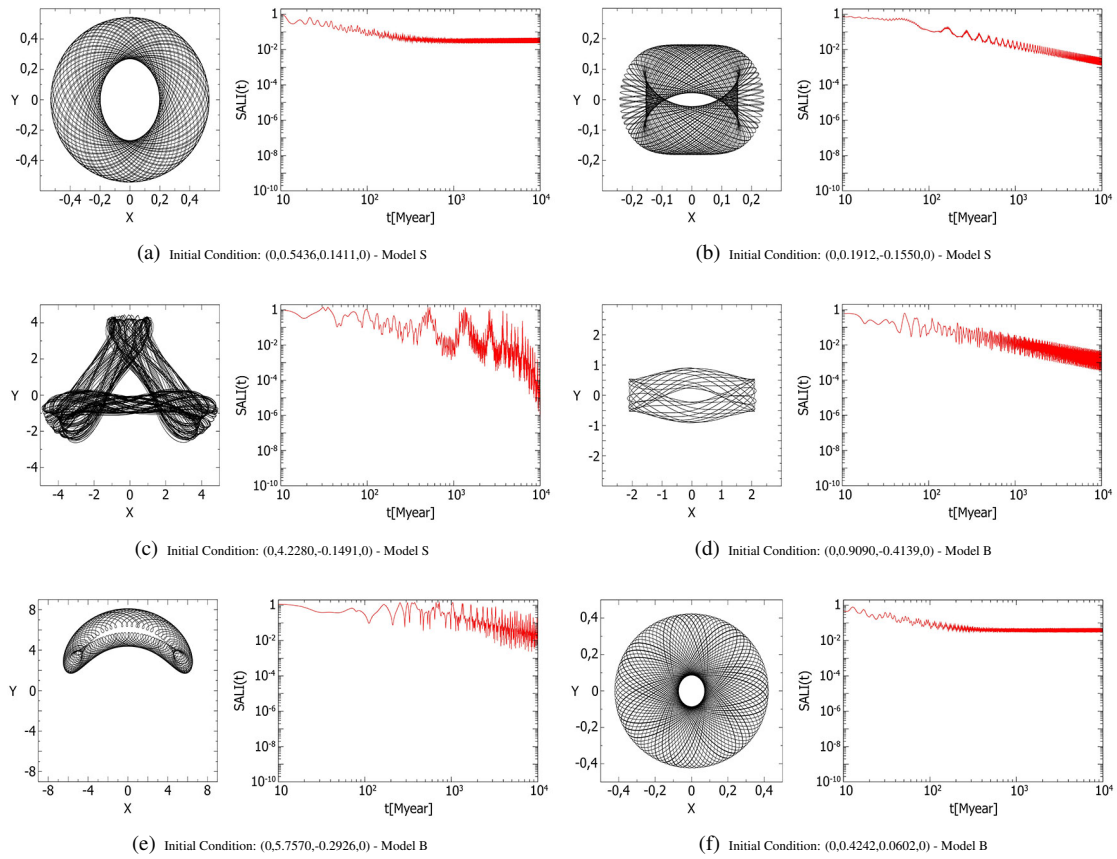


Fig. 1: Six orbits, each one with its SALI diagram. All orbits were integrated up to 10,000 Myr. Only the first 500 Myr were plotted in (a), (b), (d) and (f), for clarity.

For this Hamiltonian, the corresponding equations of motion and the corresponding variational equations that govern the evolution of a deviation vector can be found in [4]. With such equations it is possible to follow the temporal evolution of a moving particle immersed in the potential Φ_T , as well as verify if this orbit is chaotic or regular, following the evolution of deviation vectors by the SALI method.

In this work, the total potential Φ_T is composed by three components, representing the galactic bulge, disk and bar:

$$\Phi_T = \Phi_{Bulge} + \Phi_{Disk} + \Phi_{Bar}. \quad (5)$$

We represent the bulge by the Plummer Model [8]

$$\Phi_{Bulge} = -\frac{GM_S}{\sqrt{x^2 + y^2 + z^2 + \epsilon_S^2}}, \quad (6)$$

where ϵ_S is the length scale and M_S is the bulge mass.

We represent the disk by the Miyamoto-Nagai Model [6]

$$\Phi_{Disk} = -\frac{GM_D}{\sqrt{x^2 + y^2 + (A + \sqrt{z^2 + B^2})^2}} \quad (7)$$

where A and B are respectively the radial and vertical scale lengths, and M_D is the disk mass.

We represent the bar by the Ferrers Model [3]. In this model, the density is given by

$$\begin{cases} \rho_B(x, y, z) = \rho_c (1 - m^2)^2, & m < 1 \\ \rho_B(x, y, z) = 0, & m \geq 1 \end{cases} \quad (8)$$

where the central density is

$$\rho_c = \frac{105}{32\pi} \frac{GM_B}{abc},$$

M_B is the bar mass and

$$m^2 = \frac{x^2}{a^2} + \frac{y^2}{b^2} + \frac{z^2}{c^2},$$

where $a > b > c > 0$ are the semi-axes of the ellipsoid which represents the bar.

The potential created by the galactic bar is calculated with the Poisson equation (see [1]):

$$\Phi_{Bar} = -\pi G abc \frac{\rho_c}{3} \int_{\lambda}^{\infty} \frac{du}{\Delta(u)} (1 - m^2(u))^3 \quad (9)$$

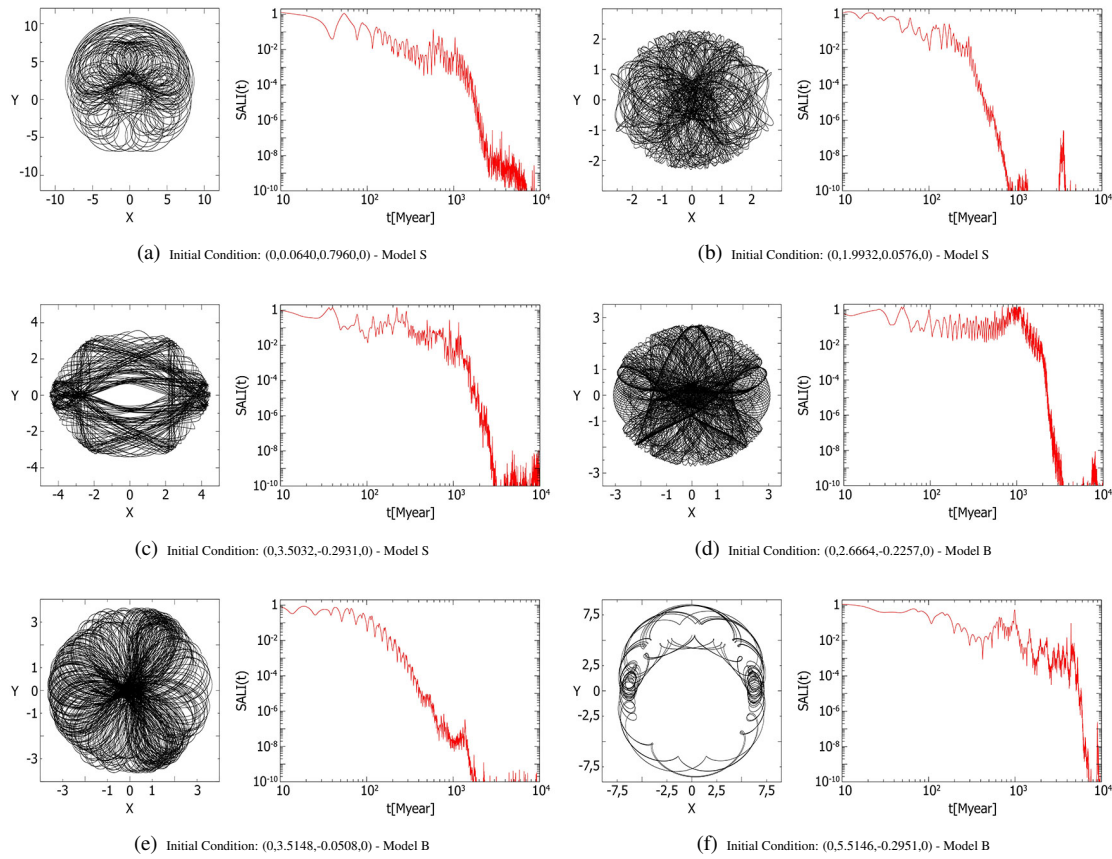


Fig. 2: The SALI graphics has both axes in logarithmic scale. All orbits were integrated into 10,000 Myr. Only the first 5,000 Myr were plotted in (b), for clarity.

where

$$m^2(u) = \frac{x^2}{a^2 + u} + \frac{y^2}{b^2 + u} + \frac{z^2}{c^2 + u},$$

$$\Delta^2(u) = (a^2 + u)(b^2 + u)(c^2 + u)$$

and λ is the positive solution of $m^2(\lambda) = 1$ for the region outside the bar ($m \geq 1$) and $\lambda = 0$ for the region inside the bar ($m < 1$).

2.3 The LP-Vicode program with minor adjustments

To perform the orbits integrations and the SALI calculation, we used the LP-Vicode program [2], which is an operational code in Fortran 77 that calculates efficiently 10 chaos indicators for dynamical systems, including SALI.

In this program, the user must provide the expressions of the potential as well the expressions of motion and variational equations. However, the general structure of motion and variational equations previously written in the main program, take into account only a static reference frame, and it is known that in order to model the galactic bar potential, it is necessary to consider a coordinate system that rotates along with the bar.

In this context, considering Ω_b the bar angular velocity, our reference frame should also rotate with angular velocity Ω_b . This affects the motion and variational equations since, as can be seen in [4], they depend on Ω_b . In order to solve this problem, adjustments were made to the main program to include the rotation in the coordinate system with the same angular velocity of the bar.

2.4 Parameters sets

We used the two parameter sets shown in Table 1 for the potential model, taken from the paper by Manos & Athanasoulas [5]. The model units adopted are: 1 kpc for length, 10^3 km s^{-1} for velocity, $10^3 \text{ km s}^{-1} \text{ kpc}^{-1}$ for angular velocity, 1 Myr for time, and $2 \times 10^{11} M_{\text{solar}}$ for mass. The universal gravitational constant G will always be considered 1 and the total mass $G(M_S + M_D + M_B)$ will be always equal to 1.

2.5 Initial conditions

We emphasize that in this paper we study orbits with two degrees of freedom. In order to do that, we consider $z = 0$ and $p_z = 0$ in the three-dimensional Hamiltonian (4).

Table 1: Parameter Sets and the Bars Co-rotation.

	M_S	ϵ_S	M_D	A	B	M_B	a	b	c	Ω_b	CR
Model S	0.08	0.4	0.82	3.0	1.0	0.1	6.0	1.5	0.6	0.054	6.04
Model B	0.08	0.4	0.82	3.0	1.0	0.1	6.0	3.0	0.6	0.054	6.06

The effective potential, which is the sum of the gravitational potential with the potential generated by the repulsive centrifugal force, is given by:

$$\Phi_{eff}(\mathbf{x}) = \Phi_T(\mathbf{x}) - \frac{1}{2}|\Omega \times \mathbf{x}|^2. \quad (10)$$

Written like that, this potential represents a rotating system.

The quantity

$$E_J = \frac{1}{2}|\mathbf{v}|^2 + \Phi_{eff}(\mathbf{x}) \quad (11)$$

is called Jacobi Energy and is conserved in the rotating system.

The curve given by $\Phi_{eff}(0, y, 0) = E_J$ is called Zero Velocity Curve and provides a good demarcation for the choice of initial conditions, since there is only possibility of orbits when $\Phi_{eff} \leq E_J$, in other words, below this curve (see [1]).

Therefore, we generated some random initial conditions initially taking a value to y_0 less than the highest possible value of y for a given energy E_J , taking $x_0 = 0$ and $v_{y_0} = 0$. This done, we could calculate v_x as follows:

$$E_J = \frac{1}{2}(v_{x_0}^2 + v_{y_0}^2) + \Phi_{eff} = \frac{1}{2}v_{x_0}^2 + \Phi_{eff} \quad (12)$$

and this implies

$$v_{x_0} = \pm \sqrt{2(E_J - \Phi_{eff})}. \quad (13)$$

Then we constructed initial conditions $(x_0, y_0, v_{x_0}, v_{y_0})$ to integrate the orbits. As $x_0 = 0$ and $v_{y_0} = 0$, the launched orbits will always be initially over the y axis and will have initial velocity only in the x direction.

Notice that we have two possible velocities from equation (13): one negative and one positive. We decided to take y_0 always positive, so that when v_{x_0} is positive, the orbits are prograde (orbits that rotate in the same direction of the bar) and when v_{x_0} is negative, the orbits are retrograde (orbits that rotate in the opposite direction of the bar).

3 Results

In our computational calculations, we consider $SALI < 10^{-8}$ close enough to zero to consider the movement chaotic.

3.1 Regular orbits

In Fig. 1 we show 6 different orbits, each one with its SALI diagram, from where we can identify them as regular orbits, as explained in section 2.1.

3.2 Chaotic orbits

Fig. 2 shows a sample of 6 chaotic orbits, identified by their SALI indexes that goes to zero after some time, as discussed in section 2.1.

4 Conclusion

In this study, we were able to reproduce a mathematical modeling of the gravitational potential of a barred galaxy and, in order to verify the stability of the orbits within, we applied the SALI method. We were able to prove the SALI efficiency in distinguishing regular or chaotic orbits. In fact, this method offers an easily observable distinction between chaotic and regular behavior.

We also perceive the LP-VIcode efficiency, which proved to be extremely competent in the orbits integration and study of stability with SALI. To make an adjustment in the variational and motion equations programmed in the LP-VIcode, we insert an adaptation in the main code to take into account a rotating system.

Therefore, we conclude that we were successful in calculating these orbits and confirm the SALI method as a new important tool in the study of stellar orbits stability.

Acknowledgements

We acknowledge the Brazilian agencies FAPESP, CAPES and CNPq (200906-2015-1), as well as the Mexican agency CONACyT (CB-2014-240426) for supporting this work. Our sincere thanks to Dr. Pfenniger, who kindly provided us with his Fortran 77 implementation of the Ferrers bar potential. All the numerical work was developed using the Hiperculo Cluster resources (FINEP 01.10.0661-00, FAPESP 2011/13250-0 and FAPESP 2013/17247-9) at IP&D–UNIVAP.

Received on May 12, 2017

References

1. Binney J. and Tremaine S. Galactic Dynamics, 2nd ed. Princeton University Press, 2008.
2. Carpintero D. D., Maffione N. and Darriba L. LP-VIcode: a program to compute a suite of variational chaos indicators. *Astronomy and Computing*, 2014, v. 5, 19–27. DOI: 10.1016/j.ascom.2014.04.001.
3. Ferrers N. M. On the potential of ellipsoids, ellipsoidal shells, elliptic laminae and elliptic rings, of variable densities. *Quarterly Journal of Pure and Applied Mathematics*, 1877, v. 14, 1–22.
4. Manos T. A Study of Hamiltonian Dynamics with Applications to Models of Barred Galaxies. PhD Thesis in Mathematics, Université de Provence and University of Patras, 2008.

5. Manos T. and Athanassoula E. Regular and chaotic orbits in barred galaxies – I. Applying the SALI/GALI method to explore their distribution in several models. *Monthly Notices of the Royal Astronomical Society*, 2011, v. 415, 629–642. DOI: 10.1111/j.1365-2966.2011.18734.x.
6. Miyamoto M. and Nagai R. Three-dimensional models for the distribution of mass in galaxies. *Astronomical Society of Japan*, 1975, v. 27, 533–543.
7. Pfenniger D. The 3D dynamics of barred galaxies. *Astronomy and Astrophysics*, 1984, v. 134, 373–386. ISSN: 0004-6361.
8. Plummer H. C. On the problem of distribution in globular star clusters. *Notices of the Royal Astronomical Society*, 1911, v. 71, 460–470. DOI: 10.1093/mnras/71.5.460.
9. Skokos Ch. Alignment indices: a new, simple method for determining the ordered or chaotic nature of orbits. *Journal of Physics: Mathematical and General*, 2001, v. 34, 10029–10043. DOI: 10.1088/0305-4470/34/47/309.
10. Skokos Ch., Antonopoulos Ch., Bountis T. C. and Vrahatis M. N. Smaller alignment index (SALI): Determining the ordered or chaotic nature of orbits in conservative dynamical systems. In Gomez G., Lo M. W., Masdemont J. J., eds. *Proceedings of the Conference Libration Point Orbits and Applications*, World Scientific, 2002, 653–664. DOI: 10.1142/9789812704849_0030.
11. Skokos Ch., Antonopoulos Ch., Bountis T. C. and Vrahatis M. N. How does the Smaller Alignment Index (SALI) distinguish order from chaos? *Prog. Theor. Phys. Supp.*, 2003, v. 150, 439–443. DOI: 10.1143/PTPS.150.439.
12. Skokos Ch., Antonopoulos Ch., Bountis T. C. and Vrahatis M. N. Detecting order and chaos in Hamiltonian systems by the SALI method. *J. Phys. A*, 2004, v. 37, 6269–6284. DOI: 10.1088/0305-4470/37/24/006.
13. Skokos Ch. and Bountis T. C. *Complex Hamiltonian Dynamics*. Springer, 2012.

A New Perspective for Kinetic Theory and Heat Capacity

Kent W. Mayhew

68 Pineglen Cres., Ottawa, Ontario, K2G 0G8, Canada. E-mail: Kent.Mayhew@gmail.com

The currently accepted kinetic theory considers that a gas' kinetic energy is purely translational and then applies equipartition/degrees of freedom. In order for accepted theory to match known empirical finding, numerous exceptions have been proposed. By re-defining the gas' kinetic energy as translational plus rotational, an alternative explanation for kinetic theory is obtained, resulting in a theory that is a better fit with empirical findings. Moreover, exceptions are no longer required to explain known heat capacities. Other plausible implications are discussed.

1 Introduction

The conceptualization of a gaseous system's kinematics originated in the writings of the 19th century greats. In 1875, Maxwell [1] expressed surprise at the ratio of energies (translational, rotational and/or vibrational) all being equal. Boltzmann's work on statistical ensembles reinforced the current acceptance of law of equipartition with a gas's energy being equally distributed among all of its degrees of freedom [2–3]. The net result being that the accepted mean energy for each independent quadratic term being $kT/2$.

The accepted empirically verified value for the energy of a N molecule monatomic gas is $kT/2$ with its isometric molar heat capacity (C_v) being $(3R/2)$. An implication is that a monatomic gas only possesses translational energy [4–5]. The reasoning for this exception is that the radius of a monatomic gas is so small that its rotational energy remains negligible, hence its energy contribution is simply ignored.

Mathematically speaking equipartition based kinetic theory states that a molecule with n'' atoms has $3n''$ degrees of freedom (f) [5–6] i.e.:

$$f = 3n'' \quad (1)$$

This leads to the isometric molar heat capacity (C_v) for large polyatomic molecules:

$$C_v = \frac{3}{2} n'' R \quad (2)$$

Interestingly, the theoretical expected heat capacity for N diatomic molecules is $7NkT/2$. This is the summation of the following three energies a) three translational degrees, i.e. $3NkT/2$. b) three rotational degrees of freedom, however since the moment of inertia about the internuclear axis is vanishing small w.r.t. other moments, then it is excluded, i.e. NkT . c) Vibrational energy, i.e. NkT . This implies a molar heat capacity $C_v = 7NkT/2 = 29.3$ J/(mol*K). However, empirical findings indicate that the isometric molar heat capacity for a diatomic gas is actually 20.8 J/(mol*K), which equates to $5RT/2$ [6]. This discrepancy for diatomic gases certainly allows one to question the precise validity of accepted kinetic theory! In 1875 Maxwell noted that since atoms have internal parts then this discrepancy maybe worse than we believe [7].

Various explanations for equipartition's failure in describing heat capacities have been proposed. Boltzmann suggested that the gases might not be in thermal equilibrium [8]. Planck [9] followed by Einstein and Stern [10] argued the possibility of zero-point harmonic oscillator. More recently Dahl [11] has shown that a zero point oscillator to be illusionary. Lord Kelvin [12–13] realized that equipartition maybe wrongly derived. The debate was somewhat ended by Einstein claiming that equipartition's failure demonstrated the need for quantum theory [14–15]. Heat capacities of gases have been studied throughout the 20th century [16–19] with significantly more complex models being developed [20–21].

It becomes a goal of this paper to clearly show that an alternative kinetic theory/model exists. A simple theory that correlates better with empirical findings without relying on exceptions while correlating with quantum theory.

2 Kinetic theory and heat capacity simplified

Consider wall molecules 1 through 8, in Fig. 1. The total mean energy along the x -axis of a vibrating wall molecule is

$$\overline{E}_x = kT \quad (3)$$

Half of a wall molecule's mean energy would be kinetic energy, and half would be potential energy. Thus, the mean kinetic energy along the x -axis, remains

$$\overline{E}_x = \frac{kT}{2} \quad (4)$$

In equilibrium, the mean kinetic energy of a wall molecule, as defined by equation (4) equals the mean kinetic energy of the gas molecule along the same x -axis. Herein, the wall in the y - z plane acts as a massive pump, pumping its mean kinetic energy along the x -axis onto the much smaller gas molecules.

In equilibrium each gas molecule will have received a component of kinetic energy along each orthogonal axis. Although there are six possible directions, at any given instant, a gas molecule can only have components of motion along three directions, i.e. it cannot be moving along both the positive and negative x -axis at the same time. Therefore, the total kinetic energy of the N molecule gas is defined by

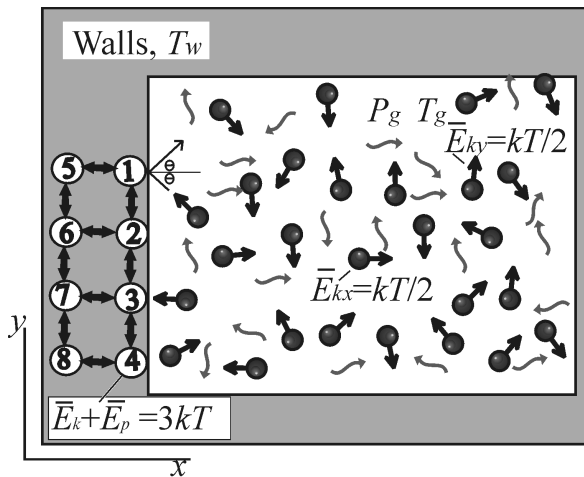


Fig. 1: Ideal monoatomic gas at pressure P_g and temperature T_g surrounded by walls at temperature $T_w = T_g$. Gas molecules have no vibrational energy.

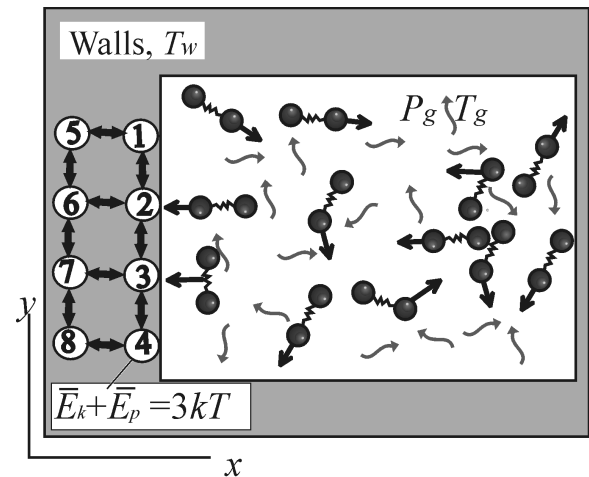


Fig. 2: Ideal diatomic gas at pressure P_g and temperature T_g surrounded by walls at temperature $T_w = T_g$. Gas molecules have vibrational energy.

equation (4) i.e. $3NkT/2$. Up to this point we remain in agreement with accepted theory.

Consider that you hit a tennis ball with a suitable racquet. If the ball impacts the racquet's face at a 90 degree angle, then the ball will have significant translational energy in comparison to any rotational energy. Conversely, if the ball impacts the racquet at an acute angle, although the same force is imparted onto that ball, the ball's rotational energy can be significant in comparison to its translational energy. The point being, in real life both the translational and rotational energy, are due to the same impact.

Now reconsider kinetic theory. Understandably, momentum transfer between both the wall's and gas' molecules result in energy exchanges between the massive wall and small gas molecules. Moreover, the exact nature of the impact will vary, even though the exchanged mean energy is constant.

Case 1: Imagine that a monatomic gas molecule collides head on with a wall molecule, e.g. the gas molecule hitting wall molecule no. 3 in Fig. 1. Herein, the gas molecule might only exchange translational energy with the wall, resulting in the gas molecule's mean kinetic energy being purely translational, and defined by equation (4).

Case 2: Imagine that a monatomic gas molecule strikes wall molecule no. 1 at an acute angle. The gas molecule would obtain both rotational and translational energy from the impact such that the total resultant mean energy of the gas molecule would be the same as it was in Case 1, i.e. defined by equation (4).

Case 3: Imagine a rotating and translating monatomic gas molecule striking the wall. Both the rotational and translational energies will be passed onto the wall molecule. Since the wall molecule is bound to its neighbors,

it cannot rotate hence both energies can only result in vibrational energy of the wall molecules along its three orthogonal axis.

After numerous wall impacts, our model predicts that an N molecule monatomic gas will have a total kinetic energy (translational plus rotational) defined by

$$E_{kT(t,r)} = \frac{3}{2} NkT. \tag{5}$$

Fig. 2 illustrates a system of diatomic gas molecules in a container. The wall molecules still pass the same mean kinetic energy onto the diatomic gas molecule's center of mass with each collision. Therefore the diatomic gas' kinetic energy is defined by equation (5). The diatomic gas molecule's vibrational energy would be related to the absorption and emission of its surrounding blackbody/thermal radiation. Therefore, the mean x -axis vibrational energy within a diatomic gas molecule remains defined by equation (3) and the total mean energy for a diatomic gas molecule becomes defined by

$$\bar{E}_{tot} = \bar{E}_{kT(t,r)} + \bar{E}_v = \frac{3}{2} kT + kT = \frac{5}{2} kT. \tag{6}$$

Therefore the total energy for an N molecule diatomic gas becomes

$$E_{tot} = E_{kT(t,r)} + E_v = \frac{3}{2} NkT + NkT = \frac{5}{2} NkT. \tag{7}$$

For an N molecule triatomic gas:

$$E_{tot} = E_{kT(t,r)} + E_v = \frac{3}{2} NkT + 2NkT = \frac{7}{2} NkT, \tag{8}$$

n'' signifies the polyatomic number. Therefore for N molecules of n'' -polyatomic gas, the vibrational energy is

$$E_v = (n'' - 1)NkT. \tag{9}$$

Therefore, the total energy for a polyatomic gas molecule is:

$$\begin{aligned} E_{tot} = E_{kT(t,r)} + E_v &= \frac{3}{2} NkT + (n'' - 1) NkT \\ &= \left(n'' + \frac{1}{2} \right) NkT. \end{aligned} \quad (10)$$

Dividing both sides by temperature and rewriting in terms of per mole ($N=6.02 \times 10^{23}$) then equation (10) becomes:

$$\frac{E_{tot}}{T} = nk \left(n'' + \frac{1}{2} \right) = R \left(n'' + \frac{1}{2} \right). \quad (11)$$

For most temperature regimes, the heat capacity of gases remains fairly constant, hence equation (11) can be rewritten in terms of the isometric molar heat capacity (C_v), i.e.

$$C_v = R \left(n'' + \frac{1}{2} \right). \quad (12)$$

The difference between molar isobaric heat capacity (C_p) and molar isometric heat capacity (C_v) for gases is the ideal gas constant (R) [see equation (15)]. Therefore, a gas's isobaric heat capacity C_p becomes

$$C_p = R \left(n'' + \frac{1}{2} \right) + R = R \left(n'' + \frac{3}{2} \right). \quad (13)$$

The adiabatic index is the ratio of heat capacities, i.e. dividing equation (13) by equation (12) gives the adiabatic index

$$\gamma = \frac{C_p}{C_v} = \frac{\left(n'' + \frac{3}{2} \right)}{\left(n'' + \frac{1}{2} \right)}. \quad (14)$$

Table 1 shows the accepted isometric and isobaric molar heat capacities for various substances for $0 > n'' > 27$. These values were calculated using data (specific heats) from an engineering table (Rolle [22]) that is shown in Table 2. Note: Engineer's use specific heats (per mass), physicists and chemists prefer heat capacity (per mole).

In Fig. 3, both our theoretical molar isometric and isobaric [equations (12) and (13)] heat capacities are plotted against the number of atoms (n'') in each molecule. The accepted empirically determined values for heat capacities versus n'' (from Table 1) are also plotted. The traditional theoretical values for molar heat capacities [eq. (2)] are also plotted.

The theory/model proposed herein remains a better fit to empirical findings for all polyatomic molecules. Importantly, it does not rely upon the exceptions that plague the traditionally accepted degrees of freedom based kinetic theory.

Interestingly, there is a discrepancy, between our model and empirical known values for $4 < n'' < 9$. Moreover, the slope of our theoretical values visually remains close to the slope of empirically determined values for $n'' > 8$. Furthermore, hydrogen peroxide (H_2O_2 , $C_v=37.8$, $n''=4$) and

acetylene (C_2H_2 , $n''=4$, $C_v=35.7$) are linear bent molecules and good fit, while pyramidal ammonia (NH_3 , $n''=4$, $C_v=27.34$) is not. Could the gas molecule's shape influence how it absorbs surrounding thermal radiation, hence its vibrational energy?

Table 2 shows the accepted adiabatic index versus our theoretical adiabatic index for most of the same substances shown in Table 1. Our theoretical adiabatic index compares rather well with the accepted empirical based values, especially for low $n'' < 4$ and high $n'' > 11$, as is clearly seen in Fig. 4. Although not 100% perfect, this new theory/model certainly warrants due consideration by others.

3 Kinetic theory and thermal equilibrium

Kinetic theory holds because the walls act as massive energy pumps, i.e. gas molecules take on the wall's energy with every gas-wall collision. For sufficiently dilute gases, this remains the dominant method of energy exchange. Mayhew [23–24] has asserted that inter-gas molecular collisions tend to obey conservation of momentum, rather than adhere to kinetic theory. Therefore, when inter-gas collisions dominate over gas-wall collisions, then kinetic theory, the ideal gas law, Avogadro's hypothesis, Maxwell's velocities etc. all can start to lose their precise validity.

It is accepted that there are changes to heat capacity in and around dissociation temperatures. Firstly, at such high temperatures, the pressure tends to be high; hence the inter-gas collisions may dominate. This author believes that this actually helps explain why kinetic theory falters in polytropic stars, wherein high-density gases collide in a condensed matter fashion hence one must use polytropic solutions. Secondly, at high temperatures a system's thermal energy density is no longer proportional to temperature, i.e. a blast furnace's thermal energy density is proportional to T^4 [22].

Blackbody radiation describes the radiation within an enclosure. For an open system and/or none blackbody, the thermal radiation surrounding the gas molecules may be better to considered. Herein thermal radiation means radiation that is readily absorbed and radiated by condensed matter and/or polyatomic gases, resulting in both intramolecular and intermolecular vibrations.

For a system of dilute polyatomic gas e.g. Fig. 2, thermal equilibrium requires that all of the following three states remain related to the same temperature (T):

1. The walls are in thermal equilibrium with the enclosed blackbody/thermal radiation.
2. The gas' translational plus rotational energy is in mechanical equilibrium with the molecular vibrations of the walls.
3. The gas' vibrational energies are in thermal equilibrium with the enclosed blackbody/thermal radiation.

Imagine that a system of dilute polyatomic gas is taken to remote outer space, and that the walls are magically re-

Table 1: Accepted isometric and isobaric heat capacities versus theoretical i.e. empirical findings versus Eqn. (12), Eqn. (13), as well as Eqn. (2). Note: Accepted heat capacities were calculated from the engineer's specific heats in Table 2 (Rolle [22]), exception being H₂O₂ which was taken from Giguere [19].

Substance		n''	Accepted C_v [J/mol*K]	Eqn. (12) C_v [J/mol*K]	Accepted C_p [J/mol*K]	Eqn. (13) C_p [J/mol*K]	Eqn. (2) C_v [J/mol*K]
Helium	He	1	12.48	12.47	20.80	20.78	
Neon	Ne	1	12.47	12.47	20.79	20.78	
Argon	Ar	1	12.46	12.47	20.81	20.78	
Xenon	Xe	1	12.47	12.47	20.58	20.78	
Hydrogen	H ₂	2	20.52	20.78	28.83	29.09	
Nitrogen	N ₂	2	20.82	20.78	29.14	29.09	
Oxygen	O ₂	2	21.02	20.78	29.34	29.09	
Nitric oxide	NO	2	21.55	20.78	29.86	29.09	
Water vapor	H ₂ O	3	25.26	29.09	33.58	37.40	37.40
Carbon dioxide	CO ₂	3	28.83	29.09	37.14	37.40	37.40
Sulfur dioxide	SO ₂	3	31.46	29.09	39.78	37.40	37.40
Hydrogen peroxide	H ₂ O ₂	4	37.4	37.73	46.05	45.71	49.86
Ammonia	NH ₃	4	27.37	37.40	35.70	45.71	49.86
Methane	CH ₄	5	27.4	45.71	35.72	54.0	62.33
Ethylene	C ₂ H ₄	6	35.24	54.02	43.54	62.33	74.79
Ethane	C ₂ H ₆	8	44.35	70.64	52.65	78.95	99.72
Propylene	C ₃ H ₆	9	53.82	78.95	63.92	87.26	112.19
Propane	C ₃ H ₈	11	65.18	95.57	73.51	103.88	137.12
Benzene	C ₆ H ₆	12	73.50	103.88	81.63	112.19	149.58
Isobutene	C ₄ H ₈	12	77.09	103.88	85.68	112.19	149.58
n-Butane	C ₄ H ₁₀	14	89.10	120.50	97.42	128.81	174.51
Isobutane	C ₄ H ₁₀	14	88.52	120.50	96.84	128.81	174.51
n-Pentane	C ₅ H ₁₂	17	111.91	145.43	120.20	153.74	211.91
Isopentane	C ₅ H ₁₂	17	111.69	145.43	119.99	153.74	211.91
n-Hexane	C ₆ H ₁₄	20	134.78	170.36	143.06	178.67	249.30
n-Heptane	C ₇ H ₁₆	23	157.62	195.29	165.94	203.60	286.70
Octane	C ₈ H ₁₈	26	180.60	220.22	188.83	228.53	324.09

moved and the gas disperses. Spreading at the speed of light the blackbody/thermal radiation density decreases faster than the density of slower moving gas molecules. As the radiation density decreases, the rate at which polyatomic gaseous molecules absorbs blackbody/thermal radiation decreases in time. Hence their vibrational energy decreases although their mean velocity remains constant. Now place a thermometer in the expanding wall-less gas, what will it read? Traditional kinetic theory claims that the temperature will be the same because the gas molecule's velocity remains constant i.e. temperature is only associated with the system's kinemat-

ics [2–3]. However, without walls the blackbody/thermal radiation decouples from thermal equilibrium i.e. the mean velocity of the gas molecules are associated with one temperature, but the radiation density is no longer associated with that temperature. This bodes the question: What is the real temperature? Of course this means accepting that the thermometer not only exchanges kinetic energy with the gas molecules, but it also exchanges blackbody/thermal radiation with its surroundings.

The above is another reason that this author hypothesizes that kinetic theory can falter in systems without walls. The

Table 2: Engineer's accepted adiabatic index compared to theoretical: Eqn. (14). Note: Data in first six columns after Rolle [22]. Rolle's reference: J.F. Masi, Trans. ASME, 76:1067 (October, 1954); National Source of Standards (U.S.) Circ. 500, Feb. 1952; Selected Values of Properties of Hydrocarbons and Related Compounds, American Petroleum Institute Research Project 44, Thermodynamic Research Center, Texas, A&M University, College Station, Texas.

Substance		n''	Molar mass [g/mol]	Engineer's R [J/kg*K]	Engineer's C_p [kJ/mol*K]	Engineer's C_v [kJ/mol*K]	Accepted adiabatic index(γ)	Theoretical index (γ) Eqn. (14)
Helium	He	1	4.00	2079	5.196	3.117	1.67	1.67
Neon	Ne	1	20.18	412	1.030	0.618	1.67	1.67
Argon	Ar	1	39.94	208	0.521	0.312	1.67	1.67
Xenon	Xe	1	131.30	63	0.1568	0.095	1.67	1.67
Hydrogen	H ₂	2	2.02	4124	14.302	10.178	1.41	1.4
Nitrogen	N ₂	2	28.02	297	1.040	0.743	1.4	1.4
Oxygen	O ₂	2	32.00	260	0.917	0.657	1.4	1.4
Nitric oxide	NO	2	30.01	277	0.995	0.718	1.39	1.4
Water vapor	H ₂ O	3	18.02	462	1.864	1.402	1.33	1.29
Carbon dioxide	CO ₂	3	44.01	189	0.844	0.655	1.29	1.29
Sulfur dioxide	SO ₂	3	64.07	130	0.621	0.491	1.26	1.29
Ammonia	NH ₃	4	17.03	488	2.096	1.607	1.30	1.22
Methane	CH ₄	5	16.04	519	2.227	1.708	1.30	1.18
Ethylene	C ₂ H ₄	6	28.05	297	1.552	1.256	1.24	1.15
Ethane	C ₂ H ₆	8	30.07	277	1.751	1.475	1.19	1.12
Propylene	C ₃ H ₆	9	42.08	198	1.519	1.279	1.19	1.11
Propane	C ₃ H ₈	11	44.10	189	1.667	1.478	1.13	1.09
Benzene	C ₆ H ₆	12	78.11	106	1.045	0.939	1.11	1.08
Isobutene	C ₄ H ₈	12	56.11	148	1.527	1.374	1.11	1.08
n-Butane	C ₄ H ₁₀	14	58.12	143	1.676	1.533	1.09	1.07
Isobutane	C ₄ H ₁₀	14	58.12	143	1.666	1.523	1.09	1.07
n-Pentane	C ₅ H ₁₂	17	72.15	115	1.666	1.551	1.07	1.06
Isopentane	C ₅ H ₁₂	17	72.15	115	1.663	1.548	1.07	1.06
n-Hexane	C ₆ H ₁₄	20	86.18	96	1.660	1.564	1.06	1.05
n-Heptane	C ₇ H ₁₆	23	100.20	83	1.656	1.573	1.05	1.04
Octane	C ₈ H ₁₈	26	114.23	73	1.653	1.581	1.05	1.04

other reason kinetic theory may falter without walls is that wall-gas interactions no longer exist, hence kinetic theory's complete virtues may be limited to systems with walls [24–25] i.e. experimental systems.

4 Discussion of other implications

This author [24–25] has hypothesized that blackbody/thermal radiation within a system has a temperature associated with it. So although the total energy associated with radiation often is infinitesimally small in comparison to the total energy associated with the kinematics of matter, the idea that black-

body radiation has a temperature associated with it, should no longer be ignored. In other words, even a vacuum can have a temperature, although it has no matter and comparatively speaking only contains a minute amount of energy.

Pressure is traditionally envisioned as being solely due to change in translational energy i.e. "every molecule that impinges and rebounds exerts an impulse equal to the difference in its momenta before and after impact" [pg. 32, 20]. Interestingly, the analysis given herein does alter such explanations just because the rotational energy plus the translational energy of the gas molecules now combine to exert pressure. Moreover, consider the tennis ball impacting a wall. Ask

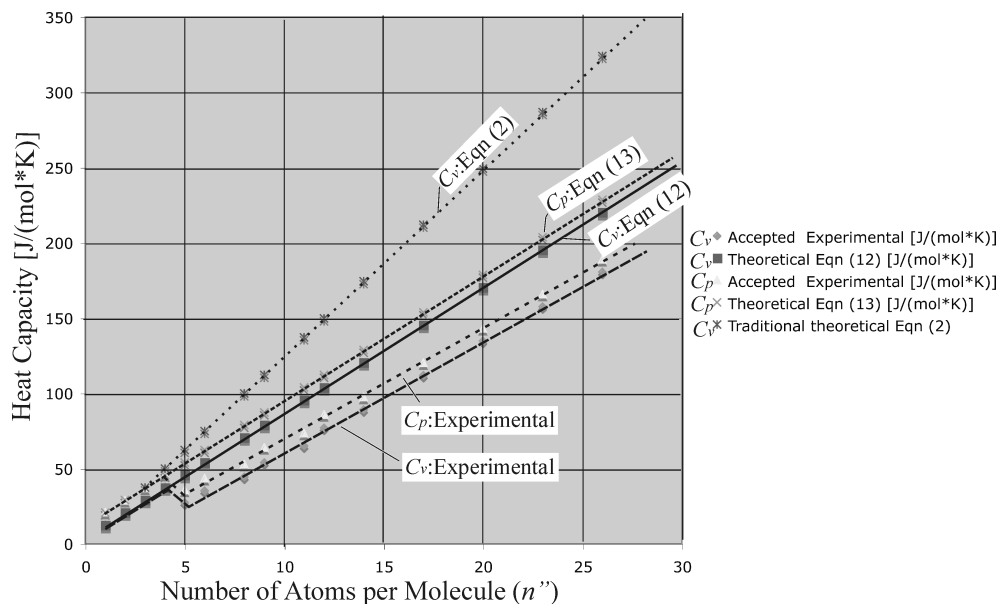


Fig. 3: Theoretical molar heat capacity based on our theoretical equations (12) and (13) versus empirical values, plus the traditional theoretical isometric molar heat capacity plot [based upon degrees of freedom, equation (2)].

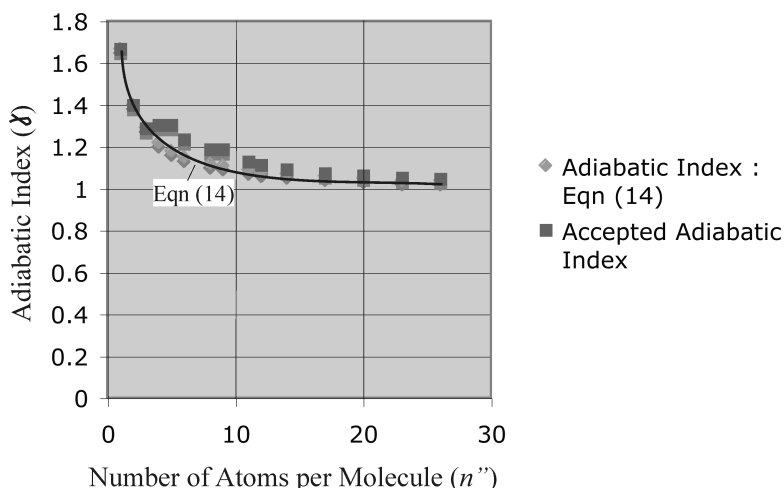


Fig. 4: Theoretical adiabatic index [eq. (14)] versus number of atoms (solid line). Adiabatic index data points based upon engineering table for gases.

yourself: Are not both the rotational and translational energy of that ball exchanged with the wall. So why would a gas molecule behave any differently? Just because wall molecules are bound i.e. cannot rotate, does not mean that they don't exchange rotational energy/momentum with an impacting gas! The gas' mean translational velocity ($mv^2/2$) can no longer be simply equated in terms of Boltzmann's constant ($kT/2$). This has consequences to fundamentals such as Maxwell's velocity distributions for gases. In our analysis, the magnitude of translational energy compared to rotational energy is not defined beyond that they add up to and equal, the summation of the walls molecule's kinetic energies! Since the

gas' total kinetic energy remains the same, then most of what is known in quantum theorem still applies with the change being how a gas' kinetic energy is expressed.

Consider the hypothesis that rotational energy of a gas is frozen out at low temperatures [26]. This is like claiming that gas molecules never impact a wall at acute angles, when in a cold environment. This author thinks in terms of thermal energy being energy that results in both intermolecular and intramolecular vibrations within condensed matter. Just consider the blackbody radiation curve for 3 K, whose peak is located at wavelength of 1 mm. Compare this to 300 K, where the radiation curves' peak occurs in the infrared spec-

trum, wavelength equals 10 micrometers. Accepting that the majority of thermal energy is in the infrared then this author also believes that somewhere between 3 K and 300 K, a system's thermal energy density will no longer proportional to temperature i.e. probably around 100 K. Perhaps it is the gas' vibrational energy that is frozen out? Understandably, at low temperatures the blackbody/thermal radiation within the system may be such that it does not provide enough thermal energy (infrared) for measurable gas vibration. However, this should equally apply to the system's walls, unless the walls have more thermal energy relative to the gas i.e. apparatus considerations? This is conjecture, as remains the current notion that rotational energies are frozen out.

For gases the accepted difference between molar isobaric heat capacity and molar isometric heat capacity is the ideal gas constant (R). Accordingly [2–3]:

$$C_p - C_v = R. \quad (15)$$

The difference in heat capacities is obviously independent of the type of gas. This implies that the difference depends upon the system's surroundings and not the experimental system, nor its contents. This fits this author's assertion that "the ideal gas constant is the molar ability of a gas to do work per degree Kelvin" [27]. This is based upon the realization that work is required by expanding systems to upwardly displace our atmosphere's weight, i.e. an expanding system does such work, which becomes irreversibly lost into the surrounding Earth's atmosphere. The lost work being [24, 28–29]

$$W_{lost} = P_{atm} dV. \quad (16)$$

This does not mean that the atmosphere is always upwardly displaced, rather that the energy lost by an expanding system is defined by equation (17). This lost energy can be associated with a potential energy increase of the atmosphere, or a regional pressure increase. Note: A regional pressure increase will result in either a volume increase, or viscous dissipation i.e. heat created = lost work. This requires the acceptance that the atmosphere has mass and resides in a gravitational field. It is no different than realizing that an expanding system at the bottom of an ocean, i.e. a nucleating bubble, must displace the weight of the ocean plus atmosphere. Accordingly, any expanding system here on Earth's surface must expend energy/work to displace our atmosphere's weight and such lost work, is immediately or eventually lost into the surrounding atmosphere. Accepting this then allows one to question our understanding of entropy [24, 29].

5 Conclusions

Kinetic theory has been reconstructed with the understanding that a gas' kinetic energy has both translational and rotational components that are obtained from the wall molecule's kinetic energy. Therefore, the gas' translational plus rotational energies along each of the x , y and z -axis, are added

and equated to the wall molecules' kinetic energy along the identical three axes. No knowledge pertaining to the magnitudes of the gas' rotational energy versus translational energy is claimed. This is then added to the gas' internal energy e.g. vibrational energy, in order to determine the gas' total energy.

The empirically known heat capacity and adiabatic index for all gases are clearly a better fit to this new theory/model, when compared to accepted theory. The fit for monatomic through triatomic gases is exceptional, without any reliance upon traditionally accepted exceptions! Moreover, our model treats all polyatomic molecules in the same manner as condensed matter.

Seemingly, Lord Kelvin's assertion that equipartition was wrongly derived, may have been right after all. Accepting that the traditional degrees of freedom in equipartition theory may be mathematical conjecture rather than constructive reasoning will cause some displeasure. Certainly, one could argue that what is said herein is really just an adjustment to our understanding. Even so, it will alter how pressure is perceived that being due to the gas molecules' momenta from both rotation and translation, which is imparted onto a surface. Ditto for the consideration of a gas' energy in quantum theory.

The consequence of a polyatomic gas' thermal vibrations being related to its surrounding thermal radiation may alter our conceptualization of temperature, i.e. a vacuum now has a temperature. The notion that rotation in cold gases is frozen out was also questioned. Perhaps it is a case that the thermal energy density does not remain proportional to temperature, as T approaches 0, which also is the case for very high temperature gases.

The difference between isobaric and isometric heat capacity is gas independent. This fits well with this author's assertion that lost work represents the energy lost by an expanding system into the surrounding atmosphere. Interestingly, for a mole of gas molecules this lost work can be related to the ideal gas constant.

To some, the combining of a gas' rotational and translational energy may seem like a minor alteration, however the significance to the various realms of science maybe shattering. Not only may this help put to rest more than a century of speculations, it also may alter the way that thermodynamics is envisioned. If accepted it actually opens the door for a simpler new thermodynamics vested in constructive logic, rather than mathematical conjecture.

A thanks goes out to Chifu E. Ndikilar for his helpful preliminary comments, as well as both Dmitri Rabounski and Andreas Ries for their insights in finalizing the paper.

6 Example calculations

1. Table 1 for $n'' = 3$; our theoretical values: [equation (12)]: I.e. $C_v = \frac{7}{2}R = \frac{7}{2} 8.31 \text{ J}/(\text{mol}\cdot\text{K}) = 29.09 \text{ J}/(\text{mol}\cdot\text{K})$.

[eq. (13)]: I.e. $C_p = \frac{9}{2}R = \frac{9}{2} 8.31 \text{ J/(mol}\cdot\text{K)}$
 $= 37.40 \text{ J/(mol}\cdot\text{K)}$.

For $n''=3$, traditional accepted theoretical value is equation (2): I.e. $C_v = \frac{9}{2}R = \frac{9}{2} 8.31 \text{ J/(mol}\cdot\text{K)}$
 $= 37.40 \text{ J/(mol}\cdot\text{K)}$.

2. Table 2, for $n'' = 3$. Accepted adiabatic index (γ) for carbon dioxide ($n'' = 3$) based upon engineering data [22] is $\gamma = 0.844/0.655 = 1.29$. Our theoretical adiabatic index (γ) is equation (14): I.e.

$$\gamma = \frac{\frac{9}{2}}{\frac{7}{2}} = 1.29.$$

Submitted on June 16, 2017

References

- Maxwell J.C. *J. Chem. Soc.* (London), 1875, 28, 493–508; [facsimile published in Mary Jo Nye, *The Question of the Atom* (Los Angeles: Tomash 1984)].
- Reif, F. *Fundamentals of Statistical and Thermal Physics*. McGraw-Hill, New York, 1965.
- Carey V. *Statistical Thermodynamics and Microscale Thermophysics*. Cambridge University press 1999.
- Kundt A, and Warburg E. Ueber die spezifische Wärme des Quecksilbergases (On the specific heat of mercury gas). *Ann. Phys.*, 1876, 157, 353–369.
- Goldstein H. *Classical Mechanics* (2nd. ed.). Addison-Wesley, 1980.
- Wüller A., *Lehrbuch der Experimentalphysik* (Textbook of Experimental Physics). Leipzig, Teubner. Vol. 2, 507 ff, (1896).
- Maxwell J.C. (1890). On the Dynamical Evidence of the Molecular Constitution of Bodies. In WD Niven. *The Scientific Papers of James Clerk Maxwell*. Cambridge University Press. Vol.2, pp.418–438. A lecture delivered by Prof. Maxwell at the Chemical Society on 18 February 1875.
- Boltzmann L. On certain Questions of the Theory of Gases. *Nature*, 1895, v. 51(1322), 413–415.
- Planck M. On the Law of the Energy Distribution in the Normal Spectrum. *Ann. Phys.*, 1901, v. 4(553), 1–11.
- Einstein A. and Stern O. Einige Argumente Fur die Annahme einer molekularen Agitation beim absoluten Nullpunkt (Some Arguments for the Assumption of Molecular Agitation at Absolute Zero). *Ann. Phys.*, 1913, v. 40(551) 551–560.
- Dahl J.P. On the Einstein–Stern model of rotational heat capacities. *J. Chem. Phys.*, 1998, v. 109, 10688.
- Thomson W. (1904). *Baltimore Lectures*. Baltimore: Johns Hopkins University Press. Sec. 27. Re-issued in 1987 by MIT Press as *Kelvin's Baltimore Lectures and Modern Theoretical Physics: Historical and Philosophical Perspectives*. (Robert Kargon and Peter Achinstein, editors).
- Rayleigh J.W.S. The Law of Partition of Kinetic Energy. *Phil. Mag.*, 1900, v. 49, 98–118.
- Pais A. *Subtle is the Lord*. Oxford University Press. Oxford UK 1982.
- Hermann Armin (1971). *The Genesis of Quantum Theory (1899–1913)* (original title: *Frühgeschichte der Quantentheorie (1899–1913)*), translated by Claude W. Nash ed.), Cambridge, MA.
- Masi J.F., Petkof B. *J. Res. Natl. Bur. Stand.*, 1952, v. 48(3), 179–187.
- Scott R.B., Mellors J.W. *J. Res. Natl. Bur. Stand.*, 1945, v. 34, 243–248.
- Prydz R., Goodwin R.D. *J. Res. Natl. Bur. Stand.*, 1970, v. 74A(5), 661–665.
- Giguere P.A. Heat capacities for water-hydrogen peroxide systems between 25 and 60. *J. Chem. Eng. Data*, 1962, v. 7(4), 526–527.
- Chapman S., Cowling T.G. *The mathematical theory of non-uniform gases*, third edition. Cambridge University Press 1970.
- Wu L., White C., Scanlon T.J., Reese J.M. and Zhang Y. A kinetic model of the Boltzmann equation for non-vibrating polyatomic gases. *J. Fluid Mechanics*, 2015, v. 763, 24–50.
- Rolle K.C. *Thermodynamics and Heat Power* 4th edition. Maxwell Macmillian Canada, 1993.
- Mayhew K. Latent heat and critical temperature: A unique perspective. *Phys. Essays*, 2013, v. 26(4), 604–611.
- Mayhew K. *Changing our Perspective: Part 1: A New Thermodynamics* (Self-published 2015) Available at <http://www.newthermodynamics.com> and <https://createspace.com/5277845>
- Mayhew K. Improving our thermodynamic perspective. *Phys. Essays*, 2011, v. 24(3), 338–344.
- Levin K., Fetter, A., Stampur-Kurn, D. *Ultracold Bosonic and Fermionic gases*. Elsevier Press Oxford UK (2012).
- Mayhew K., A new thermodynamics. *IJRDO*, Vol. 2 Issue 1, 45 (2016) (Note: Concerning this paper: Publication has numerous equations wrong and journal did not care. Please see <http://www.newthermodynamics.com/ijrdojournaljan2016.pdf>)
- Mayhew K. Second law and lost work. *Phys. Essays*, 2015, v. 28(1), 152–155.
- Mayhew K. Entropy: an ill-conceived mathematical contrivance? *Phys. Essays*, 2015, v. 28(3), 352–357.

Exotic Matter: A New Perspective

Patrick Marquet

18 avenue du Président Wilson, 62100 Calais, France
E-mail: patrick.marquet6@wanadoo.fr

In this paper we suggest a possible theoretical way to produce negative energy that is required to allow hyperfast interstellar travels. The term “Exotic Matter” was first coined by K. Thorne and M. Morris to identify a material endowed with such energy in their famous traversable space-time wormhole theory. This possibility relies on the wave-particle dualism theory that was originally predicted by L. de Broglie and later confirmed by electrons scattering experiments. In some circumstances, an electron interacting with a specific dispersive and refracting medium, has its velocity direction opposite to that of the phase velocity of its associated wave. However, it is here shown that a positron placed in the same material exhibits a negative mass. Generalizing the obtained equations leads to an energy density tensor which is de facto negative. This tensor can be used to adequately fit in various “shortcut theories” without violating the energy conditions.

Introduction

In this paper we show that it is possible to obtain a negative energy provided the associated proper particle’s mass is variable. The basis for this study starts with the associated wave that was originally detected on electrons diffraction experiments [1]. In some circumstances, L. de Broglie showed that a particular homogeneous refractive and dispersive material may cause the tunnelling particle to reverse its velocity with respect to its wave phase propagating velocity [2]. In this case, and under the assumption that the proper mass of the particle is subject to a ultra high frequency vibration synchronized with the wave frequency, it is formally shown that an anti-particle exhibits a negative mass (energy). This energy could be extracted to sustain for example the space-time wormhole, set forth by K. Thorne and M. Morris [3, 4]. To be physically viable, it is well known that it requires a so-called exotic matter endowed with a negative energy density which violates all energy conditions [5]. However, if the exotic matter threading the inner throat of the wormhole is likened to the specific dispersive material wherein circulates a stream of antiparticles, our model does not conflict with classical physics restrictions and can be fully applied.

Notations

In this paper we will use a set of orthonormal vector basis denoted by $\{e_0, e_a\}$, where the space-time indices are $a, b = 0, 1, 2, 3$, while the spatial indices are $\mu, \nu = 1, 2, 3$. The space-time signature is $\{-2\}$.

1 Proper mass variation

1.1 Phase velocity and group velocity

It is well known that the classical wave with a frequency n

$$\psi = a(n) \exp [2\pi i(\nu t - \mathbf{k}\mathbf{r})] \quad (1)$$

propagates along the direction given by the unit vector N . Here \mathbf{k} is the 3-wave vector, $\mathbf{k}\mathbf{r} = \phi$ is the wave spatial phase, and n is the refractive index of the medium. Equation (1) is a solution of the wave propagation equation

$$\Delta\psi = \frac{1}{w^2} \frac{\partial^2\psi}{c^2\partial t^2}, \quad (1)\text{bis}$$

where w is the wave phase velocity of the wave moving in a dispersive medium whose refractive index is $n(\nu)$ generally depending of the coordinates, and which is defined by:

$$\frac{1}{w} = \frac{n(\nu)}{c}. \quad (2)$$

In our study, the medium is assumed to be homogeneous but it can be anisotropic and it will depend on the frequency ν . In this material, the phase ϕ of the wave is progressing along the given direction with a separation given by a distance

$$\lambda = \frac{w}{\nu} = \frac{c}{n\nu} \quad (2)\text{bis}$$

called the wavelength. Consider now the superposition of two stationary waves along the x -axis having each close frequencies $\nu' = \nu + \delta\nu$ and close velocities $w' = w + (dw/d\nu)\delta\nu$, so that their superposition can be expressed by:

$$\begin{aligned} & \sin 2\pi\left(\nu t - \frac{\nu x}{w}\right) + \sin 2\pi\left(\nu' t - \frac{\nu' x}{w'}\right) = \\ & = 2 \sin 2\pi\left(\nu t - \frac{\nu x}{w}\right) \cos 2\pi\left[\delta\left(\frac{\nu}{2}\right)t - x \frac{d}{d\nu} \frac{\nu}{w} \delta\frac{\nu}{2}\right]. \end{aligned}$$

The resulting wave displays a wave packet (or beat) that varies along with the so-called group velocity ($\mathbf{v} = v^g$):

$$\frac{1}{\mathbf{v}_g} = \frac{d}{d\nu} \frac{\nu}{w}. \quad (3)$$

The wave mechanics shows that the momentum 3-vector of an electron of a rest mass m_0 (in vacuum) is given by the de Broglie relation

$$\mathbf{p} = m_0 \mathbf{v} = \frac{h}{\lambda} \tag{4}$$

which completes the Einstein relation $E = h\nu$.

1.2 The plane wave spinor

Since we deal here with a spin 1/2-fermion, we must introduce the four components wave function Ψ_A expressed with the non local 4×4 Dirac trace free matrices γ_a (capital latin spinor indices are $A = B = 1, 2, 3, 0$). They display here the following real components [8]:

$$\gamma_0 = \begin{pmatrix} 0 & 0 & 0 & -1 \\ 0 & 0 & -1 & 0 \\ 0 & 1 & 0 & 0 \\ 1 & 0 & 0 & 0 \end{pmatrix}, \quad \gamma_1 = \begin{pmatrix} 0 & 0 & 0 & -1 \\ 0 & 0 & 1 & 0 \\ 0 & 1 & 0 & 0 \\ -1 & 0 & 0 & 0 \end{pmatrix},$$

$$\gamma_2 = \begin{pmatrix} 1 & 0 & 0 & 0 \\ 0 & 1 & 0 & 0 \\ 0 & 0 & -1 & 0 \\ 0 & 0 & 0 & -1 \end{pmatrix}, \quad \gamma_3 = \begin{pmatrix} 0 & 0 & -1 & 0 \\ 0 & 0 & 0 & -1 \\ -1 & 0 & 0 & 0 \\ 0 & -1 & 0 & 0 \end{pmatrix}.$$

These matrices are said standard representation as opposed for example to the Majorana representation. Moreover, they verify

$$\gamma_a \gamma_b + \gamma_b \gamma_a = -2\eta_{ab} \mathbf{I} \tag{5}$$

where η_{ab} is the Minkowski tensor and \mathbf{I} is the unit matrix. In what follows, Λ^* is the complex conjugate of an arbitrary matrix Λ , ${}^T \Lambda$ is the transpose of Λ , and $\tilde{\Lambda}$ is the classical adjoint of Λ .

Introducing now the Hermitean matrix $\beta = i\gamma_0$

$$\beta = \begin{pmatrix} 0 & 0 & 0 & -i \\ 0 & 0 & -i & 0 \\ 0 & i & 0 & 0 \\ i & 0 & 0 & 0 \end{pmatrix},$$

which verifies $\beta^2 = \mathbf{I}$, we derive the important relation

$$\beta \gamma_a \beta^{-1} = -\tilde{\gamma}_a \tag{5bis}$$

with β and the spinor Ψ , we form the Dirac conjugate [9]

$${}^\circ \Psi = t \tilde{\Psi} \beta, \tag{5ter}$$

where t is the time orientation. or the electron, the Dirac equation is written as

$$[W - (m_0)_{\text{elec}} c] \Psi = 0, \tag{6}$$

where $W = \gamma_B^A \partial_a$ is the Dirac operator and it is customary to omit the spinor indices A, B by simply writing $\gamma_a = \gamma_a^A_B$ so that this operator becomes $\gamma^a \partial_a$, or in the slash notation (Feynman), $\not{\partial}_a$. The monochromatic wave associated with the

electron can be approximated to a plane wave spinor without loss of generality [10]:

$$\Psi_A = a(x^a) \exp 2\pi i (p_a x^a), \tag{6bis}$$

where

$$p_a x^a = Et - p_\mu x^\mu. \tag{6ter}$$

The 4-vector p_a is the 4-momentum of the electron. The spinor ‘‘amplitude’’ $a(x^a)$ satisfies the Dirac equation

$$[\gamma^a (p_a)_{\text{elec}}] a = [(m_0)_{\text{elec}} c] a \tag{7}$$

where the operator $[\gamma^a (p_a)_{\text{elec}}]$ is here substituted to the Dirac operator $\gamma^a \partial_a$. We now re-write (6)bis as

$$\Psi = a(x^a) \exp(2\pi i/h) \phi, \tag{7bis}$$

where the global phase is $\phi = h[\nu - (\alpha x + \beta y + \gamma z)/\lambda] t$ (here α, β, γ are the direction cosines). The energy and momentum of the electron located at x^a are then related with the wave phase by:

$$E = \partial_t \phi, \quad \mathbf{p} = -\text{grad } \phi. \tag{7ter}$$

Now, if the electron moves at a velocity $\mathbf{v} = \beta c$ within a slight variation $\beta, \beta + \delta\beta$, corresponding to the frequency interval $\nu, \nu + \delta\nu$, w and ν are functions of β . The wave phase velocity (in vacuum) can be expressed as $w = c^2/\nu = c/\beta$ and since $\nu = (1/h) m_0 c^2 / \sqrt{1 - \beta^2}$, it is easy to infer that:

$$\mathbf{v}_g = \frac{d\nu}{d\beta} \frac{1}{\frac{d\nu}{d\beta} w} = \beta c = \mathbf{v}. \tag{8}$$

The group velocity \mathbf{v}_g of the wave packet associated with the electron of rest mass m_0 , coincides with its velocity \mathbf{v} . The group velocity is thus also expressed by the Hamiltonian form $\mathbf{v}_g = \partial E / \partial \mathbf{k}$ which corresponds to the particle’s velocity $\mathbf{v} = \partial E / \partial \mathbf{p}$. Recalling (2) and (2)bis to as $1/w = n(\nu)/c$, $\lambda = w/n\nu$, we easily infer the Rayleigh’s formulae [11]:

$$\frac{1}{\mathbf{v}_g} = \frac{1}{c} \frac{\partial n\nu}{\partial \nu} = \frac{\partial (\frac{1}{\lambda})}{\partial \nu}. \tag{9}$$

1.3 Making the electron vibrate

In the framework of the special theory of relativity, the proper frequency ν_0 of a plane monochromatic wave is transformed as

$$\nu = \frac{\nu_0}{\sqrt{1 - \mathbf{v}^2/c^2}}. \tag{10}$$

Constraint A: We assume that the electron is subject to an ultra high stationary vibration having a proper frequency ν_0 .

When moving at the velocity \mathbf{v} , this frequency is known to transform according to:

$$\nu_e = \nu_0 \sqrt{1 - \mathbf{v}^2/c^2}. \tag{11}$$

We clearly see that its frequency ν_e differs from that of its associated wave denoted here by ν .

If N is the unit vector normal to the associated wave phase, the electron subject to the frequency $\nu_0 = m_0 c^2 / h$ has traveled a distance dN during a time interval dt , so that we may define an electronic phase ϕ_e which has changed by:

$$d\phi_e = h\nu_0 \sqrt{(1 - \mathbf{v}^2/c^2)} dt = m_0 c^2 \sqrt{(1 - \mathbf{v}^2/c^2)} dt. \quad (12)$$

Simultaneously, the corresponding wave phase variation is

$$d\phi = \partial_t \phi dt + \partial_N \phi dN = (\partial_t \phi + \mathbf{v} \text{grad } \phi) dt \quad (12)\text{bis}$$

and by analogy to the classical formula (7)ter, one may write

$$\mathbf{p} = -\text{grad } \phi = \frac{m_0 \mathbf{v}}{\sqrt{1 - \mathbf{v}^2/c^2}}, \quad E = \partial_t \phi = \frac{m_0 c^2}{\sqrt{1 - \mathbf{v}^2/c^2}}$$

so we find

$$d\phi = \left[\frac{m_0 c^2}{\sqrt{1 - \mathbf{v}^2/c^2}} - \frac{m_0 \mathbf{v}^2}{\sqrt{1 - \mathbf{v}^2/c^2}} \right] dt. \quad (13)$$

Constraint B: We set the following phase synchronization:

$$d\phi = d\phi_e, \quad (14)$$

which leads to:

$$\begin{aligned} \left[\frac{m_0 c^2}{\sqrt{1 - \mathbf{v}^2/c^2}} - \frac{m_0 \mathbf{v}^2}{\sqrt{1 - \mathbf{v}^2/c^2}} \right] dt &= \\ &= \left[m_0 c^2 \sqrt{1 - \mathbf{v}^2/c^2} \right] dt. \end{aligned} \quad (15)$$

Dividing through by dt , we retrieve the famous Planck-Laué equation

$$\frac{m_0 c^2}{\sqrt{1 - \mathbf{v}^2/c^2}} = m_0 c^2 \sqrt{1 - \mathbf{v}^2/c^2} + \frac{m_0 \mathbf{v}^2}{\sqrt{1 - \mathbf{v}^2/c^2}}, \quad (15)\text{bis}$$

which holds provided the proper mass is slightly variable. (see proof in Appendix A). In the frameworks of our postulate, the ultra high frequency vibration imparted to the electron can be viewed as apparently reflecting its stationary mass variation which is likened to a fluctuation.

From now on, ${}^{\#}m_0$ will denote the variable rest mass of the electron so that the Planck-Laué relation becomes:

$$\begin{aligned} {}^{\#}E &= \frac{{}^{\#}m_0 c^2}{\sqrt{1 - \mathbf{v}^2/c^2}} = \\ &= {}^{\#}m_0 c^2 \sqrt{1 - \mathbf{v}^2/c^2} + \frac{{}^{\#}m_0 v^2}{\sqrt{1 - \mathbf{v}^2/c^2}}. \end{aligned} \quad (15)\text{ter}$$

This formulae will be required to determine the explicit form of the dispersive material which is the key point of our theory.

2 Exotic matter

2.1 Dynamics in a refracting material

Let us first recall the relativistic form of the Doppler formulae:

$$\nu_0 = \frac{\nu(1 - \mathbf{v}/w)}{\sqrt{1 - \mathbf{v}^2/c^2}}, \quad (16)$$

where as before, ν_0 is the wave's frequency in the frame attached to the electron. With the latter equation and taking into account the classical Planck relation $E = h\nu$, we find

$$E = \frac{E_0 \sqrt{1 - \mathbf{v}^2/c^2}}{1 - \mathbf{v}/w}. \quad (17)$$

However, inspection shows that the usual equation

$$E = \frac{E_0}{\sqrt{1 - \mathbf{v}^2/c^2}} \quad (18)$$

holds only if

$$1 - \frac{\mathbf{v}}{w} = 1 - \frac{\mathbf{v}^2}{c^2}, \quad (19)$$

which implies

$$w \mathbf{v} = c^2. \quad (20)$$

The latter relation is satisfied provided we set

$${}^{\#}E = \frac{{}^{\#}m_0 c^2}{\sqrt{1 - \mathbf{v}^2/c^2}}, \quad (21)$$

$${}^{\#}\mathbf{p} = \frac{{}^{\#}m_0 \mathbf{v}}{\sqrt{1 - \mathbf{v}^2/c^2}}. \quad (22)$$

Constraint C: ${}^{\#}E$ depends on a specific dispersive and refracting material through which the electron is tunnelling.

Let us define this influence by a function $Q(n)$ where n is the refractive index of the material. Note: The variation of the proper mass is independent on $Q(n)$. Equation (21) is modified to as

$${}^{\#}E = \frac{{}^{\#}m_0 c^2}{\sqrt{1 - \mathbf{v}^2/c^2}} + Q(n) \quad (23)$$

from which Eq. (22) can be expressed as:

$${}^{\#}\mathbf{p} = \frac{{}^{\#}m_0 \mathbf{v}}{\sqrt{1 - \mathbf{v}^2/c^2}} = \frac{\mathbf{v} [{}^{\#}E - Q(n)]}{c^2}. \quad (24)$$

Now taking into account the Doppler formulae (16), and the Planck-Laué relation (15)ter, we find

$${}^{\#}E - \frac{\mathbf{v}^2 [{}^{\#}E - Q(n)]}{c^2} = {}^{\#}E \left(1 - \frac{\mathbf{v}}{w} \right) \quad (25)$$

wherefrom is inferred

$$Q(n) = \#E \left(1 - \frac{c^2}{w \mathbf{v}}\right) = h\nu \left(1 - \frac{c^2}{w \mathbf{v}}\right) \quad (26)$$

and with the Rayleigh formulae (4), we eventually obtain the explicit form of $Q(n)$:

$$Q(n) = \#E \left[1 - \frac{n\partial(n\nu)}{\partial\nu}\right]. \quad (27)$$

2.2 Specific dispersive material

Depending on the nature of the dispersive material, thus its index (n), it is well known that the tunnelling electron's 3-velocity \mathbf{v} can be directed either in the direction of the associated wave phase velocity w or in the opposite direction. The electron then moves backward through the specific material.

Let N be the 3-unit vector directed to the wave phase direction (chosen positive) so that the wave number is given by:

$$\mathbf{k} = \frac{Nh}{\lambda}. \quad (28)$$

By applying the Rayleigh formulae (4) to this particular case where \mathbf{v} is opposite to the wave phase propagation, we have $\mathbf{v} < 0$. Hence, from $Q(n) = \#E (1 - c^2/w \mathbf{v})$, we find

$$\#E - Q(n) = \frac{\#Ec^2}{w \mathbf{v}} \quad (29)$$

which is negative.

Then, with $\mathbf{p} = \#m_0 \mathbf{v} / \sqrt{1 - \mathbf{v}^2/c^2}$, we infer from (24):

$$\frac{\#m_0}{\sqrt{1 - \mathbf{v}^2/c^2}} = \frac{\#E - Q(n)}{c^2}. \quad (29)\text{bis}$$

In order to maintain the variable proper mass $\#m_0$ positive i.e.

$$\#m_0 = \sqrt{(1 - \mathbf{v}^2/c^2)} \frac{\#E}{w \mathbf{v}} > 0 \quad (30)$$

we must have necessarily: $\mathbf{p} = -\mathbf{k}$.

2.3 Matching the exotic matter definition

Now consider a stream of electrons and positrons placed in the specific material whose respective associated wave (positive) direction is given by the same unit vector N (i.e. $w > 0$). From the Dirac theory, we know that the electron momentum 3-vector \mathbf{p}_{elec} and that of the positron momentum 3-vector \mathbf{p}_{pos} are opposed. (See proof in Appendix B). Therefore we have here $\mathbf{p}_{\text{pos}} = \mathbf{k}$, however the dispersive material yet imposes $\mathbf{v}_{\text{pos}} < 0$, hence, we are led to the fundamental conclusion:

A positron moving at the backward velocity \mathbf{v}_{pos} through the specific dispersive refracting material defined above and

subject to Constraints A, B and C, will exhibit a negative mass given by:

$$(\#m_0)_{\text{pos}} = \sqrt{1 - \mathbf{v}_{\text{pos}}^2/c^2} \frac{\#E}{w \mathbf{v}} < 0, \quad (30)\text{bis}$$

where $\#E - Q(n) = \#Ec^2/w_{\text{pos}} < 0$ in accordance with Eq. (29).

Let us write the mass (30)bis as:

$$(\#m_0)_{\text{pos}} = \int (\#\rho_0)_{\text{pos}} \sqrt{-g} dV, \quad (31)$$

where $(\#\rho_0)_{\text{pos}}$ is the variable proper density of the positronic massive flow. The integral is performed over the 3-volume V delimiting the variable proper mass $(\#m_0)_{\text{pos}}$ boundary. We then readily infer the familiar form of the energy density tensor in the static case

$$(\#T_0^0)_{\text{pos}} = (\#\rho_0)_{\text{pos}} c^2, \quad (32)$$

which is de facto negative.

So, within the scheme of the wave-particle picture, we have been able to give a consistent picture of what could be the united conditions to reach our goal :

The so-called "exotic matter" required to assemble a space-time distortion can be provided by the negative energy extracted from a stream of vibrating antifermions interacting with a specific dispersive refracting material adequately engineered.

3 Concluding remarks

Without going into details of a sound engineering, we have here only scratched the surface of a basic theory describing the ability of a system composed of antiparticles to interact with a specific refracting and dispersive material in order to exhibit a dynamical negative mass.

Thus, our approach mainly relies on de Broglie's theory which has been verified for the electron.

Upon Constraints A, B, and C, we might as well consider other heavier particles such as the antiproton to produce negative energy.

Once these conditions are fulfilled, the concept of hyperfast interstellar travel is viable if one can "handle" routinely antimatter, and envision a sufficient amount of negative energy density. These orders of magnitude are beyond the scope of this text.

Without any doubt, some advanced civilizations have already long mastered the negative energy obtained by this process, to achieve superluminal travels as described by space-time warp drive theories [12–14].

For us, a huge research work is still ahead, but if we have contributed to open a small door, then the challenge is widely available for physicists.

Appendix A: The Planck-Laué relation

The Planck-Laué relation is a relativistic equation which has been derived when the proper mass is assumed to slightly fluctuate. This proper mass is here denoted by ${}^{\#}m_0$. Under this circumstance, the relativistic dynamics of ${}^{\#}m_0$ can now be extended as follows.

We first write the Lagrange function for an observer who see the particle moving at the velocity \mathbf{v}

$$L = -{}^{\#}m_0 c^2 \sqrt{1 - \mathbf{v}^2/c^2}$$

so that the least action principle applied to this function is still expressed by

$$\delta \int_{t_0}^{t_1} L dt = \delta \int_{t_0}^{t_1} -{}^{\#}m_0 c^2 \sqrt{1 - \mathbf{v}^2/c^2} = 0.$$

From this principle the equations of motion

$$\frac{d}{dt} \left(\frac{\partial L}{\partial \dot{x}_a} \right) = \frac{\partial L}{\partial x_a}, \quad \dot{x}_a = \frac{dx_a}{dt},$$

are inferred, which lead to

$$\frac{d{}^{\#}\mathbf{p}}{dt} = -c^2 \sqrt{1 - \mathbf{v}^2/c^2} \text{grad } {}^{\#}m_0 \quad (\text{A.1})$$

(since ${}^{\#}m_0$ is now variable). Hence, by differentiating the relativistic relation ${}^{\#}E^2/c^2 = {}^{\#}p^2 + {}^{\#}m_0^2 c^2$, we obtain

$$\frac{d{}^{\#}E}{dt} = c^2 \sqrt{1 - \mathbf{v}^2/c^2} \frac{\partial {}^{\#}m_0}{\partial t}. \quad (\text{A.2})$$

Combining (A.1) and (A.2) readily gives

$$\frac{d{}^{\#}E}{dt} - \mathbf{v} \cdot \frac{d{}^{\#}\mathbf{p}}{dt} = c^2 \sqrt{1 - \mathbf{v}^2/c^2} \frac{d{}^{\#}m_0}{dt}, \quad (\text{A.3})$$

where $d{}^{\#}m_0/dt = \partial {}^{\#}m_0/\partial t + \text{grad } {}^{\#}m_0$ is the variation of the mass in the course of its motion. On the other hand, we have

$$\begin{aligned} \frac{d({}^{\#}\mathbf{p} \cdot \mathbf{v})}{dt} &= \frac{\mathbf{v} \cdot d{}^{\#}\mathbf{p}}{dt} + {}^{\#}m_0 c^2 \frac{(\mathbf{v}/c) d(\mathbf{v}/c) dt}{\sqrt{1 - \mathbf{v}^2/c^2}} = \\ &= \mathbf{v} \cdot \frac{d{}^{\#}\mathbf{p}}{dt} - {}^{\#}m_0 c^2 \frac{d}{dt} (1 - \mathbf{v}^2/c^2) \end{aligned} \quad (\text{A.4})$$

i.e.

$$\begin{aligned} \frac{d}{dt} [{}^{\#}m_0 c^2 \sqrt{1 - \mathbf{v}^2/c^2}] &= \\ &= c^2 \sqrt{1 - \mathbf{v}^2/c^2} \frac{d{}^{\#}m_0}{dt} + {}^{\#}m_0 c^2 \frac{d}{dt} \sqrt{1 - \mathbf{v}^2/c^2} \end{aligned}$$

hence (A.3) can be re-written as

$$\frac{d}{dt} [{}^{\#}E - \mathbf{v} \cdot {}^{\#}\mathbf{p} - {}^{\#}m_0 c^2 \sqrt{1 - \mathbf{v}^2/c^2}] = 0 \quad (\text{A.5})$$

which is satisfied when the particle is at rest, that is: $\mathbf{v} = 0 \Rightarrow {}^{\#}E_0 = {}^{\#}m_0 c^2$. Therefore, we must always have:

$${}^{\#}E = \frac{{}^{\#}m_0 c^2}{\sqrt{1 - \mathbf{v}^2/c^2}} = {}^{\#}m_0 c^2 \sqrt{1 - \mathbf{v}^2/c^2} + \frac{{}^{\#}m_0 \mathbf{v}^2}{\sqrt{1 - \mathbf{v}^2/c^2}}. \quad (\text{A.6})$$

It is important to note that this variable (proper) mass, ${}^{\#}m_0$, is purely intrinsic, i.e. its motion is unaffected.

Equation (A.6) is known as the Planck-Laué formula.

Appendix B: Dirac currents

Let us consider the real Dirac current as

$$J^a = i ({}^{\circ}\Psi \gamma^a \Psi) = (J^a)_1 - (J^a)_2,$$

where

$$(J^a)_1 = i {}^{\circ}\Psi_A \gamma_B^{aA} \Psi^B, \quad (J^a)_2 = i \Psi^B \gamma_B^{aA} {}^{\circ}\Psi_A.$$

The charge conjugate of J^a is first calculated

$$[(J^a)_1]^{(C)} = i \Psi_A^* \gamma_B^{aA} \Psi^{*B} = i t^T \Psi_A \beta_B^A \gamma_C^{aB} \Psi^{*C}$$

i.e.

$$[(J^a)_1]^{(C)} = i t \Psi^A \beta_B^A \gamma_B^{aC} \Psi^{*C}.$$

From the antisymmetry of β , and remembering that the γ^a are here *real*, we have

$${}^T \gamma^a \beta = -\tilde{\gamma}^a \beta = \beta \gamma^a$$

from which we infer

$$[(J^a)_1]^{(C)} = i t \Psi^A \gamma_A^{aB} \beta_B^C \tilde{\Psi}_C = i \Psi^A \gamma_A^{aB} {}^{\circ}\Psi_B$$

hence, we see that

$$[(J^a)_1]^{(C)} = (J^a)_2$$

and similarly

$$[(J^a)_2]^{(C)} = (J^a)_1$$

therefore, we obtain the most important relation:

$$-(J^a)^{(C)} = J^a \quad (\text{B.1})$$

The Dirac current orientation is opposed to that of its Dirac conjugate [15]. The Dirac conjugate ${}^{\circ}\Psi$ of the plane wave spinor (6)bis is here:

$${}^{\circ}\Psi = {}^{\circ}a \exp -2\pi i (p_a x^a). \quad (\text{B.2})$$

With the Dirac conjugate spinor amplitude ${}^{\circ}a = a^* \gamma^0$, that is equivalent to (5)ter, we first set the normalization condition:

$${}^{\circ}a a = m_0 c. \quad (\text{B.3})$$

Besides, the Dirac equation reads:

$$(\gamma^a p_a) {}^{\circ}a = m_0 c {}^{\circ}a. \quad (\text{B.4})$$

Due to the property of $(\gamma^a)^2$, Equations (7) and (B.4) are both satisfied for:

$$(p_a)^2 = (m_0 c)^2. \quad (\text{B.5})$$

Multiplying now Equation (7) on the left with ${}^\circ a$, we obtain with (B.2) and (B.5)

$$({}^\circ a \gamma^a a) p_a = (m_0 c)^2 = (p_a)^2 \quad (\text{B.6})$$

from which we infer:

$${}^\circ a \gamma^a a = p^a. \quad (\text{B.7})$$

The Dirac current density vector $J^a = {}^\circ \Psi \gamma^a \Psi$ will here yield

$$J^a = {}^\circ a \gamma^a a = p^a \quad (\text{B.8})$$

with

$$p^a = m_0 c^2 + p^\mu \quad (\text{B.9})$$

([16]: compare with formulae (23.6) there).

From the charge conjugate $\Psi^{(C)}$ corresponding to the positron plane spinor, we define the Dirac current for the positron $(J^a)^{(C)}$. However, it was shown that $(J^a)^{(C)} = -J^a$. Therefore, assuming that $(m_0)_{\text{elec}} = (m_0)_{\text{posit}}$ in vacuum, we must then have

$$(J^\mu)^{(C)} = (p^\mu)_{\text{posit}} = -(p^\mu)_{\text{elect}}. \quad (\text{B.10})$$

This clearly means that in vacuum, $\mathbf{v}_{\text{posit}} = -\mathbf{v}_{\text{elect}}$.

Submitted on May 15, 2017

References

1. Davisson C.J., Germer L.H. The Diffraction of electrons by a crystal of Nickel. *Proc. of the National Acad. of Sci. of the USA*, 1 April 1928, v. 14, no. 4, 317–322.
2. de Broglie L. Etude du mouvement des particules dans un milieu réfringent. *Ann. Inst. Henri Poincaré*, 1973, v. XVIII, no. 2, 89–98.
3. Morris M., Thorne K. Wormholes in spacetime and their use for interstellar travel. *Am. J. Phys.*, 1988, v. 56, 395.
4. Morris M., Thorne K., Yurtzever U. *Phys. Rev. Letters*, 1988, v. 61, 1446.
5. Hawking S.W., Ellis G.F.R. *The Large Scale Structure of Space-Time*. Cambridge University Press, 1987.
6. Kramer D., Stephani H., Hertl E., MacCallum M. *Exact Solutions of Einstein's Field Equations*. Cambridge University Press, 1979.
7. Marquet P. A space-time wormhole sustained by the electromagnetic field. *The Abraham Zelmanov Journal*, 2011, v. 4, 92–107.
8. Lichnérowicz A. Champs spinoriels et propagateurs en Relativité Générale. *Bulletin. Soc. Mathématique de France*, 1964, t. 92. p. 11 à 100.
9. Moret-Bailly F. Le champ neutrinique en Relativité Générale. *Ann. Institut Henri Poincaré*, sec. A: 1966, v. 4, 301–355.
10. Marquet P. On the physical nature of the de Broglie wave. *Progress in Physics*, 2016, v. 12, issue 4, 318–322.
11. de Broglie L. *Éléments de la théorie des quanta et de la mécanique ondulatoire*. Gauthier-Villars, Paris, 1959.
12. Alcubierre M. The Warp Drive: hyper fast travel within General Relativity. *Class. Quantum Gravity*, 1994, v. 11, L73–L77.
13. Natario J. Warp Drive with zero expansion. *Class. Quantum Gravity*, 2002, v. 19, no. 6, 1157–1165.
14. Krasnikov S. The quantum inequalities do not forbid spacetime shortcuts. arXiv: gr-qc/020705.
15. Lichnérowicz A. Champ de Dirac, champ du neutrino et transformations C, P, T sur un espace courbe. *Ann. Institut Henri Poincaré*, sec. A: 1964, v. 3, p.233–290.
16. Bereteviski V.L., Lifshitz E., Pitayevski L. *Electrodynamique Quantique*. Edition Mir, Moscow, 1973.

Testing 5D Gravity with LIGO for Space Polarization by Scalar Field

T. X. Zhang

Department of Physics, Alabama A & M University, Normal, Alabama 35762
E-mail: tianxi.zhang@aamu.edu

Whether LIGO detectors can directly detect the scalar field dark energy and thus test the five-dimensional (5D) gravity or not is examined analytically in terms of the author previously well-developed 5D fully covariant theory of gravitation with a scalar field. It is shown that an object with some thousand kilograms (e.g. 4700 kg), if electrically charged up to some ten kilovolts (e.g. 40 kV), can polarize the space or vacuum by the scalar field dark energy of the charged object and thus be able to extend the optical path length of a laser beam that travels through one LIGO arm with some hundred reflections (e.g. 280) by approximately 4×10^{-19} m (or the space-polarization strain of 10^{-22}), which is the amount of 4 times greater than that to be detected by the LIGO detectors. Switching on and off the power to the object, we can carry out tests of this 5D gravity by examining whether the converging laser beams become out of phase and thus the interference pattern varies or not. We can also apply a harmonically varying voltage with a frequency, e.g. 100 Hz, to charge the object and thus produce a varying optical length difference in the specific frequency range of LIGO detectors. Therefore, being added a highly charged sphere into the experimental setup, LIGO, which has recently detected first ever the gravitational waves from binary black hole mergers, can directly examine the existence of the scalar field dark energy of 5D gravity in a ground-base experiment. This study provides a design criterion for this new approach and experiment of discovering dark energy as well as testing 5D gravity.

1 Introduction

The observed acceleration of the present universe is generally attributed to the existence of dark energy throughout the universe [1-2]. A direct detection of the dark energy, whose true nature remains elusive, has become one of the most important issues in the modern astrophysics and cosmology since the discovery of acceleration of the universe. Two commonly accepted candidates of dark energy are the cosmological constant and the quintessence. Unlike the cosmological constant, which Albert Einstein first introduced into his general theory of relativity in order for the universe to be static, the quintessence is a scalar field Φ that varies throughout space-time and has been modeled in various theories of gravitation such as the four-dimensional (4D) Brans-Dicke scalar-tensor gravity [3] and the five-dimensional (5D) Kaluza-Klein scalar-vector-tensor gravity (shortened by 5D gravity) [4-6].

The scalar field of 5D gravity, which has been recently related to the Higgs field of 4D particle physics in [7], were theoretically shown to be capable of polarizing the space or vacuum [8-9] and thus able to extend the optical path length of a laser beam that travels through the polarized vacuum. The vacuum polarization by a scalar field has been studied in the Schwarzschild spacetime [10], in a waveguide [11], in the de Sitter spacetime with the presence of global monopole [12], and in a homogeneous space with an invariant metric [13]. Recently, the author, in terms of his 5D fully covariant theory of gravitation, has quantitatively determined the dielectric constant of the polarized vacuum in accordance with

the charge-mass ratio of a charged object [14].

In this paper, we will further analytically demonstrate that the vacuum polarization by the scalar field dark energy of 5D gravity can increase the relative optical path length (i.e. the strain) above a factor of 10^{-22} and therefore can be directly detected via the extremely accurate LIGO detectors that have recently detected first ever the gravitational waves from the binary black hole merger as declared in [15]. We will use a harmonic voltage to charge the object, which leads to a varying optical length difference in the frequency range of the LIGO detection. A positive result of detecting the scalar field dark energy by LIGO will provide a fundamental test of 5D gravity.

2 5D gravity and vacuum polarization by scalar field dark energy

2.1 5D gravity with scalar field and field solution

A 5D gravity is a Kaluza-Klein theory that unifies the 4D Einsteinian general relativity (GR) and Maxwellian electromagnetism (EM). Without a scalar field (i.e. $\Phi = 1$), the 5D unification is trivial because, in the (4+1) split form, it is identical to GR and EM. With a scalar field, however, a 5D gravity can lead to a sequence of new effects such as the space or vacuum polarization [8-9, 14], electric redshift [16], gravitational field shielding [17-18], gravitationless black hole [19], modified neutron star mass-radius relation [20], and so on. A 5D gravity with the Friedmann-Lemaître-Robertson-Walker (FLRW) metric of the universe modifies the Friedmann equa-

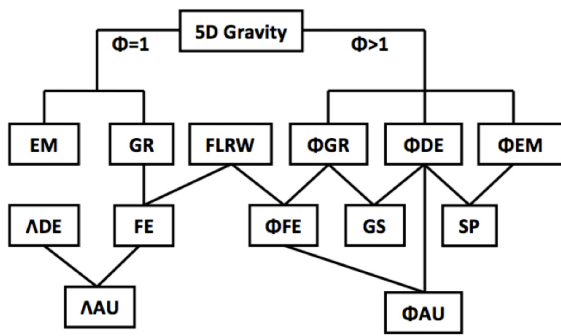


Fig. 1: Characteristics of 5D gravity with and without a scalar field dark energy (Φ DE). Without a scalar field (i.e. $\Phi = 1$), 5D gravity just trivially unifies the 4D Einsteinian general relativity (GR) and Maxwellian electromagnetism (EM). Combining with the Friedmann-Lemaître-Robertson-Walker (FLRW) metric of 4D spacetime, the field equation given in GR derives the Friedmann equation (FE) that governs the dynamic and development of the universe. Including the cosmological constant dark energy (Λ DE), FE explains the acceleration of the universe (Λ AU). With a scalar field (i.e. $\Phi > 1$), 5D gravity modifies the general relativity (Φ GR) and electromagnetism (Φ EM) through the scalar field dark energy (Φ DE). These modifications lead to a sequence of new effects such as the space or vacuum polarization (SP) and the gravitational field shielding (GS). Combining with the FLRW metric of 4D spacetime, Φ GR derives a modified Friedmann equation (Φ FE), which can also explain the acceleration of the universe (Φ AU) but due to the scalar field dark energy (Φ DE). The space polarization (SP) or the effect on light by the Φ DE of 5D gravity can be significant enough for the accurate LIGO detectors to detect.

tion with a scalar field, which plays the role of dark energy and explains the acceleration of the universe [21-23]. These new effects are results of the scalar field that modulates both gravitational and electromagnetic fields as shown in the (4+1) split form of the 5D field equation or as seen in the field solutions [14, 24]. Figure 1 shows the characteristics of a 5D gravity with and without a scalar field dark energy and its role to the cosmology.

The metric of 5D spacetime is usually given by [25]:

$$\bar{g}_{\alpha\beta} = \begin{pmatrix} g_{\mu\nu} + q^2\Phi^2 A_\mu A_\nu & q\Phi^2 A_\nu \\ q\Phi^2 A_\mu & \Phi^2 \end{pmatrix} \quad (1)$$

where α and β are the subscripts for the 5D coordinates, running through 0 - 4; μ and ν are the subscripts for the 4D coordinates, running through 0 - 3; $g_{\mu\nu}$ is the metric of 4D spacetime; A_μ is the standard 4D electromagnetic potential; Φ is the scalar field, which is an effectively massless 4D scalar; q is a scale constant defined by $q = 2\sqrt{G}$ with G the gravitational constant. The fifth dimension is compact [26]. In isotropic coordinates, the line element ds^2 of 4D spacetime can be represented according to the metric as [27]

$$ds^2 = -g_{\mu\nu} dx^\mu dx^\nu$$

$$ds^2 = -e^\nu dt^2 + e^\lambda (dr^2 + r^2 d\theta^2 + r^2 \sin^2 \theta d\phi^2), \quad (2)$$

where e^λ and e^ν are the metric rr - and tt -components as functions of the radial distance r . Then, the exact static spherically symmetric solution of gravitational, electromagnetic, and scalar fields of a charged body is given by [24]

$$e^\lambda = \left(1 - \frac{B^2}{r^2}\right)^2 \Psi^{-2}, \quad (3)$$

$$e^\nu = \Psi^2 \Phi^{-2}, \quad (4)$$

$$H_{01} = -H_{10} = -\frac{Q}{r^2} e^{(\nu-\lambda)/2}, \quad (5)$$

$$\Phi^2 = a_1 \Psi^{p_1} + a_2 \Psi^{p_2}, \quad (6)$$

where the function Ψ is defined by

$$\Psi = \left(\frac{r-B}{r+B}\right)^{C/2B}, \quad (7)$$

and the seven constants (K , p_1 , p_2 , B , C , a_1 , and a_2) are constrained by the following five relations:

$$K = 4(4B^2 - C^2)C^{-2}, \quad (8)$$

$$a_1 + a_2 = 1, \quad (9)$$

$$p_1 = 1 + \sqrt{1+K}, \quad (10)$$

$$p_2 = 1 - \sqrt{1+K}, \quad (11)$$

$$Q^2 = -a_1 a_2 C^2 (1+K)G^{-1}. \quad (12)$$

Here H_{01} and H_{10} are non-zero components of the effective 4D electromagnetic field $H_{\mu\nu} \equiv \phi^3 F_{\mu\nu}$ with $F_{\mu\nu} = \partial_\nu A_\mu - \partial_\mu A_\nu$. At $r \rightarrow \infty$, the limits of e^λ , e^ν , and Φ are the unity. The parameter Q denotes the electric charge. It is obvious that the above 5D solution of the fields includes two independent constants.

In a traditional 5D gravity, one usually assumes or hypothetically forms the fifteenth component (\bar{T}^{44}) of the 5D energy-momentum tensor by including an undetermined parameter called scalar charge S , e.g. $\bar{T}^{44} = S\rho$ as done by [24] with ρ the density of matter. Since it lacks of any measurement and short of any observational support, the undetermined parameter makes all results obtained from the traditional 5D gravity to be non-decisive and hence non-conclusive in comparison with other theories of gravitation, observations, and experiments. Describing the matter to be also covariant in the 5D spacetime as the fields are, however, this author analytically derived the fifteenth component of the 5D energy-momentum tensor without assuming any unknown parameter ([14] and references therein such as the early studies by the author [28-29]),

$$\bar{T}^{44} = \frac{\rho\alpha^2}{\Phi^2 \sqrt{\Phi^2 + \alpha^2}}, \quad (13)$$

where α is a non-dimensional constant (or charge-mass ratio) defined by

$$\alpha = \frac{Q}{2\sqrt{GM}}, \quad (14)$$

with M the mass of matter, and therefore analytically determined all the constants in the solution as follows

$$K = 8, \quad p_1 = 4, \quad p_2 = -2, \quad (15)$$

$$a_1 = -\alpha^2, \quad a_2 = 1 + \alpha^2, \quad (16)$$

$$C = \frac{2GM}{3c^2\sqrt{1+\alpha^2}}, \quad B = \frac{GM}{c^2\sqrt{3(1+\alpha^2)}}. \quad (17)$$

Here the cgs or Gaussian unit system is adapted. This set of constants is the simplest and most elegant, because of $K = 8$ that leads to p_1 and p_2 to be whole numbers, for the solution to be non-trivial. Therefore, according to this solution with the constants obtained, the gravitational, electromagnetic, and scalar fields of a charged spherically symmetric object are completely determined from the charge and mass of the object.

In the Einstein frame, this field solution simply reduces to the Schwarzschild solution of the Einsteinian general relativity when matter is neutral and fields are weak [14,17]. This guarantees that the fundamental tests of the Einsteinian general relativity in the case of weak fields are also the tests of this 5D gravity. In the case of strong fields, especially when matter is electrically charged, however, the results obtained from this 5D gravity are significantly different from the Einsteinian general relativity. These new strong field effects include the space polarization [8, 14], electric redshift [16], gravitational field shielding [17-18], and so on. At $\Phi = 1$, the 5D gravity is trivially equivalent to GR and EM, where the Reissner-Nordstrom solution determines the standard GR metric of a charged, massive particle [30-31]. The solution of this 5D gravity Eq. (3) is obtained at $\Phi \neq 1$ and thus cannot be limited to the Reissner-Nordstrom solution for a charged, massive particle. But when fields are weak and matter is weakly charged, the effect of the scalar field on both gravitational and electromagnetic fields are negligible.

2.2 Vacuum polarization by scalar field

In terms of this 5D gravity and the field solution obtained, the electric field of a charged body can be defined as

$$E \equiv H_{10} = -H_{01} = \frac{Q}{r^2} e^{(\nu-\lambda)/2}, \quad (18)$$

and then the dielectric constant (or relative permittivity) ϵ_r of the vacuum that is polarized by the scalar field can be determined by

$$\epsilon_r \equiv \frac{E_C}{E} = e^{(\lambda-\nu)/2} = \left(1 - \frac{B^2}{r^2}\right) \Phi \Psi^{-2}, \quad (19)$$

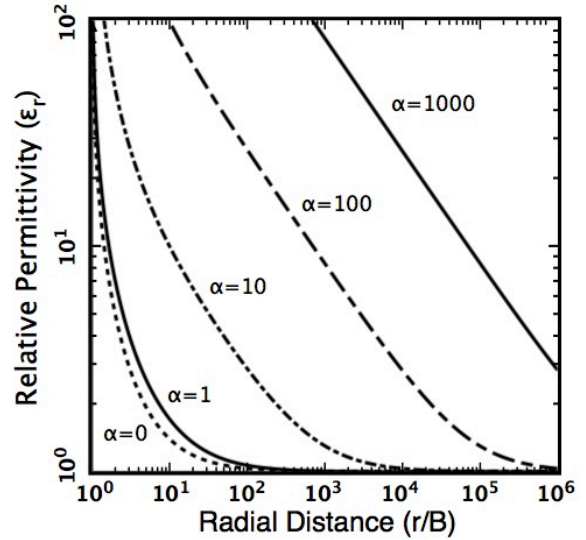


Fig. 2: The relative permittivity ϵ_r or the electric field ratio E_C/E versus the normalized radial distance r/B for a charged object with $\alpha = 0, 1, 10, 100, 1000$, respectively.

where $E_C = Q/r^2$ is the Coulomb electric field of the charged object. To see how significant the space or vacuum polarization is, we plot, in Figure 2, the relative permittivity ϵ_r as a function of the normalized radial distance r/B for a charged object with five different charge-mass ratios $\alpha = 0, 1, 10, 100, 1000$.

The result indicates that the electric field of the charged object asymptotically approaches the Coulomb electric field (i.e. $\epsilon_r \rightarrow 1$), when r is getting larger ($r \gg B$) or approaches infinity. When r becomes small, however, the electric field significantly deviates from the Coulomb electric field (i.e. $\epsilon_r \gg 1$) due to the vacuum space to be extensively polarized by the strong scalar field. When r tends to B , the relative permittivity approaches infinity and the electric field becomes weaker and weaker as compared with the strength of the Coulomb electric field, especially when the object is highly charged. In the limit case of $\epsilon_r = \infty$, the vacuum space is completely polarized by the extremely strong scalar field. It should be noted that a big deviation at $r \sim B$ still exists even if the object is weakly charged ($\alpha \ll 1$) or neutral. The deviation increases as the charge increases. For instance, at $\alpha = 100$ and $r/B = 10^3$, the electric field is only 10% of the Coulomb electric field. The electric field is significantly weakened as compared with the strength of the Coulomb electric field and the vacuum space is greatly polarized, especially when the object is highly charged.

Only for a massive, compact and charged object, we can have a B not to be too small in comparison with its radius and can see a significant polarization of the vacuum. For a lab-sized object, the polarization of the vacuum can only be extremely weak. Figure 3 plots the deviation of the rel-

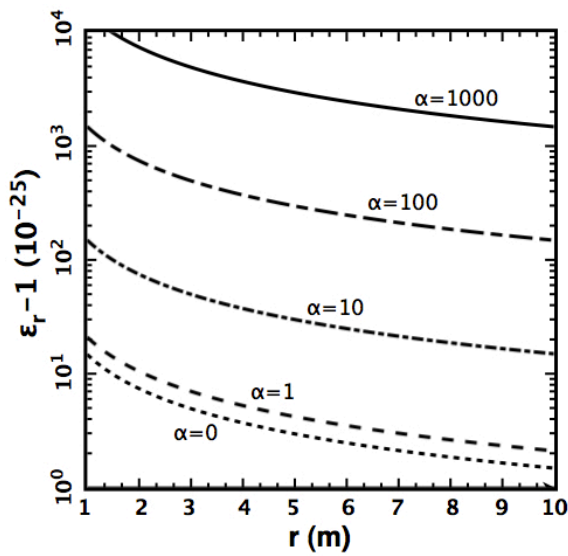


Fig. 3: The change of the relative permittivity $\epsilon_r - 1$ or the change of relative electric field $(E_c - E)/E$ versus the radial distance r for a charged object with mass of 1000-kg and charge-mass ratio $\alpha = 0, 1, 10, 100, 1000$, respectively.

ative permittivity of the vacuum from the unity, $\epsilon_r - 1$, due to the polarization as a function of the radial distance r for a charged object with mass of 1000 kilograms and charge in a range of $\alpha = 0 - 1000$. It is seen that, because the fields of a non-massive object are too weak, the polarization of the vacuum by the scalar field dark energy of 5D gravity is very very small and thus extremely difficult to be detected in laboratory, except for us to have an extremely accurate detector with an appropriate approach. In the following section, we will examine whether the LIGO detectors can detect such small vacuum polarization or not. The answer as shown in the next section is positive when the charge-mass ratio of the charged body is much greater than 1.

3 Can LIGO detect the scalar field dark energy?

In accordance with the relative permittivity determined above, we can find the refractive index of the vacuum that is polarized by the scalar field of 5D gravity as,

$$n \equiv \sqrt{\epsilon_r} = e^{(\lambda-v)/4}. \quad (20)$$

For the non-polarized vacuum, we have $n = 1$ and $\epsilon_r = 1$. Substituting Eqs. (3) and (4) into Eq. (20), we have

$$n = \Phi^{1/2} \Psi^{-1} \left(1 - \frac{B^2}{r^2} \right)^{1/2}. \quad (21)$$

In the case of weak fields, we can obtain the change of the refractive index for the polarized vacuum as,

$$\delta n = n - 1 \simeq \frac{\sqrt{1 + \alpha^2} GM}{c^2 r}, \quad (22)$$

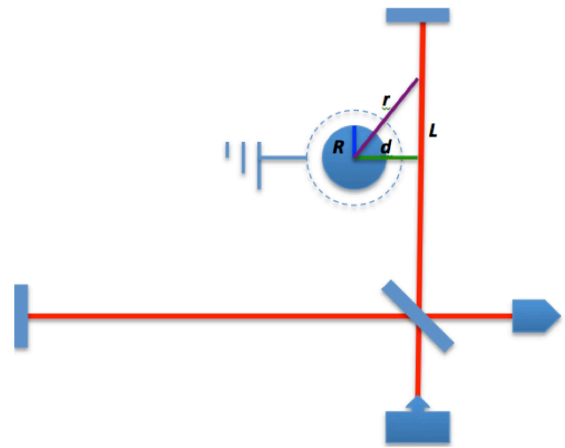


Fig. 4: A schematic diagram for LIGO with a charged object to detect the scalar field dark energy of 5D gravity. When we place a highly charged object, whose strong electromagnetic fields are shielded by a conductor shell that is grounded, nearby one path of the LIGO laser beams. The space surrounding the charged object and the vacuum travelled through by the laser beam back and forth are polarized by the scalar field of the charged object. This polarization extends the optical path length of the laser beam to be significant enough for the accurate LIGO to detect the scalar field dark energy.

When $\alpha \gg 1$, δn is about linearly increasing with α . Then, the change of the optical path length of the polarized space or vacuum can be obtained by the following path line integration

$$\delta l = \int_C \delta n ds. \quad (23)$$

To quantitatively estimate the polarization, we consider a metal (e.g. copper) sphere with radius $R = 0.5$ m. From the mass density of copper $\rho = 9 \times 10^3$ kg/m³, we can find the mass of the sphere to be $M = 4\pi\rho R^3/3 \sim 4.7 \times 10^3$ kg. Now, if the sphere is electrically charged up to $V = 10^5$ V, we can also calculate the charge Q and charge-mass ratio α of the sphere as $Q = 4\pi\epsilon_0 R V \sim 5.6 \times 10^{-6} C = 1.7 \times 10^4$ esu and $\alpha \sim 7$, respectively. Then, from Eq. (22), we can find the change of the refractive index in the space surrounding the charged sphere to be $\delta n = 1.2 \times 10^{-23}$. Here, we have chosen as an example the radial distance to be 4 radii of the object, i.e. $r = 2$ m. This result indicates that the scalar field of the charged object can extend the optical path length relatively by $\sim 1.2 \times 10^{-23}$ m for each meter, which is significant enough for the accurate LIGO detectors to detect.

Now, we suggest to place this charged object into the LIGO system nearby the middle of the path of one of the two perpendicular arms or laser beams (Figure 4). Then, the variation of the optical path length due to the space polarization by the scalar field dark energy can be estimated by,

$$\Delta L = (N + 1) \int_{-L/2}^{L/2} \delta n ds$$

$$\Delta L = \frac{(N+1)\sqrt{1+\alpha^2}GM}{c^2} \ln \frac{L + \sqrt{L^2 + 4d^2}}{-L + \sqrt{L^2 + 4d^2}}, \quad (24)$$

where N is the number of reflections of the laser beam, L is the geometric length of the arm, d is the minimum distance from the center of the charged object to the laser beam, and s is the coordinate of position to be integrated along the path from $-L/2$ to $L/2$. For the LIGO working parameters, we can choose $N = 280$ and $L = 4$ km. The distance can be chosen again as 4 radii of the charged object, i.e. $d = 2$ m. Then, we can obtain that the optical length of the 4 km path of the LIGO laser beam with 280 times reflections is increased due to the space polarization by $\Delta L \sim 10^{-18}$ m, about the amount of one order higher than that being detectable by LIGO. Similarly to the gravitational-wave strain defined in [15], we can define a strain for the space polarization by scalar field, h , as the change of the optical length dividing by the length of the LIGO arm L ,

$$h \equiv \frac{\Delta L}{L} \simeq \frac{2(N+1)\sqrt{1+\alpha^2}GM}{c^2L} \ln \frac{L}{d}. \quad (25)$$

Here, we have approximate the expression or Eq. (24) by considering $d \ll L$. For $\alpha \gg 1$, we have that the strain is proportional to the charge Q but independent of the mass M .

$$h \simeq \frac{(N+1)\sqrt{G}Q}{c^2L} \ln \frac{L}{d} \propto Q. \quad (26)$$

Here, the cgs units are adapted since we have used Eq. (14).

To see the charge dependence, we plot in Figure 5 the increase of the optical path length as a function of the voltage of the charged object. The result indicates that the extension of the optical path length remains a constant as the mass is fixed when the object is weakly charged ($V < 500$ V) and linearly increases with the voltage when the object is highly charged. For instance, when $V = 40$ kV, the charged object can cause the optical path length of one laser beam in a LIGO arm with 280 times reflections to extend up to about $\Delta L \sim 4 \times 10^{-19}$ m (or the strain $h \sim 10^{-22}$), which is the amount of 4 times greater than that to be detectable by the LIGO detectors [15]. For LIGO to detect the scalar field dark energy or to test the 5D gravity, we can switch on and off the power to the object and check whether the converging laser beams become out of phase and thus the interference pattern varies or not. In addition, to have a timely varying optical length difference in a specific range of 20-2000 Hz that LIGO can measure, we consider a harmonically varying voltage or power to charge the sphere, $V(t) = V_0 \sin(2\pi ft)$, with $V_0 = 10^5$ V and $f = 100$ Hz. Figure 6 plots the the varying optical length change between two laser beams as a function of time. Therefore, the accurate LIGO detectors that have recently detected first ever the gravitational waves from a binary black hole merger are capable to be detectors and testers for the scalar field dark energy of 5D gravity. This study provides a creative approach for LIGO to detect the vacuum polarization by the scalar field

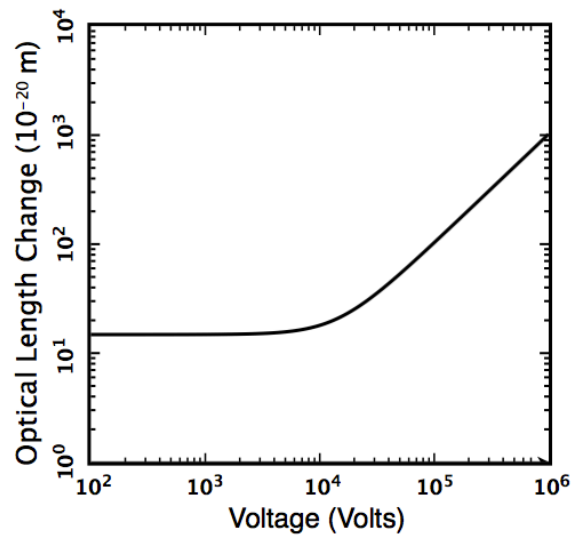


Fig. 5: Space polarization by the scalar field dark energy of 5D gravity. The increase of the optical path length of a laser beam in one LIGO arm that is polarized by a charged object is plotted as a function of the voltage applied to the object. In the case of the object to be only weakly charged ($V < 500$ V), the extension of the optical path length remains a constant as the mass is fixed. When the object is highly charged, however, the optical path length linearly increases with the voltage. At $V = 40$ kV, the charged object can extend the optical path length of one laser beam in a LIGO arm with 280 times reflections up to about $\Delta L \sim 4 \times 10^{-19}$ m (or the strain $h \sim 10^{-22}$), about one order higher than that to be detected by LIGO.

of 5D gravity, a candidate of dark energy that drives the universe in its accelerating expansion. It should be noted that this paper only focuses on the variation in optical length due to the vacuum polarization by the scalar field. To include the variation in optical length due to other fields, we need compute it based on the full solution of all fields. This leaves for future study.

4 Discussions and conclusions

LIGO uses the interference pattern where the beams combine to determine if the optical length down the two laser arms is changing. Possible physical causes for the change of the optical length down the two laser beams can be various sources such as seismic disturbances, gravitational waves from binary black hole mergers, space polarizations by scalar field, and so on. When a gravitational wave passes through the interferometer, the spacetime in the local area is altered, disturbed, and curved. This results in an effective change in the optical length of one or both of the laser beams, which is estimated by $\Delta L(t) = h(t)L$, where $h(t)$ is the gravitational-wave strain amplitude projected onto the detector [15]. The advanced LIGO detectors can have sensitive responses to a strain of $h(t) \sim 10^{-21} - 10^{-23}$. This change of the optical length causes the light currently very slightly out of phase with the incom-

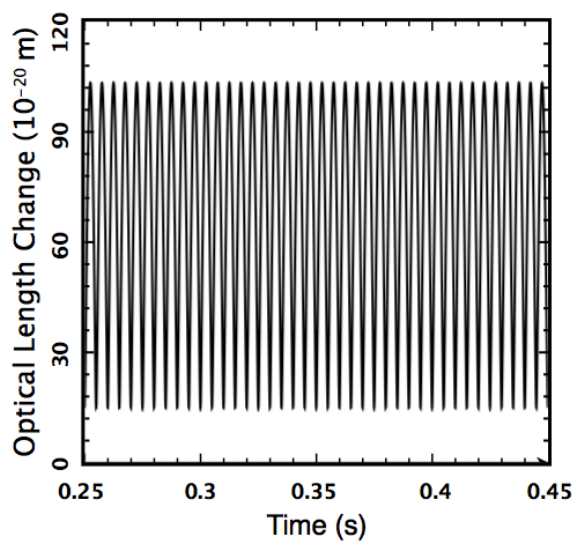


Fig. 6: The optical length difference between the two laser beams is plotted as a function of time when a 100-Hz harmonically varying voltage is applied to charge the sphere. LIGO detectors that have detected the gravitational waves from binary black hole mergers can measure the varying optical length change.

ing light and thus varies the interference pattern. The effective optical length change due to the spacetime disturbances and distortions by the passing of gravitational waves is calculated from the solution of the deviating geodesics equation with a gravitational wave from a binary black hole merger. For the space polarization by scalar field, as analyzed in this paper, we calculate the change of the optical length in accordance with the solution of the deviating index refraction. Seismic disturbances can also result in the converging laser beams being out of phase.

As a consequence, we have in terms of a 5D gravity found that a some-thousand-kilogram (e.g., 4700 kg) sphere electrically charged to some ten kilovolts (e.g. 40 kV) can polarize the vacuum by its scalar field dark energy and thus extend the optical path length of a laser beam that travels through one LIGO arm with some hundred (e.g. 280) reflections by approximately 4×10^{-19} m (or the strain of $h \sim 10^{-22}$), which is the amount of 4 times greater than that to be detected by the LIGO detectors. Switching on and off the power to the object allows to check whether the LIGO detectors can detect the scalar field dark energy and thus test the 5D gravity or not. For a harmonic voltage with frequency, e.g. 100 Hz, we have a varying optical length difference between the two laser beams in the frequency range of the LIGO detection. Therefore, being added a highly charged sphere into the experimental setup, LIGO, which has recently detected first ever the gravitational waves from the binary black hole merger, may directly discover first ever the scalar field dark energy of 5D gravity. This study also provides a design criterion for a

new approach and experiment of discovering dark energy.

Acknowledgement

This work was partially supported by the NSF/REU programs (Grant #: PHY-1263253, PHY-1559870) at Alabama A & M University.

Submitted on June 20, 2017

References

1. Riess A.G. et al. Observational evidence from supernovae for an accelerating universe and a cosmological constant. *Astronomical Journal*, 1998, v. 116, 1009–1038.
2. Perlmutter S. et al. Measurements of Ω and Λ from 42 high-redshift supernovae. *The Astrophysical Journal*, 1999, v. 517, 565–586.
3. Brans C.H., Dicke R.H. Mach's principle and a relativistic theory of gravitation. *Physical Review*, 1961, v. 124, 925–935.
4. Kaluza T. On the problem of unity in physics. *Sitz. Preuss. Akad. Wiss. (Phys. Math.)*, 1921, K1, 966–972.
5. Klein O. Quantum theory and five-dimensional theory of relativity. *Zeitschrift fur Physik*, 1926a, v. 37, 895–906.
6. Klein O. The atomicity of electricity as a quantum theory law. *Nature*, 1926b, v. 118, 516–516.
7. Wesson P.S. The scalar field of 5D gravity and the Higgs field of 4D particle physics: A possible connection, *eprint arXiv:1003.2476*, 2010, arXiv: 1003.2476.
8. Nodvik J.S. Suppression of singularities by the g55 field with mass and classical vacuum polarization in a classical Kaluza-Klein theory. *Physical Review Letters*, 1985, v. 55, 2519–2522.
9. Dragilev V.M. Vacuum polarization of a scalar field in anisotropic multidimensional cosmology. *Theoretical and Mathematical Physics*, 1990, v. 84, 887–893.
10. Frolov V.P., Zelnikov A.I. Vacuum polarization by a massive scalar field in Schwarzschild spacetime. *Physics Letters*, 1982, v. B115, 372–374.
11. Rodrigues R.B., Svaiter N.F. Vacuum fluctuations of a scalar field in a rectangular waveguide. *Physica A: Statistical Mechanics and Its Applications*, 2003, v. 328, 466–492.
12. Bezerra de Mello E.R. Vacuum polarization by a scalar field in de Sitter spacetime in the presence of a global monopole. *Gravitation and Cosmology*, 2010, v. 16, 92–104.
13. Breev A.I. Scalar field vacuum polarization on homogeneous spaces with an invariant metric. *Theoretical and Mathematical Physics*, 2014, v. 178, 59–75.

14. Zhang T.X. The 5D fully-covariant theory of gravitation and its astrophysical applications. *Galaxies*, 2015, v. 3, 18–53.
15. Abbott B.P. et al. Observation of gravitational waves from a binary black hole merger. *Physical Review Letters*, 2016, v. 116, id. 061102.
16. Zhang T.X. Electric redshift and quasar. *The Astrophysical Journal Letters*, 2006, v. 636, L61–L63.
17. Zhang T.X. Gravitational field shielding and supernova explosions. *The Astrophysical Journal Letters*, 2010, v. 725, L117–L120.
18. Zhang B.J., Zhang T.X., Guggilla P., Dokhanian M. Gravitational field shielding by a scalar field. *Progress in Physics*, 2013, v. 1, 69–73.
19. Zhang T.X. Gravitationless black holes. *Astrophysics and Space Science*, 2011, v. 334, 311–316.
20. Zhang B.J., Zhang T.X., Guggilla P., Dokhanian M. Neutron star mass-radius relation with gravitational field shielding by a scalar field. *Research in Astronomy and Astrophysics*, 2013a, v. 13, 571–578.
21. Dvali G., Turner S. Dark energy as a modification of the Friedmann equation. *arXiv: astro-ph/0301510*, 2003.
22. Jadhav M. Five-dimensional fully covariant Kaluza-Klein cosmology with scalar field dark energy. *PhD Thesis* (Advisor: T. X. Zhang), 2013, Alabama A & M University
23. Sharif M., Khanum F. Kaluza-Klein cosmology with modified holographic dark energy. *General Relativity and Gravitation*, 2011, v. 43, 2885–2894.
24. Chodos A., Detweiler S. Spherically symmetric solutions in five dimensional general relativity. *General Relativity and Gravitation*, 1982, v. 14, 879–890.
25. Overduin J.M., Wesson P.S. Kaluza-Klein gravity. *Physics Reports*, 1997, v. 283, 303–378.
26. Souriau J.M. Five-Dimensional Relativity. *Nuovo Cimento*, 1963, v. 30, 565–578
27. Weinberg S. *Gravitation and Cosmology*, Wiley: New York, 1980.
28. Zhang T.X. Static spherically symmetric solution of Kaluza-Klein theory with scalar field and its experimental examination. *Thesis* (Advisor: Z.T. Yang), Yunnan University, 1987.
29. Zhang T.X. Kaluza-Klein theory with five-dimensionally complete covariance. *Journal of Jiangxi University: Natural Science*, 1993, v. 17, 63–70.
30. Reissner H. Über die Eigengravitation des elektrischen Fields nach der Einsteinschen Theorie. *Annalen der Physik (in German)*, 1916, v. 355, 106–120.
31. Nordström G. On the Energy of the Gravitational Field in Einstein's Theory. *Koninklijke Nederlandsche Akadademie van Wetenschappen Proceedings*, 1918, v. 20, 1238–1245.

Progress in Physics is an American scientific journal on advanced studies in physics, registered with the Library of Congress (DC, USA): ISSN 1555-5534 (print version) and ISSN 1555-5615 (online version). The journal is peer reviewed and listed in the abstracting and indexing coverage of: Mathematical Reviews of the AMS (USA), DOAJ of Lund University (Sweden), Scientific Commons of the University of St.Gallen (Switzerland), Open-J-Gate (India), Referential Journal of VINITI (Russia), etc. **Progress in Physics** is an open-access journal published and distributed in accordance with the Budapest Open Initiative: this means that the electronic copies of both full-size version of the journal and the individual papers published therein will always be accessed for reading, download, and copying for any user free of charge. The journal is issued quarterly (four volumes per year).

Electronic version of this journal: <http://www.ptep-online.com>

Advisory Board of Founders:

Dmitri Rabounski, Editor-in-Chief
Florentin Smarandache, Assoc. Editor
Larissa Borissova, Assoc. Editor

Editorial Board:

Pierre Millette
Andreas Ries
Gunn Quznetsov
Felix Scholkmann
Ebenezer Chifu

Postal address:

Department of Mathematics and Science, University of New Mexico,
705 Gurley Avenue, Gallup, NM 87301, USA
